이학박사 학위논문

Decadal Changes in the Physical Mechanisms of Summertime Precipitation Variability in Korea

한국 여름 강수 변동성 기작의 십년 규모 변화

2012 년 8 월

서울대학교 대학원

지구환경과학부

노 준 우

한국 여름 강수 변동성 기작의 십년 규모 변화

Decadal Changes in the Physical Mechanisms of Summertime Precipitation Variability in Korea

지도교수 김 광 열

이 논문을 이학박사 학위논문으로 제출함
2012 년 5 월

서울대학교 대학원
지구환경과학부
노 준 우

노준우의 박사학위논문을 인준함
2012 년 6 월

위 원 장 임 유 호 (인)

부위원장 김 광 열 (인)

위 원 이 동 규 (인)

위 원 전 종 갑 (인)

위 원 서 경 환 (인)

Abstract

Decadal Changes in the Physical Mechanisms of Summertime Precipitation Variability in Korea

Roh, Joon-Woo
School of Earth and Environmental Sciences
The Graduate School
Seoul National University

Issues related to precipitation changes are currently of great practical importance in association with the impact of climate changes. Areas of extreme precipitation changes compared to the respective mean are limited to a few regions rather than the whole globe. Thus, studies focusing on the detailed physical mechanisms of heavy rainfall on a regional scale are needed. Summertime precipitation variability in Korea has also changed significantly in recent years.

Three distinct physical mechanisms in the seasonal cycle of the 120-day (May 19-September 15) summer precipitation in Korea (126°-130°E × 33°-38°N) were identified by cyclostationary empirical orthogonal function (CSEOF) analysis with using the 1979-2008 observed precipitation records at 61 Korea Meteorological Administration stations. Detailed space-time structures of the physical mechanisms of precipitation variability were derived using the daily NCEP/NCAR reanalysis data over Asia (80°-180°E, 0°-60°N). The seasonal cycle

of summertime precipitation in Korea exhibits three principal temporal scales—seasonal, sub-seasonal, and high-frequency components—of variability with distinct physical mechanisms. The seasonal component represents the variability associated with the evolution of the Asian summer monsoon, specifically the East Asia summer monsoon, governed primarily by large-scale circulation as a result of varying sea level pressure contrasts between the Asian continent and the surrounding oceans. The arrival and the duration of a monsoon front primarily shape the seasonal evolution of precipitation in Korea. The bimodal peaks are due to the low-level circulation change as a result of temperature and subsequently sea level pressure redistribution during summer. The sub-seasonal component has characteristic time scales of 10-30 days and is associated with eastward moving upper-level disturbances at ~40°N. The upper-level disturbances affect the meridional circulations resulting in low-level convergence/divergence underneath and also to the south and to the north of the disturbance. From mid-July to mid-August, the sub-seasonal component is more clearly observable and the period of oscillations is generally shorter than during early or late summer. The high-frequency component with time scales less than 10 days is associated with mid-latitude baroclinic Rossby waves; synoptic-scale variations of upper-level geopotential height and low-level moisture convergence are well correlated with the high-frequency variability of precipitation in Korea. Positive precipitation anomalies over Korea correspond

to an upper-level divergence with anti-cyclonic wind anomalies due to baroclinic Rossby waves with their axis around ~40°N. The vertical structures of key physical variables are well explained in the context of baroclinic instability with the geopotential height anomaly field connecting the upper-level divergence and the lower-level convergence tilted westward with height and the temperature anomaly field slanting slightly in the opposite direction.

Since various physical mechanisms potentially contribute to changes in Korean summertime precipitation, distinct physical mechanisms with different time scales help analyze the summertime precipitation variability. 61 KMA summertime precipitation data in South Korea for 1996-2008 (POS) in comparison with those for 1979-1995 (PRE) were also analyzed via CSEOF technique. Detailed physical change by extracting space-time structures of the physical mechanisms of precipitation variability were derived from using the daily NCEP/NCAR reanalysis data over East Asia (80°-180°E, 0°-60°N) by CSEOF analysis with the same design to the previous analysis.

In the seasonal component, which represents the variability associated with the evolution of the East Asian summer monsoon, due to the change of low-level circulation patterns in the Asian region, the commencement, duration, and retreat of the East Asian monsoon front has varied significantly over recent years. Specifically, the first peak of the bimodal precipitation pattern in Korea

has started earlier and significantly increased in intensity. The second peak has broadened in recent years and the typical seasonal period of decreased precipitation has weakened.

The strength of the sub-seasonal component has increased in recent years due to the strengthening of meridional circulation between the subtropics and the mid-latitudes. A conspicuous change in the vertical structure of the sub-seasonal component is seen in recent records. Increased warm and moist advections from the south and decreased cold and dry advections from the north seem to be the primary reasons for such a change. Relatively strong sub-seasonal precipitation activity with an averaged period of ~15 days has shifted from late June through mid July in the PRE years to early August through early September in the POS years. The high-frequency component, which is formed by the baroclinic instability, has increased in the POS years by ~25% particularly in early- to mid-August in Korea since dynamical and thermodynamical processes have strengthened.

The second and third CSEOF modes in the entire period explain the localized heavy rainfall events, which are mainly associated with the direct/indirect effect of tropical cyclones. The extreme localized heavy rainfall event appeared in the southern provinces of Korea as September 3 in the second CSEOF of 1979-1995. In the second CSEOF of 1996-2008, however, the extreme

heavy rainfall events at August 7 and August 31 occur dominantly in the central-western region and in the eastern part of the Korean Peninsula, respectively. This change in the localized heavy rainfalls could be due to the tropical cyclone or depression activities.

Keywords: Physical mechanism, summertime precipitation variability, cyclostationary EOF, decadal change

Student number: 2005-30139

Table of Contents

List of figures

List of tables

1. Introduction

1.1. Background on summertime precipitation variability in Korea

Korean summertime rainfalls accounting for about three-fourth of the mean yearly precipitation are primarily caused by Changma, which includes continuous rainfalls along the Changma front, localized heavy rainfalls with convective instability, and rainfalls due to direct/indirect typhoons (Lee et al., 2008; Lee, 2004). The rainy season in Korea, the so-called Changma, accompanied by a belt-like peak rainfall zone, begins with the influence of the quasi-stationary convergence zone between the tropical maritime air mass from the south, and both continental and maritime polar air masses from the north (e.g., Lee, 2004; Ding, 2004). Changma is considered a part of the East Asian summer monsoon (Ding, 2004) and, more generally, a part of the Asian monsoon (Lim et al., 2002).

The Changma front is, in a sense, a quasi-stationary front between the continental cold low from the Asian continent and the subtropical high from the western North Pacific (Lee, 2005; Ninomiya and Mizuno, 1987). Changma is regarded as a part of the East Asian summer monsoon (Ding, 2004; Wang and Ho, 2002; Tao and Chen, 1987) or, more generally, a part of the Asian summer monsoon (Lim et al., 2002) as a result of the land/ocean thermal contrast. The

synoptic-scale structure related to the fronts, which are caused by a quasi-stationary moisture convergence zone or band between the tropical maritime air mass from the south and the continental and maritime polar air masses from the north (Qian and Lee, 2000; Lau et al., 1988), is one of the main rain-bearing synoptic systems in northeast Asia. The East Asian summer monsoon advances northward with time as the front migrates poleward. This migration is manifested in the movement of the major seasonal rain belt from south China to the Yangtze River basin and Japan, reaching northern China and Korea. The seasonal cycle of Changma in Korea are primarily determined by the movement and location of the precipitation bands. The primary rainy spell diminishes briefly and then the second rainy spell develops as circulation pattern changes with the temperature distribution over the continent and over the ocean (Lim et al., 2002; Chen et al., 2003; Ding, 2004).

The Asian monsoon system, which is associated to Changma, exhibits significant quasi-periodic variations on intraseasonal time scales (Webster et al., 1998). The intraseasonal variability has been studied in regard to the South China Sea monsoon (Kajikawa and Yasunari, 2005) and the Asian monsoon (Annamalai and Slingo, 2001; Lau et al., 1988). Annamalai and Slingo (2001) remarked that the intraseasonal variability has two temporal scales with distinct physical properties: 30-60 days with northward propagation, and westward propagating oscillations with a shorter period (10-25 days) in South Asia. It is

not clear how these explanations are linked with the sub-seasonal variability of Korean summer precipitation.

In additional to the seasonal variability, precipitation records in Korea exhibit a substantial amount of synoptic-scale variability. Hong (2004) remarked that the synoptic conditions producing heavy summer precipitations over Korea are characterized by a strong baroclinicity. Further, summer precipitation is associated with thermodynamically neutral atmosphere over Korea in contrast to large convective available potential energy, which is typical over the central United States. In addition, the low-level vortices over the Tibetan Plateau play a role in developing a unique weather system on a synoptic scale in the EASM regions (Ding, 2004).

1.2. Motivation and objective

Precipitation change and its social and economical effects are currently of great practical importance. Groisman et al. (2005) found a widespread increase in the frequency of very heavy precipitation in the mid-latitudes during the past 50 to 100 years. Emory and Brown (2005) suggested that a greater increase in global mean water vapor tends to yield a greater global mean thermodynamic increase in extreme precipitation based on model results. Mitas and Clement (2005) showed that water vapor has increased in recent years.

Held and Soden (2006) used numerical models to examine changes in the hydrological cycle. Such changes include a decrease in convective mass fluxes, an increase in horizontal moisture transport, associated enhancement of the pattern of evaporation minus precipitation and its temporal variance, and a decrease in the horizontal sensible heat transport in the extratropics. An issue of local importance in recent years is the significant change in local precipitation levels. Extreme precipitation events have been projected to increase, but the cause and the mechanism of increase are not clear. However, global warming, one of the biggest environmental issues in recent years, is generally suspected to be responsible for such changes.

Trenberth (1999) asserted that the enhancement of atmospheric moisture content feeds increased moisture to all weather systems. On a global mean basis, annual mean precipitation is constrained by the energy balance between atmospheric radiative cooling and latent heating, which is expected to limit the mean precipitation increase to be lower than the rate of atmospheric moisture increase (Allen and Ingram, 2002). On a regional basis, however, Emori and Brown (2005) showed that areas of extreme changes in precipitation are limited to a few regions. Thus, detailed mechanisms of heavy rainfall need to be examined individually on regional scales. Summertime precipitation variability in Korea has also changed significantly in recent years. Observational records exhibit a strong decadal change in the East Asian summer monsoon. In

the current decade, for example, negative correlations between the intensity of the East Asian summer monsoon and that of the western North Pacific summer monsoon are much stronger compared with the last decade (Kwon et al., 2005). In this study, local changes in summer precipitation variability in Korea are investigated.

There are various physical mechanisms potentially exerting influences on the Korean summer precipitation. Kim et al. (2010) showed that the seasonal cycle of the summertime precipitation variability in Korea consists of three different physical mechanisms; the seasonal evolution, the sub-seasonal evolution, and the high-frequency evolution. This study aims at characterizing the summertime precipitation change in Korea in the context of distinct physical mechanisms of precipitation variability. Instead of simply addressing precipitation amount change, this study focuses more on how distinct physical mechanisms contribute to precipitation change in Korea. In order to understand the decadal (climatological) changes of the physical mechanisms, summertime precipitation in Korea are analyzed for two periods, which were divided based on the estimated time of shift in the patterns of precipitation; this will help us understand the change of summertime precipitation variability in Korea in terms of dynamical and physical viewpoints, which is a primary goal this research.

Kim and Suh (2009) examined the multiple change-point and change pattern of the annual precipitation and the heavy rainfall characteristics averaged over South Korea during 1954-2007 based on a Bayesian approach. A statistically significant change has occurred around 1996 or 1997 in the heavy precipitation days and amounts (Kim and Suh, 2009; Kim et al., 2009). We investigated precipitation variability for the period 1979-1995 (PRE) and the period 1996-2008 (POS) using the observed precipitation records at 61 Korea Meteorological Administration stations. Detailed physical structures of precipitation changes will be extracted by applying the cyclostationary EOF (CSEOF) technique (Kim et al., 1996; Kim and North, 1997) on various physical variables. The primary motivation for using the CSEOF technique is to extract physical evolutions from atmospheric variables in such a way that they are physically consistent with each other. The technique has been used successfully in many previous studies (e.g., Seo and Kim, 2003; Kullgren and Kim, 2006; Kim et al., 2006; Lim and Kim, 2007)

2. Data and methods

The detailed descriptions of the data used in this study are first given. Then, methods of explaining more detailed causes of summertime precipitation variability in Korea and decadal change of physical mechanisms were described.

2.1. Data

The primary data used in the present study is the 30-year (1979-2008) daily precipitations at 61 Korean Meteorological Administration (KMA) stations distributed in the republic of Korea (~126°E - 130°E, ~33°N - 38°N). Table 2.1 shows the arranged numbers, station numbers, locations, and name of KMA stations. The arranged numbers of 61 KMA stations were rearranged for considering sequential latitudinal and longitudinal locations. The station numbers of KMA stations indicated the identified numbers. Figure 2.1 shows the locations and the arranged station numbers of 61 KMA stations. Then, in order to investigate decadal change of summertime precipitation variability in Korea, two periods were considered to previous 17-year (1979-1995) and recent 13-year (1996-2008) (Kim and Suh, 2009). For the present analysis, 120 summer days set from 19 May through 15 September.

In order to draw a connection between the local precipitation variability and physical processes around Korea and over Asia, 2.5° × 2.5° daily geopotential height, temperature, zonal wind, meridional wind, omega, and specific humidity fields for 11 layers from 200-hPa to 1000-hPa were taken from the National Center for Environmental Prediction/National Center for Atmospheric Research (NCEP/NCAR) reanalysis product (Kalnay et al., 1996). Gridded daily NCEP/NCAR precipitation rates are available in the form of 1.875° × 94 Gaussian array in order to investigate a relationship between Korean summertime precipitation and Asian summertime precipitation.

Table 2.1. The arranged number (ARR NUM), station number (STN NUM), latitude (LAT) of station, longitude (LON) of station, and station name (STN NAME) list for 61 Korean Meteorological Administration stations in the Republic of Korea.

ARR NUM	STN NUM	LAT (°N)	LON (°E)	STN NAME
1	108	37.57	126.97	Seoul
2	112	37.47	126.63	Incheon
3	119	37.27	126.98	Suwon
4	202	37.48	127.50	Yangpyeong
5	203	37.27	127.48	Icheon
6	211	38.05	128.17	Inje
7	101	37.90	127.73	Chuncheon
8	114	37.33	127.95	Wonju
9	212	37.68	127.88	Hongcheon
10	221	37.15	128.20	Jecheon
11	105	37.75	128.90	Gangneung
12	90	38.25	128.57	Sokcho
13	100	37.68	128.77	Daegwallyeong
14	115	37.48	130.90	Ulleungdo
15	127	36.97	127.88	Chungju
16	131	36.63	127.45	Cheongju
17	135	36.22	128.00	Chupungnyeong
18	226	36.48	127.73	Boeun
19	232	36.78	127.12	Cheonan
20	129	36.77	126.50	Seosan
21	133	36.37	127.37	Daejeon
22	235	36.32	126.57	Boryeong
23	236	36.27	126.92	Buyeo
24	238	36.10	127.48	Geumsan
25	243	35.73	126.72	Buan
26	143	35.88	128.62	Daegu
27	152	35.55	129.32	Ulsan
28	244	35.62	127.28	Imsil
29	245	35.57	126.87	Jeongeup
30	247	35.40	127.33	Namwon
31	256	35.07	127.23	Suncheon
32	159	35.10	129.03	Busan

33	168	34.73	127.75	Yeosu
34	184	33.52	126.53	Jeju
35	170	34.40	126.70	Wando
36	260	34.68	126.92	Jangheung
37	261	34.55	126.57	Haenam
38	262	34.62	127.28	Goheung
39	265	33.38	126.88	Seongsanpo
40	130	36.98	129.42	Uljin
41	138	36.03	129.38	Pohang
42	140	35.98	126.70	Gunsan
43	146	35.82	127.15	Jeonju
44	272	36.87	128.52	Yeongju
45	273	36.62	128.15	Mungyeong
46	277	36.53	129.42	Yeongdeok
47	278	36.35	128.68	Uiseong
48	279	36.13	128.32	Gumi
49	281	35.97	128.95	Yeongcheon
50	162	34.85	128.43	Tongyeong
51	156	35.17	126.90	Gwangju
52	165	34.82	126.38	Mokpo
53	201	37.70	126.45	Ganghwa
54	284	35.67	127.92	Geochang
55	285	35.57	128.17	Hapcheon
56	288	35.48	128.75	Miryang
57	289	35.42	127.88	Sancheong
58	294	34.88	128.60	Geoje
59	295	34.82	127.93	Namhae
60	189	33.25	126.57	Seogwipo
61	192	35.20	128.12	Jinju

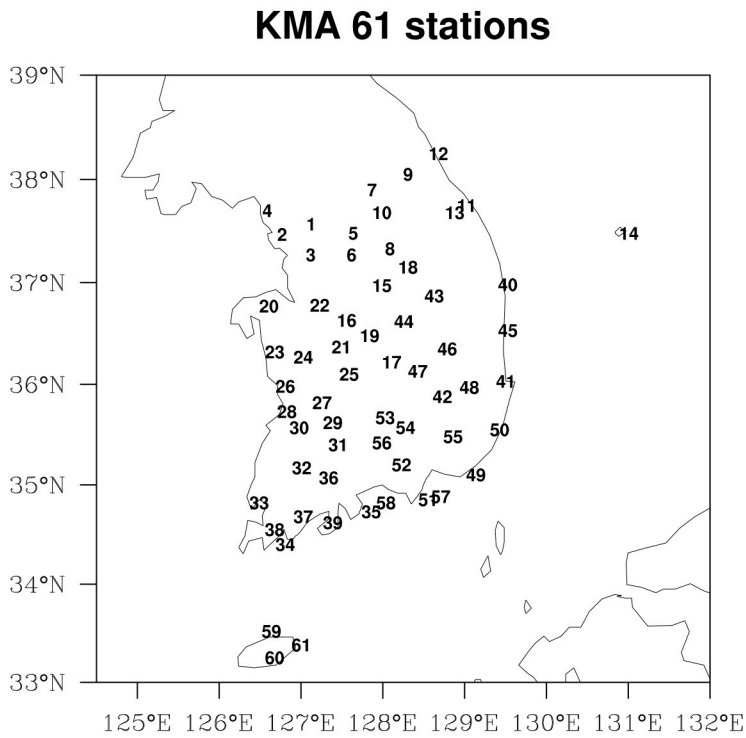

Figure 2.1. The locations and arranged station numbers of 61 Korean Meteorological Administration stations in the Republic of Korea.

2.2. Cyclostationary Empirical Orthogonal Function analysis

Physical processes in the datasets were extracted by using the cyclostationary empirical orthogonal function technique (CSEOF) (Kim and North, 1997) for extracting the spatiotemporal evolution of physical modes and their long-term amplitude variations. At first, in order to investigate the more detailed summertime precipitation variability, CSEOF analysis was conducted on the 30-year record (**TOT**). Then, In order to understand the long-term changes of the resulting physical processes, the same analysis for three different periods, which were 17-year (1979-1995; **PRE**), and recent 13-year (1996-2008; **POS**) of the 120-day summer precipitations at 61 KMA stations in Korea, were carried out. The nested period was set to be 120 days (1 summer year). Similarly, CSEOF analysis was conducted on key physical variables over the Asian domain (80°E - 180°E, 0°N - 60°N) in order to investigate the physical processes associated with summertime precipitation variability in Korea. In this method, space-time data are written as a linear combination of CSEOF,

$$P(r,t) = \sum_n B_n(r,t) T_n(t), \tag{2.1}$$

where $B_n(r,t)$ and $T_n(t)$ are cyclostationary loading vectors (CSLV) and principal component (PC) time series, respectively. CSLVs can be derived from a space-time covariance function, $C_n(r,t;r't')$ by solving

$$C_n(r,t;r',t')B_n(r',t') = \lambda_n B_n(r,t), \tag{2.2}$$

where λ_n are the eigenvalues and inner product is assumed by the repeated indices r' and $,t'$. The assumption of cyclostationarity is invoked here in order to estimate the space-time covariance statistics from a given data set. An important process when performing CSEOF analysis is to set the nested period (i.e., the inherent period of covariance statistics). The CSLVs are periodic and time dependent since the CSLVs are eigen-functions of a time-dependent and periodic covariance statistics.

$$\begin{aligned} C_n(r,t;r',t') &= \langle T(r,t)T(r',t')\rangle = \langle T(r,t+d)T(r',t'+d)\rangle \\ C_n(r,t;r',t') &= C_n(r,t+d;r',t'+d), \end{aligned} \tag{2.3}$$

Note that each random variable $T(r,t)$ is correlated in space and in time as reproduced in the corresponding space-time covariance statistics $c(r,t;r',t')$. The angle brackets denote ensemble averaging. The so-called nested period is set to be 120 days in the present study assuming that physical conditions of every summer days are statistically the same as implied in equation (2.3). That is, physical conditions for each summer represent one realization of the same set of random variables. This is an important consensus of CSEOF analysis in the present study.

$$\sum_{r=1}^{N}\sum_{t=1}^{d} B_n(r,t)B_m(r,t) = \delta_{nm}, \tag{2.4}$$

where δ_{nm} is the *Kronecker delta* and N is the number of spatial points (here, stations). The PC time series are also uncorrelated, that is,

$$\sum_{t=1}^{T} T_n(t)T_m(t) = \lambda_n \delta_{nm} \,, \tag{2.5}$$

where T is the sample size (i.e., total number of time points. Here, T =3600 day (120 summer days x 30 years). While EOFs are independent of time, CSLVs depend on time and are periodic with the time. Thus, this representation of data is similar to but differs from EOF technique in that the loading vectors are time dependent and periodic, i.e.,

$$B_n(r,t) = B_n(r,t+d). \tag{2.6}$$

The CSEOF loading vectors are time dependent because they are eigen-functions of a space-time covariance function instead of a spatial covariance function as in conventional EOF analysis. It is emphasized that CSEOF loading vectors represent temporally evolving physical processes, while PC time series represent the amplitude modulation of the physical processes on longer time scales. Examples of physical and dynamical interpretations of CSEOFs can be found in Seo and Kim (2003), Kullgren and Kim (2006), Kim et al. (2006), and Lim and Kim (2007). The nested periodicity, d, denotes the inherent timescale of the climate system and is chosen to be 120 days (=1 summer year). Thus, CSLV, $B_n(r,t)$ describes the evolution of spatial patterns over the period of the

nested period as in extended EOFs (Weare and Nasstrom, 1982). The amplitude time series fluctuates slowly showing how the strength of evolution depicted in $B_n(r,t)$ varies on a time scale longer than that of $B_n(r,t)$. Since the amplitude, $T_n(t)$, does not vary significantly over the period of the nested period, d, $B_n(r,t)$ describes the evolution of correlated spatial patterns [i.e., $B_n(r,t=1), B_n(r,t=2), ..., B_n(r,t=d)$]. Thus, a physical mode exhibiting a discrete periodicity such as the seasonal cycle is captured as a single mode in the CSEOF analysis.

2.3. Regression analysis

In order to understand the detailed nature of physical processes, many physical variables are subject to CSEOF analysis in the present study. CSEOFs are computed independently for individual variables so that resulting PC time series are generally different between two different variables. Hence, to obtain dynamically consistent patterns between two variables, a regression or projection method is required. This means that physically and dynamically consistent patterns should be derived from many variables, which is accomplished in the following manner. A CSEOF analysis is conducted on each physical variable. Then, regression analysis is conducted between the PC time

series of a target variable (precipitation in Korea) and the PC time series of a predictor variable (physical variables over the Asian domain) in order to construct the evolution of a predictor variable, which is consistent with the evolution of precipitation in Korea (Seo and Kim, 2003). One needs only to find a set of regression coefficients, such that a residual error is minimized. The PC time series of a predictor variable are regressed onto the PC time series of the target variable:

$$T_i(t) = \sum_n a_n^{(i)} P_n(t) + \varepsilon^{(i)}(t), \quad i = 1,2,3,\cdots, \tag{2.7}$$

where $T_i(t)$ are the CSEOF PC time series of the target variable (precipitations at 61 KMA stations), $P_n(t)$ are the CSEOF PC time series of the predictor variables (physical variables from daily NCEP/NCAR reanalysis data), and $a_n^{(i)}$ are the regression coefficients. The degree of fitting for each mode is estimated by a determination coefficient, $r_i^2 = \langle \varepsilon^2(t) \rangle / \langle PCT_i^2(t) \rangle$, where the angle brackets denote ensemble averaging. Then, the evolution of a predictor variable is obtained from

$$\Psi_i(r,t) = \sum_n a_n^{(i)} C_n(r,t), \quad i = 1,2,3,\cdots \tag{2.8}$$

where $C_n(r,t)$ are the CSLVs of a predictor variable. Then, As a result of CSEOF analysis followed by regression analysis, entire data can be written as

$$Data(r,t) = \sum_n \{P_n(r,t), H_n(r,t), V_n(r,t), ..., T_n(r,t)\} PC_n(t) \tag{2.9}$$

where $\{P_n(r,t), H_n(r,t), V_n(r,t), ..., T_n(r,t)\}$ denotes the physical evolutions of various physical variables investigated in the present study. These spatial and temporal patterns of evolutions, $\{P_n(r,t), H_n(r,t), V_n(r,t), ..., T_n(r,t)\}$, describe the detailed nature of individual physical processes associated with the variability of precipitation in Korea. Physical consistency between physical variables of $\{P_n(r,t), H_n(r,t), V_n(r,t), ..., T_n(r,t)\}$ is argued that they have a common evolution history, $PC_n(t)$, whereas the physical evolutions in the individual variables may not be the same. In fact, $\{P_n(r,t), H_n(r,t), V_n(r,t), ..., T_n(r,t)\}$ are physically connected in terms of dynamical and thermo-dynamical equations governing the physics of each mode.

In a conventional approach, one assumes that the two spatial patterns are physically consistent if they have a common evolution history:

$$Data(r,t) = \sum_n \{\phi_n(r), \psi_n(r)\} PC_n(t) \tag{2.10}$$

Physical interpretations based on equation (6) are seriously hampered, however, since a single spatial pattern cannot adequately describe a physical process (such as the seasonal cycle) because the evolution of one variable is not identical with that of another variable. CSEOF analyses take into account the fact that the

physical evolutions of two or more variables are generally different; they are, of course, not independent of each other but are related in terms of a governing equation describing a specific physical process, say, the seasonal cycle (e.g. Seo and Kim, 2003).

3. Results

3.1. Three distinct physical mechanisms of summertime precipitation variability in Korea

Figure 3.1, which shows the first CSEOF of summertime precipitations at 61 KMA stations in Korea, explains ~16% of the total variability. The variance explained by the seasonal cycle may look small, but the seasonal cycle explains ~88% of the total magnitude of precipitation. This mode represents the seasonal cycle, as also can be inferred from the corresponding PC time series (Figure 3.1e). The evolution in Figure 3.1a is nearly identical in shape and in magnitude with the summer composite based on the same record. The amplitude of the seasonal cycle fluctuates annually around 7.71 mm/day (standard deviation, 2.44 mm/day). The PC time series shows a fairly well defined periodicity at ~3 years. A biennial component of variability is clearly seen in the precipitation record over India (Meehl and Arblaster, 2001), but 2-year periodicity is not seen in the precipitation record in Korea.

The solid line in Figure 3.1a denotes the averaged daily precipitation amount over all 61 KMA stations. The broken curve is the seasonal component of daily precipitation variability after removing high-frequency variability with time scales shorter than 30 days. Summertime precipitation variability is characterized by two periods of heavy rainfall separated by a period of

decreased precipitation. A comparison with other panels in Figure 3.1 shows a reasonable physical consistency between the precipitation over Korea and other collocated physical variables associated with convection. Specific humidity is sufficiently high for precipitation throughout the summer and is not a limiting factor for precipitation. Also, in a climatological sense, atmosphere is conditionally unstable throughout summer, as seen in the vertical structure of equivalent potential temperature (data not shown). A similarity between Figure 3.1a and Figures 3.1c and 3.1d indicates that dynamical and thermodynamical processes shape the seasonal precipitation pattern in the area (see Figures 3.1c and 3.1d). Under the conditional instability of the atmosphere, vertical velocity is favorable for precipitation from June through August, which is a major precipitation period in Korea. Low-level moisture convergence governed essentially by low-level winds also exhibits a bimodal structure, another characteristic feature of summer precipitation in Korea (Lim et al., 2002; Qian et al., 2002; Chen et al., 2003; Lee et al., 2010).

The seasonal cycle of summertime precipitation in Korea consists mainly of three different physical mechanisms with corresponding characteristic time scales: the seasonal component, with time scales longer than 30 days; the sub-seasonal component, with time scales of 10–30 days; and the high-frequency component, with time scales of less than 10 days. These three components of variability have distinct physical characteristics as described in

following sections. Although these sub-seasonal and high-frequency components of variability may also be found in higher CSEOF modes, the precipitation variability is strictly confined in the seasonal cycle. The sub-seasonal and the high-frequency components of precipitation were separated from the seasonal component by conducting 10–30 day band-pass filtering and 10-day high-pass filtering, respectively (Newton, 1988).

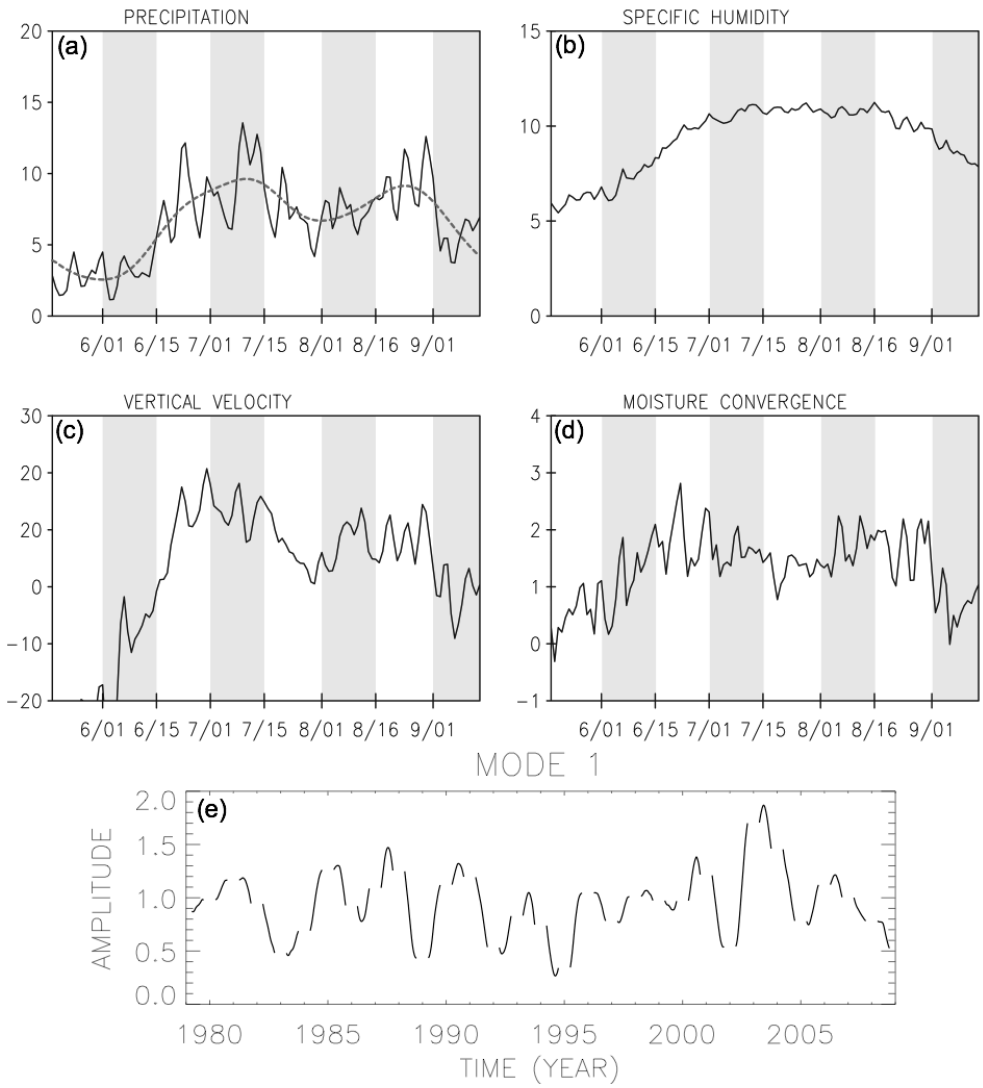

Figure 3.1. The first CSEOF of summertime precipitations at 61 KMA stations in Korea: (a) precipitation (mm/d) averaged over all 61 stations (solid line) and the seasonal evolution (dotted line) after removing high-frequency (<10 days) and subseasonal (10-30 days) components of variability; (b) specific humidity (g/kg); (c) -Ω velocity (10^{-3} Pa/sec); (d) moisture convergence (10^{-8} kg/kg/sec); and (e) corresponding normalized PC time series. Figure 1b-1d represent 850 hPa at 127.5-130°E, 32.5-37.5°N and were derived from the NCEP/NCAR daily reanalysis data.

3.1.1. Seasonal Component of the seasonal cycle of variability

The dotted curve in Figure 3.1a depicts the seasonal component in the seasonal cycle of the summertime precipitation in Korea after removing the sub-seasonal and the high-frequency components of precipitation variability. The seasonal evolution exhibits a typical bimodal structure, consisting of the first major precipitation spell (Changma) followed by the second major precipitation spell (post-Changma); a period of weakened precipitation occurs between the two (Lim et al., 2002; Wang et al., 2007).

As described in section 2.1, various NCEP/NCAR variables in Asian domain were made to be physically consistent with the seasonal cycle of the Korea summer precipitations for multi-level. Figure 3.2 shows the spatial patterns of physical variables associated with the first spell of precipitation in Korea. The low-level circulation pattern exhibits strong wind anomalies along the eastern coast of the Asian continent in association with the negative GPH anomalies over the continent and positive GPH anomalies over the western Pacific (Figure 3.2c). The negative GPH anomaly over the continent is due to continental warming, whereas the pair of GPH anomalies with opposite signs, over the western Pacific, is due to the fact that the latitude of the North Pacific High is slightly lower than the average latitude during summer. With strong southwesterly wind anomalies along the continent, significant moisture

convergence is shown over eastern China, Japan, and Korea, marking the active phase of the regional monsoons, designated Meiyu, Baiu, and Changma, respectively (Figure 3.2a). The vertical section along 127.5°E–130°E also hints the shifted position of the North Pacific High and the resulting change in the low-level moisture convergence. The upper-level wind pattern shows decreased westerlies to the north of 40°N and increased easterlies to the south of 30°N (Figure 3.2b); an exception is the northwestern Pacific, where the North Pacific High is still at a southern location and is weaker than normal, as can be inferred from the 850 hPa GPH anomalies and the 200 hPa wind anomalies over the northwestern Pacific. There is a strong sign of upper-level divergence over Korea, Japan, and east China, where strong low-level moisture convergence is also observed. The low- level and upper-level spatial patterns of physical variables associated with the seasonal evolution of precipitation in Korea are fairly similar to those described by Lim et al. (2002, their Figure 9).

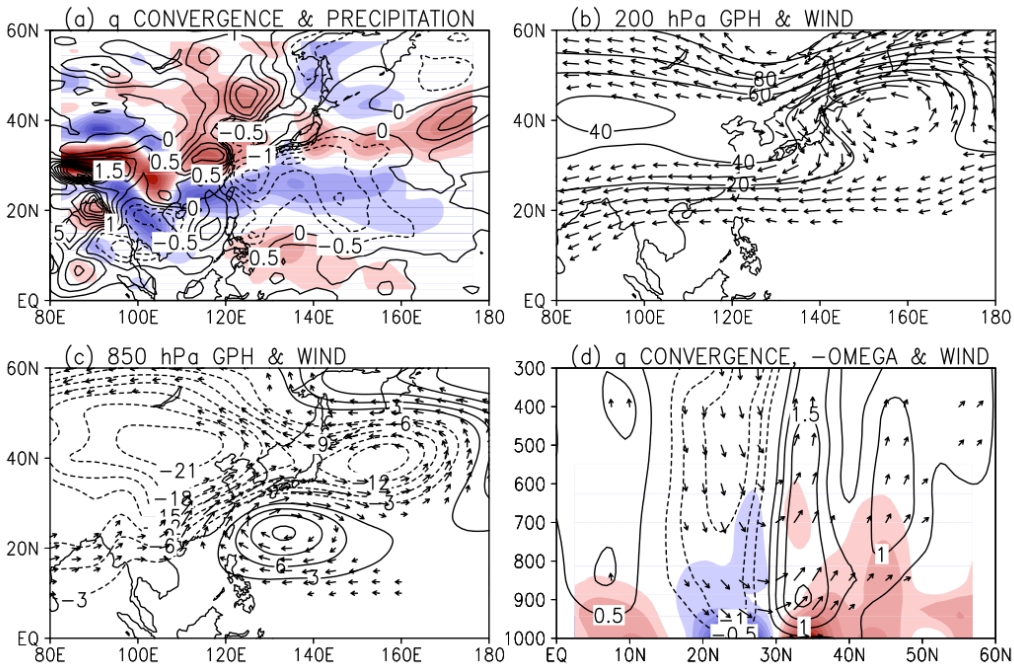

Figure 3.2. The 7 July patterns of the seasonal evolution in (a) low-level (850-1000 hPa) total moisture convergence (shaded at 1×10^{-8} kg/kg/sec intervals) and precipitation (contoured at 1 mm/day intervals) anomalies, (b) 200 hPa geopotential height anomalies (contoured at 20 m interval) and wind > 2 m/sec (vector), (c) 850 hPa geopotential height (contoured at 3 m) and wind anomalies > 1 m/sec (vector), and (d) vertical section of moisture convergence (shaded at 0.3×10^{-8}), -Ω (contoured at 1×10^{-2} Pa/sec) and wind along 127.5°-130°E. The vertical component of winds has been exaggerated by multiplying 100. Red shades denote positive values, and blue shades negative values. Solid lines, positive contours; broken lines, negative contours; vertical axis unit, hPa.

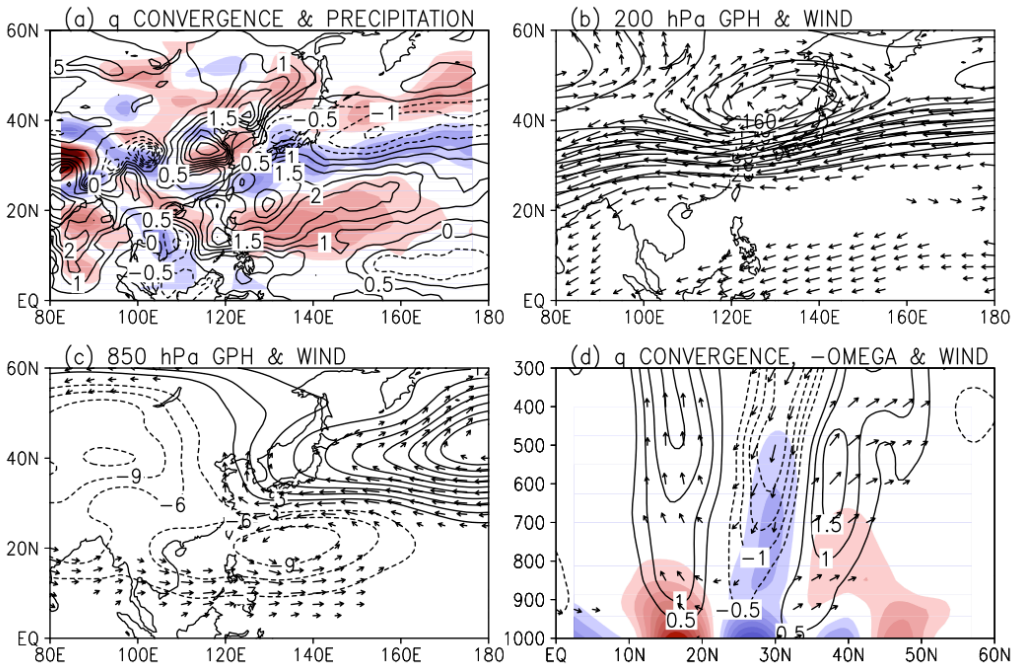

Figure 3.3. The 31 July patterns of the seasonal evolution in (a) low-level (850-1000 hPa) total moisture convergence (shaded at 1×10^{-8} kg/kg/sec intervals) and precipitation (contoured at 1 mm/day intervals) anomalies, (b) 200 hPa geopotential height anomalies (contoured at 20 m interval) and wind > 2 m/sec (vector), (c) 850 hPa geopotential height (contoured at 3 m) and wind anomalies > 1 m/sec (vector), and (d) vertical section of moisture convergence (shaded at 0.3×10^{-8}), -Ω (contoured at 1×10^{-2} Pa/sec) and wind along 127.5°-130°E. The vertical component of winds has been exaggerated by multiplying 100. Red shades denote positive values, and blue shades negative values. Solid lines, positive contours; broken lines, negative contours; vertical axis unit, hPa.

Figure 3.3 shows the spatial patterns of physical variables on 31 July, representing the period of decreased precipitation in Korea (Figure 2a). The North Pacific High has extended slightly toward the continent and migrated to its northern position in summer (Figure 3.3c). Consequently, a negative GPH anomaly developed over the southwestern Pacific, and a pressure gradient along the Asian coast decreased significantly (Figure 3.3c). As a result, low-level moisture convergence has dwindled significantly over Japan and Korea (Figures 3.3a and 3.3d). This marks the period of weakened precipitation in Japan and Korea (Figure 2.1a). The GPH anomalies at the 200 hPa level indicate that warming has spread all over the domain, although its effect in the change of GPH is stronger over the high-latitude continental area than over the ocean. Thus, it seems that upper-level jet is much weaker since 200 hPa wind anomaly corresponding to upper-level jet is changed to weak east wind anomaly. Upper-level jet is one of the important causes of heavy rainfall in Korea summer. A well-developed trough in the upper atmosphere to the west of Korea promotes a favorable condition for precipitation over eastern China (Figures 3.3a and 3.3b). By this time, moisture convergence is much weaker than during the first spell of precipitation, and location of high moisture convergence zone along ~130°E is to the north of Korea.

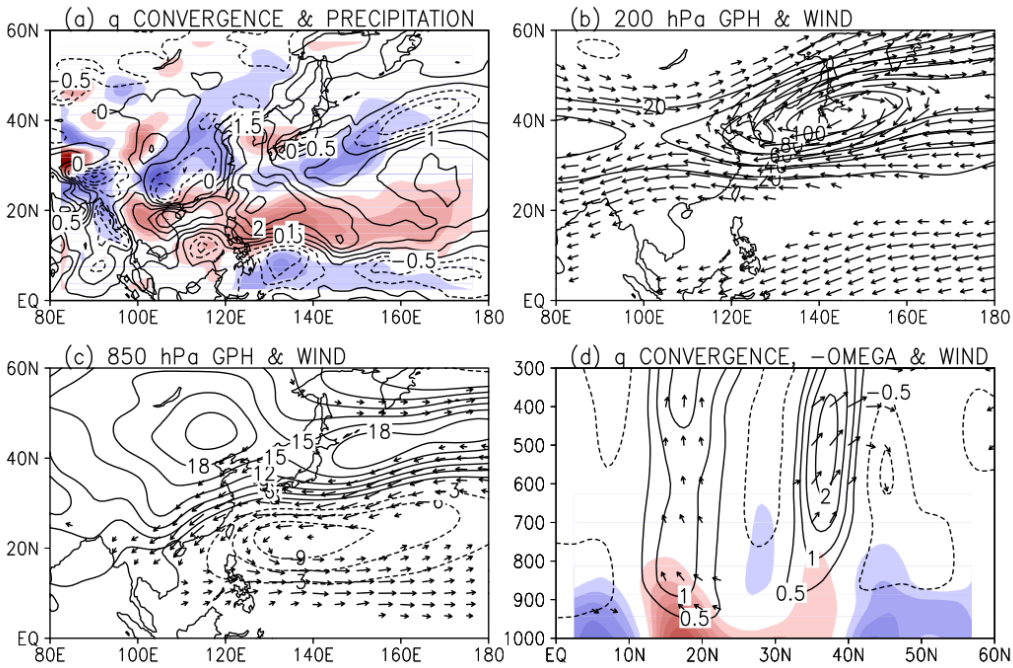

Figure 3.4. The 26 August patterns of the seasonal evolution in (a) low-level (850-1000 hPa) total moisture convergence (shaded at 1×10^{-8} kg/kg/sec intervals) and precipitation (contoured at 1 mm/day intervals) anomalies, (b) 200 hPa geopotential height anomalies (contoured at 20 m interval) and wind > 2 m/sec (vector), (c) 850 hPa geopotential height (contoured at 3 m) and wind anomalies > 1 m/sec (vector), and (d) vertical section of moisture convergence (shaded at 0.3×10^{-8}), -Ω (contoured at 1×10^{-2} Pa/sec) and wind along 127.5°-130°E. The vertical component of winds has been exaggerated by multiplying 100. Red shades denote positive values, and blue shades negative values. Solid lines, positive contours; broken lines, negative contours; vertical axis unit, hPa.

Figure 3.4 represents the second spell of precipitation in Korea. By this time, positive GPH anomalies are seen at 850 hPa over the Asian continent because of cooling (Figure 3.4c); the corresponding air temperature clearly shows cooling over the continent (data not shown). The North Pacific High has retreated northward, resulting in a negative GPH anomaly to the south and a positive GPH anomaly to the north over the western Pacific. This configuration develops low-level easterly anomalies carrying moisture from the northwestern Pacific toward Japan, Korea, and eastern China. In association with the cyclonic vortex, significant moisture convergence is observed over the subtropical western Pacific (Figures 3.4a and 3.4d). A limited amount of convergence is also seen over Korea and the southern part of Japan; this convergence is associated with the second spell of precipitation in Korea and Japan, although the second precipitation is weak in Japan because of the influence of the North Pacific High over Japan. The upper-level GPH anomaly and the resulting circulation patterns also reflect the decreased temperature over the continent and the northward migration of the North Pacific High (Figure 3.4b). Specifically, Korea is to the western flank of the upper-level divergence, which helps prolong the second precipitation spell in Korea.

As can be seen in these figures, sea level pressure contrasts between the Asian continent and the surrounding oceans essentially dictate both the low-level transport of moisture and the magnitude of moisture convergence, thereby shaping the seasonal evolution of precipitation in Korea during the summer monsoon period in Asia. The differential heat capacity between the continent and the oceans is an important ingredient for the evolution of the sea level pressure contrast between the continent and the ocean, thereby determining the direction of moisture transport during summer. Specifically, the bimodal structure of precipitation arises from the circulation change as a result of surface temperature redistribution and the resulting change in sea level pressure (Lim et al., 2002). Excessive moisture is transported primarily from low latitudes (Indian Ocean and tropical western Pacific Ocean) along the coast of the Asian continent to Korea during the first precipitation spell, whereas it is primarily from higher latitudes (northwestern Pacific Ocean) during the second precipitation spell.

3.1.2. Sub-seasonal component of the seasonal cycle of variability

Figure 3.5 shows that 10–30 day band-pass-filtered precipitation and low-level moisture convergence anomalies derived from the NCEP/NCAR daily reanalysis product are physically consistent with the seasonal cycle of precipitation in Korea. Sub-seasonal component of low-level moisture convergence, which is calculated to add moisture convergences vertically from 850-hPa height to 1000-hPa height, is seen to be well matched to sub-seasonal component of daily NCEP precipitation reanalysis data. As shown in Figure 3.5, daily NCEP reanalysis precipitation anomalies and low-level moisture convergence anomalies with alternating signs appear to propagate northward with an average period of ~15 days (e.g., Wang et al., 2007). A comparison of Figures 3.5a and 3.5b shows the sub-seasonal component of precipitation with meridional extent of South Korea appears to derive from the sub-seasonal fluctuations of precipitation over the Asian domain; correlation coefficient between time series of the averaged 61 KMA precipitation in Figure 3.5a and time series of the NCEP daily precipitation reanalysis data averaged over South Korea (126°E–130°E, 33°N–38°N) in Figure 3.5a is 0.58, indicating that the sub-seasonal component of summertime precipitation in South Korea is associated with a seemingly northward propagation of precipitation anomalies from lower latitudes. Especially, when the stronger activity of precipitation, northward

propagation is much seen clearly from early July to early September. However, when the weaker activity of precipitation in late May, in June, and in mid September, northward propagation is not seen clearly in this domain (Fig. 3.5).

The sub-seasonal component of precipitation in Korea should be compared with the intraseasonal variability in the South China Sea monsoon (Kajikawa and Yasunari, 2005) and in the Asian monsoon (Lau et al., 1988; Annamalai and Slingo, 2001). These studies report two dominant time scales with distinct physical characteristics in the intraseasonal variability in South Asia: 30–60 days with northward propagation and 10–25 days with westward propagation. The present study shows a significant northward component in the 10–30 day sub-seasonal variability, although northward migration of precipitation is not quite outstanding in the onset and the termination stages of the summer monsoon (Figure 3.5).

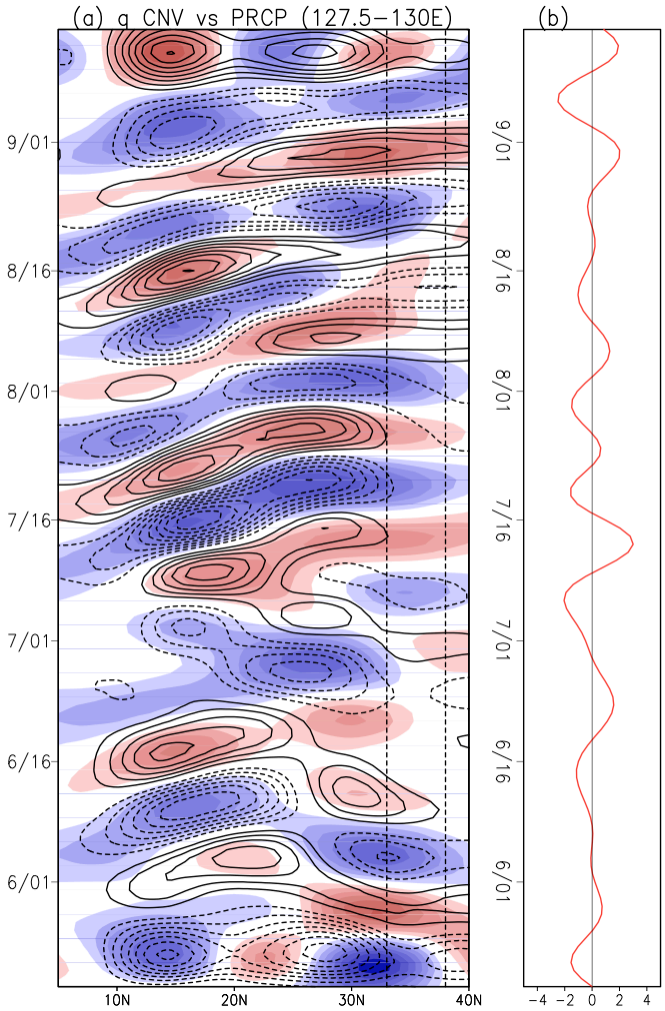

Figure 3.5. (a) Northward propagation of sub-seasonal (10-30 day) component of precipitation (PRCP; contours; 0.2 mm/day) and low-level (850-1000 hPa) moisture convergence (q CNV; shades; 1×10^{-9} kg/kg/sec) anomalies along 127.5°-130°E in the seasonal cycle. The two vertical dotted lines denote the meridional extent of the 61 KMA stations. (b) Sub-seasonal component of precipitation in Korea averaged over 61 KMA stations.

Figure 3.6 is the positive composite of various physical variables associated with the sub-seasonal oscillations. A positive composite pattern is defined by

$$C^{(+)}(r) = \sum_{P_f(t)>1.0} P_f(t) \cdot LVP_f(r,t) \Big/ \sqrt{\sum_{P_f(t)>1.0} P_f^2(t)}\,, \tag{3.1}$$

where $P_f(t)$ is the 10-30 day band-pass filtered precipitation, which is sub-seasonal component of precipitation variability over Korea (Fig. 3.5). $LVP_f(r,t)$ is the similarly filtered physical evolution of a predictor variable regressed onto the seasonal cycle of precipitation in Korea. Equation (3.1) is essentially a weighted average of $LVP_f(r,t)$ with respect to the weights $P_f(t)$. Note that $LVP_f(r,t)$ is averaged only when $P_f(t) > 1.0$ mm/day in order to capture the pattern associated with the positive phase of the oscillations in the precipitation. A negative composite pattern can be obtained in a similar manner.

The physical mechanism of the sub-seasonal oscillations is summarized in Figure 3.6. During the peak of a positive phase, strong positive precipitation anomalies and low-level moisture convergence anomalies are located over South Korea (Figure 3.6a). In comparison to alternating signs of moisture convergence anomalies and precipitation anomalies in Figure 3.5a, sub-seasonal component of moisture convergence anomalies and precipitation anomalies are well explained in aspect of horizontal distributions.

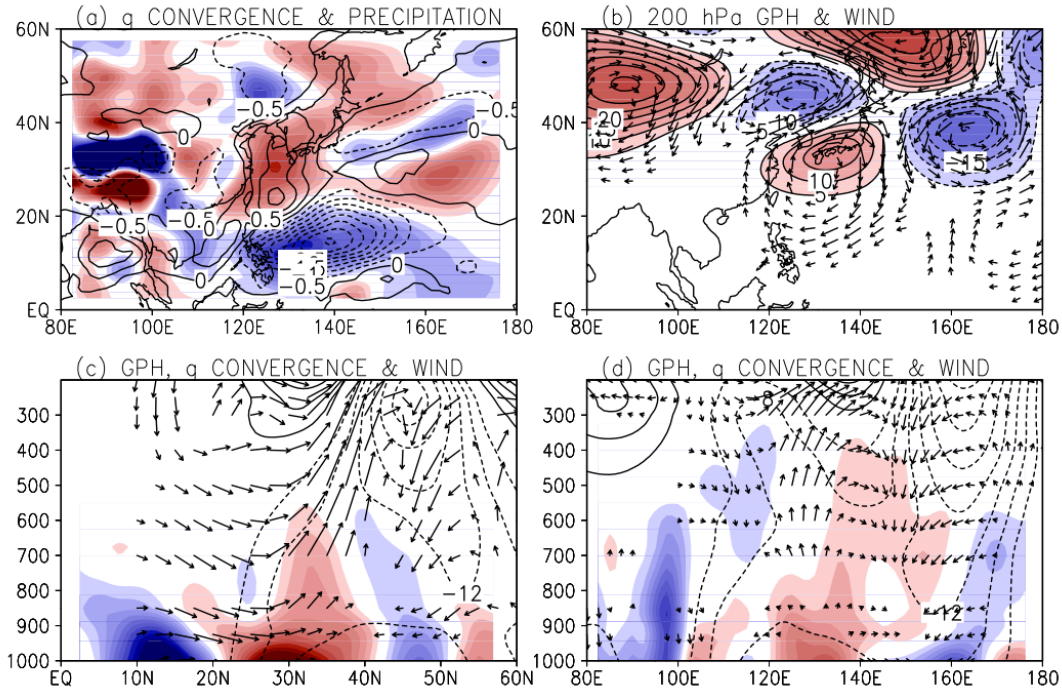

Figure 3.6. Positive composite of the subseasonal component of variability: (a) low-level (850-1000 hPa) moisture convergence (shade; 0.5×10^{-9} kg/kg/sec) and precipitation rate (contour; 0.5 mm/day); (b) 200 hPa GPH (5 m) and wind > 1.0 m/sec; (c) moisture convergence (shade; 2×10^{-9} kg/kg/sec), GPH (contour; 4 m) and wind (v, $-\Omega$) along the 127.5°-130°E band; and (d) moisture convergence (shade; 2×10^{-9} kg/kg/sec), GPH (contour; 4 m) and wind (u, $-\Omega$) along the 35°-40°N band. The vertical velocity, $-\Omega$ (Pa/sec), has been exaggerated by multiplying 100.

Increased GPH is clearly seen slightly to the east of Korea, and decreased GPH is seen to the north of it at 200 hPa (Figure 3.6b). The upper-level GPH anomaly pattern seems to be associated with variation of the jet stream; at the entry of a stronger jet stream, upper-level divergence is observed to the south of the increased jet, and convergence is seen to the north, although not shown here (Bluestein, 1993; Grotjahn, 1993). Along 35°N–40°N, upward motion is seen to the west of the upper-level disturbance, and downward motion is seen to the east (Figure 3.6d). This zonal structure implies that the upper-level GPH anomaly moves eastward; GPH decreases to the west of the center, leading to an upward motion, and increases to the east of the center, yielding a downward motion. Along a band at ~127.5°E– 130°E, upward motion is seen at ~40°N between the two upper-level GPH anomalies with opposite signs (Figure 3.6c). This upward motion is associated with the deepening of the trough by the eastward movement of the upper-level disturbance. As shown in Figure 3.6c, downward motion is observed to the south (~10°N–20°N) and north (~40°N–50°N) of the upward motion at ~40°N. At lower levels, anomalous moisture convergence is observed between ~25°N and 35°N slightly to the south of the upper-level upward motion (Figures 3.6a and 3.6c). As can be seen in Figure 7c, the upper- level upward motion is accompanied by a lower-level moisture convergence underneath and decreased moisture convergence to the north (~40°N–50°N) and to the south (~5°N–20°N).

The low-level moisture divergences to the south and to the north of the disturbance appear to be connected with the meridional circulation change as a result of upper-level disturbance (Figure 3.6c). Figure 3.7 is the map of correlation between the sub-seasonal component of KMA precipitation with moisture convergence, vertical velocity, and wind along the 127.5°E–130°E band. This map exhibits a reasonably concerted change of meridional circulation with the upper- level disturbance in Figure 3.6b. Specifically, deepening of the wave trough is accompanied by upward motion and moisture convergence beneath and by downward motion and moisture divergence to the north and to the south of the disturbance.

The vertical zonal and meridional structures of anomalies in Figures 3.6c and 3.6d, together with those shown in Figure 3.7, suggest an intriguing connection between the midlatitude upper-level disturbance and the anomalous low-level moisture convergence or divergence at low latitudes. Specifically, as the strength of the jet stream increases (Figure 3.8a), the downward branch of the Hadley circulation weakens with anomalous upward motion at ~30°N–40°N and anomalous downward motions to the north (~40°N–50°N) and to the south (~10°N – 20°N), as shown in Figure 3.8b. The upward motion induces the lower-level convergence underneath and the lower-level divergence to the north and south of it (Figure 3.8c). Figure 9d also shows that lower-level specific humidity increases (decreases) as lower-level moisture convergence increases

(decreases). Although the upper-level disturbance is confined to the midlatitude, significant changes in vertical velocity and moisture convergence are also seen at low latitudes, suggesting a midlatitude–subtropical teleconnection. Note that the response at low latitudes lags the upper-level disturbance by ~2 days (Figures 3.8b and 3.8c).

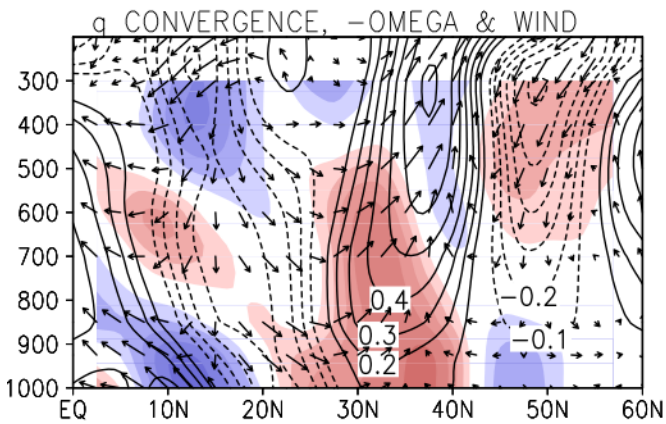

Figure 3.7. Correlation of moisture convergence (shade), −Ω velocity (contour) and wind (v, −Ω) along the 127.5°-130°E band with the sub-seasonal component of 61 averaged KMA precipitation. The vertical velocity, −Ω (Pa/sec), has been exaggerated by multiplying 100. The ordinate denotes vertical height [hPa]

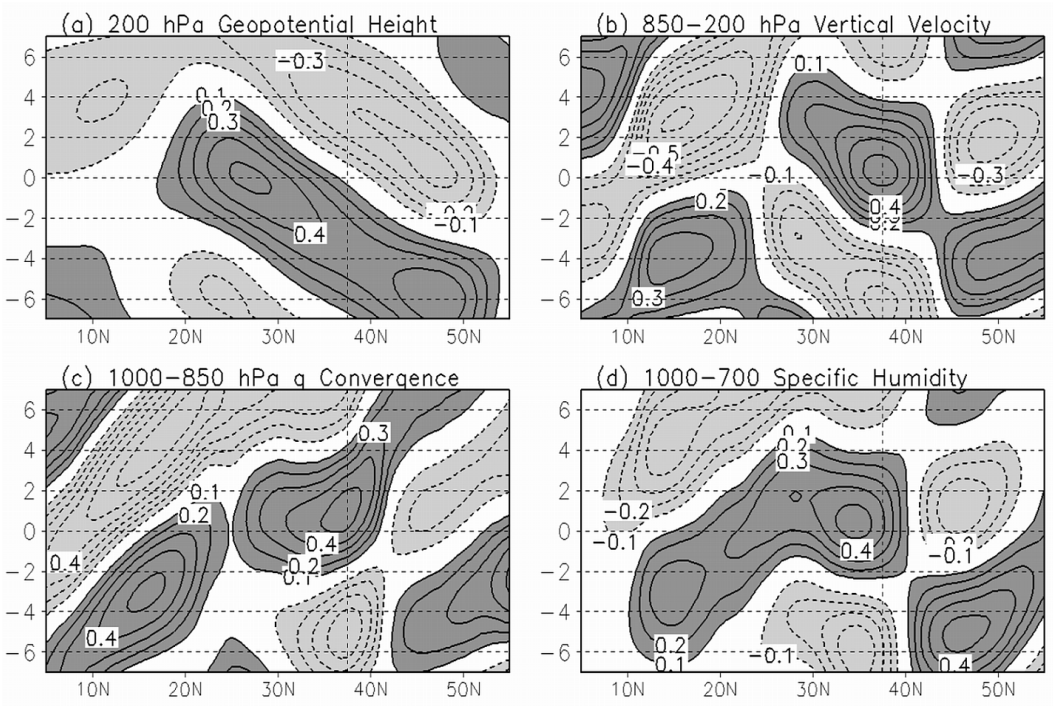

Figure 3.8. Correlation of the sub-seasonal component of 61 averaged KMA precipitation with (a) 200 hPa GPH, (b) 200-850 hPa $-\Omega$ velocity, (c) 850-1000 hPa moisture convergence, and (d) 700-1000 hPa specific humidity along the 127.5°-130°E band. The ordinate denotes time in days with respect to the reference time (peak sub-seasonal precipitation over Korea).

With the connection of the upper-level GPH anomaly and the meridional circulation in mind, the northward propagation of the sub-seasonal component of precipitation can be explained as follows. With the development of upper-level disturbance, as reflected in the pair of GPH anomalies in Figure 3.6b, upward motion and moisture convergence are established underneath the upper-level GPH anomaly with downward motions to the north and to the south of the moisture convergence. As the upper level disturbance moves eastward and is replaced by a disturbance of the opposite sign (Figure 3.6a), the existing anomalous moisture divergence at low-latitude gradually migrates northwestward and merges with the newly established disturbance (Figures 3.6b–d). Simultaneously, anomalous moisture convergence appears to the north and to the south of the newly established downward motion at ~30°N–40°N (Figures 3.6b and 3.6c). Thus, it is the emergence of a new moisture convergence anomaly at ~30°N–40°N and the subsequent merger with the existing moisture convergence anomaly that gives the appearance of a northward propagation of precipitation field (Figure 3.5). This explanation is not necessarily in conflict with previous studies (e.g., Kemball-Cook and Wang, 2001) since the existing moisture convergence anomaly at low latitude is attracted to the moisture convergence anomaly of the same sign to the north. It is clear, however, that the low-latitude precipitation variability is not a direct source of the sub-seasonal precipitation variability in Korea.

3.1.3. High-Frequency component of the seasonal cycle of variability

In addition to the seasonal and the sub-seasonal evolution of precipitation, the seasonal cycle of precipitation is populated with high-frequency undulations as shown in Figure 3.1a. To understand the nature of these high-frequency undulations, high-pass filtering has been conducted on the seasonal cycle with a 10-day cutoff period. Figure 3.9 shows the high-pass-filtered GPH anomalies and the low-level moisture convergence anomalies compared with the precipitation anomalies over Korea. As shown, high-frequency variation of precipitation over Korea is significantly correlated with the upper-level (200–600 hPa) GPH anomalies (correlation coefficient is 0.451) and the lower-level (850–1000 hPa) moisture convergence anomalies (correlation coefficient is 0.571) during the summer 120 days.

The positive composite pattern of NCEP daily precipitation depicts a region of positive precipitation anomalies around Korea. The precipitation anomaly patterns over the entire domain, however, are fairly complex, having significant zonal and meridional variations (Figure 3.10a). Precipitation anomalies over Korea appear to be associated with the overhead 200 hPa divergence with anti-cyclonic wind anomalies; the center of the divergence is slightly to the southeast of that of the precipitation anomalies (Figure 3.10b).

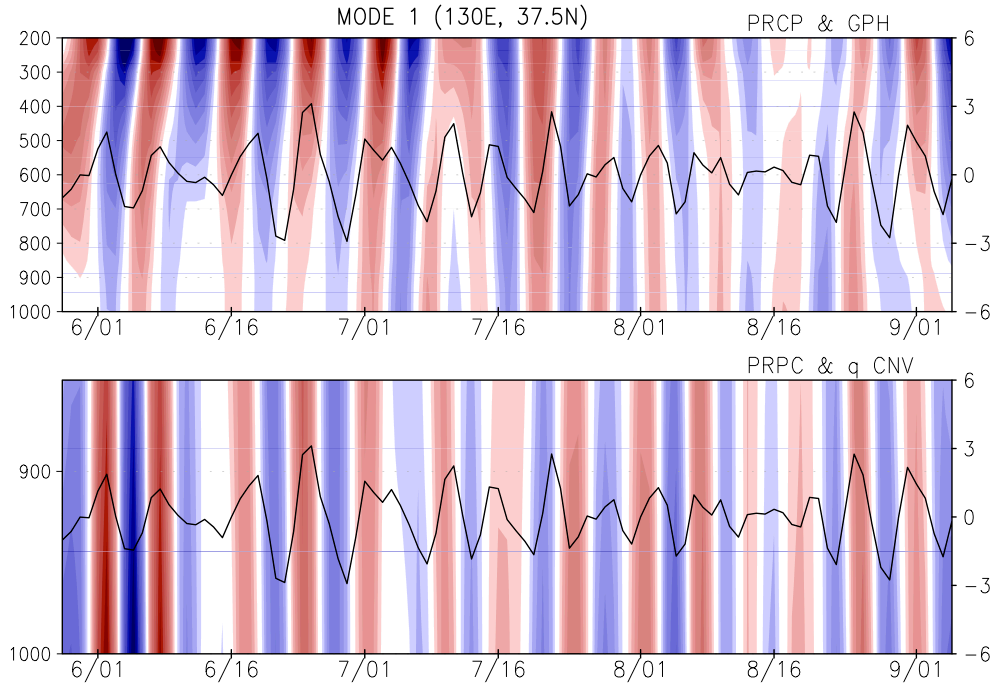

Figure 3.9. High-pass filtered precipitation (PRCP; line) and anomalies in GPH at 200-1000 hPa (shaded) (upper panel) and low-level moisture convergence (q CNV) at 850-1000 hPa (shaded) (bottom panel) in the seasonal cycle of precipitation in Korea. The right axis denotes the precipitation scale (mm/day).

Upward motion and moisture convergence increase below the 200 hPa divergence, which is consistent with the increased precipitation in the neighborhood of Korea (Figure 3.10c). Straddling the 200 hPa divergence in the zonal direction are decreased GPH anomalies and downward motions, indicating that Rossby waves are a crucial ingredient in the high-frequency components of precipitation fluctuations around Korea (Figure 3.10d). The negative composite patterns are essentially the same as the positive composite patterns but with the sign reversed (data not shown).

The tilting of the column of GPH anomalies suggests that the high-frequency fluctuations of precipitation with the period of ~6–8 days are due to the instability of baroclinic Rossby waves. Below the 200 hPa divergence, positive temperature anomalies are tilted slightly in the opposite direction from that of positive GPH anomalies (Figure 3.10d), a prototypical picture of baroclinic instability (Holton, 1992). To the west and east of the 200 hPa divergence, similar temperature and GPH structures with opposite signs are observed.

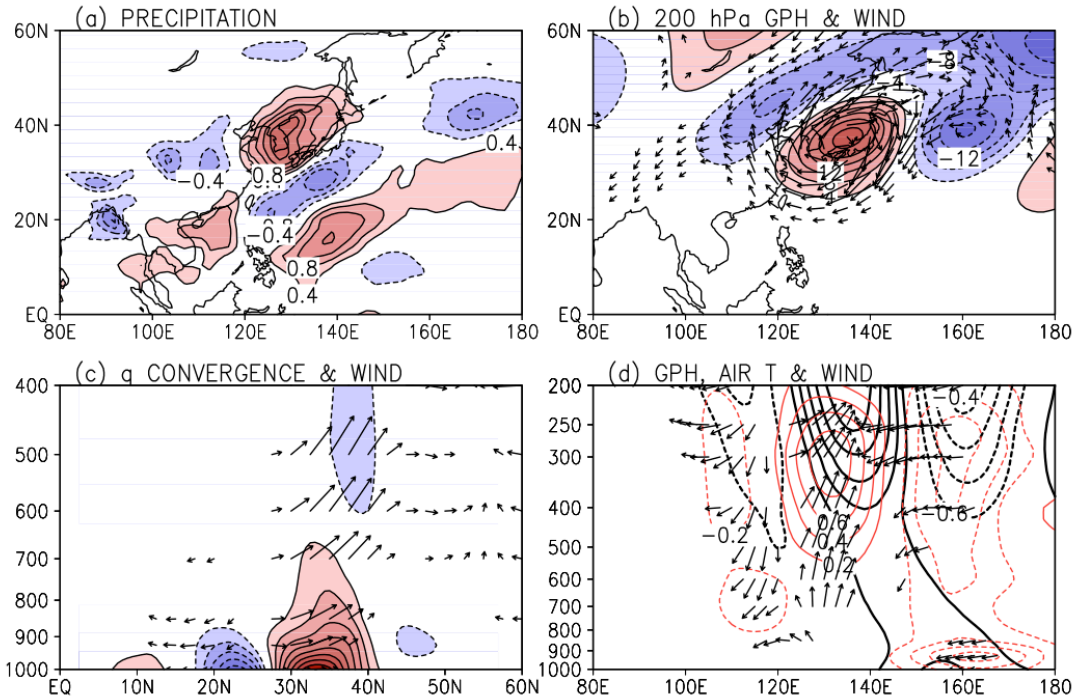

Figure 3.10. Positive composite of 10-day high-pass filtered anomalies of physical variables: (a) precipitation rate (0.4 mm/day); (b) 200 hPa GPH (4 m contours) and wind > 1 m/sec; (c) moisture convergence (4×10^{-9} kg/kg/sec) and wind (v, $-\Omega$) along 127.5°E-130°E; and (d) GPH (4 m; heavy contours), temperature (0.2 °K; light contours) and wind (u, $-\Omega$) along 35°N-40°N. The vertical velocity, $-\Omega$ (Pa/sec), has been exaggerated by multiplying 100.

3.2. Decadal change of seasonal component in the seasonal cycle

Though the trends are not set to the exact quantitatively, consistent and comprehensive evidences for the increasing trends of extreme weather, such as maximum precipitation, has been observed over the last several decades in many regions, including South Korea (Karl and Knight, 1998; Easterling et al., 2000; Haylock and Nicholls, 2000; Solomon et al., 2007). Increases in the magnitude and frequency of heavy rainfall are some of the potential consequences related to climate change (Easterling et al., 2000; Houghton et al., 2001; Chu and Zhao, 2004; Min and Hense, 2006, 2007; Khaliq et al., 2007). Consequentially, heavy rainfall events, one of typical extreme weather, have drawn increased attention in recent decades because of the huge potential power for the loss of life and property (Iwashima and Yamamoto 1993; Haylock and Nicholls, 2000; Meehl et al., 2000; Roy and Balling, 2004; Zhai et al., 2005). Many studies have been performed on the trends or change point of extreme (heavy) precipitation related to climate change (Meehl et al., 2000; Groisman et al., 2001; Booij, 2002). The detailed descriptions of decadal change in the physical mechanism of summertime precipitation variability in Korea in the seasonal cycle are described. The description of change point of decadal change for summertime precipitation variability in South Korea is first given. Then, changes of physical structures related to the decadal change of summertime

precipitation variability in the seasonal cycle are represented for three distinct components; Seasonal, Sub-seasonal, and High-frequency component. At the end, summertime precipitation variability related to localized heavy rainfall, which is explained in the second and the third CSEOF modes, is described.

3.2.1. Change point of daily precipitation over South Korea

In order to investigate the existence of a change point in the area-averaged annual maximum precipitation using Bayesian change-point analysis during a 30-year period (1976-2005) over South Korea (Kim et al., 2009). Bayesian model was selected and estimated for three types of univariate normal models with a no-change model, a mean change model, and mean and variance changes model. The Bayesian method detects a change point at an unknown time point in the time series of the area-averaged annual maximum precipitation by independent normal random variables. Using non-informative priors, Bayesian model selection is performed by posterior probability through the Bayes factor, and the exact Bayes estimators of the parameters and unknown change point for the selected change model are obtained. A single change occurred around 1997 in the area-averaged annual maximum precipitation without regard to the accumulated time periods over South Korea. This is strongly consistent with the abrupt increases in the intensity and frequency of heavy precipitation after 1997 (Kim et al., 2009). Meanwhile, the multiple

change-point and change pattern in the 54-years (1954-2007) time series of the annual and the heavy precipitation characteristics, such as amount, days and intensity, averaged over South Korea was examined (Kim and Suh, 2009). Using a Bayesian approach, mean and variance changes in a sequence of independent univariate normal observation were detected. Using non-informative priors for the parameters, the Bayesian model selection is performed by the posterior probability through the intrinsic Bayes factor. In order to investigate the significance of the changes in the precipitation characteristics between before and after the change-point, the posterior probability and 90% highest posterior density credible intervals are examined. The heavy rainfall days and amounts changed around 1996 or 1997 by a statistical significant single change. The heavy rainfall amount and days have increased after the change-point (Kim and Suh, 2009). Therefore, on considering previous results, the change point in decadal change of summertime precipitation is selected at 1996 in this study.

3.2.2. Decadal change of summertime precipitation in South Korea

As shown in section 2.1, daily precipitation data observed in 61 KMA stations are also used. The method of investigation of precipitation variability is the same way to the previous section 2.2, too. Figure 3.11 shows the first CSEOF of the summertime precipitations at the 61 KMA stations in Korea in the entire years, in 1979-1995 years, and in 1996-2008 years. All solid lines are the

precipitation averaged over the 61 KMA stations (Figures 3.11a, 3.11b, and 3.11c). The first CSEOF in the entire years was described in previous section 3.1. Figures 3.11b and 3.11c show the first CSEOFs of summertime precipitations during the PRE and the POS years respectively and explain ~18% and ~20% of the total variability, respectively (Table 2.2). Likewise in the TOT years, the seasonal cycle explains ~88% of the total magnitude of precipitation in PRE years, and ~90% of the total precipitation amounts in POS years. The amplitude of the seasonal cycle fluctuate annually around 7.77 mm/day and 8.66 mm/day with the standard deviation of 2.93 and 3.93 in the PRE and the POS years, respectively. It can be explained that the difference of the periods between PRE years and POS years. However, increased standard deviation in POS years is seem that heavy rainfall events had been increased in recent decade. The concept of increased standard deviation is well corresponded to the recent trends of increased extreme rainfalls and strong heat waves in the middle latitude (Karl and Knight, 1998; Easterling et al., 2000; Haylock and Nicholls, 2000; Solomon et al., 2007).

The PC time series shows a fairly well defined periodicity at 2~3 years (Fig. 3.11d). A biennial component of variability is clearly seen in the precipitation record over India (Meehl and Arblaster, 2001), but 2-year periodicity is not clearly seen in the precipitation record in Korea, too.

Table 2.2. Variance of the top five CSEOF modes of summertime precipitations at 61 KMA stations in South Korea in the entire record, and in PRE and POS years.

	Variance (%)				
Mode number	1	2	3	4	5
PRCP in entire record	15.7	7.0	5.6	5.1	4.9
PRCP in PRE years	18.0	10.5	8.3	7.7	7.3
PRCP in POS years	19.9	14.0	9.7	9.4	8.8

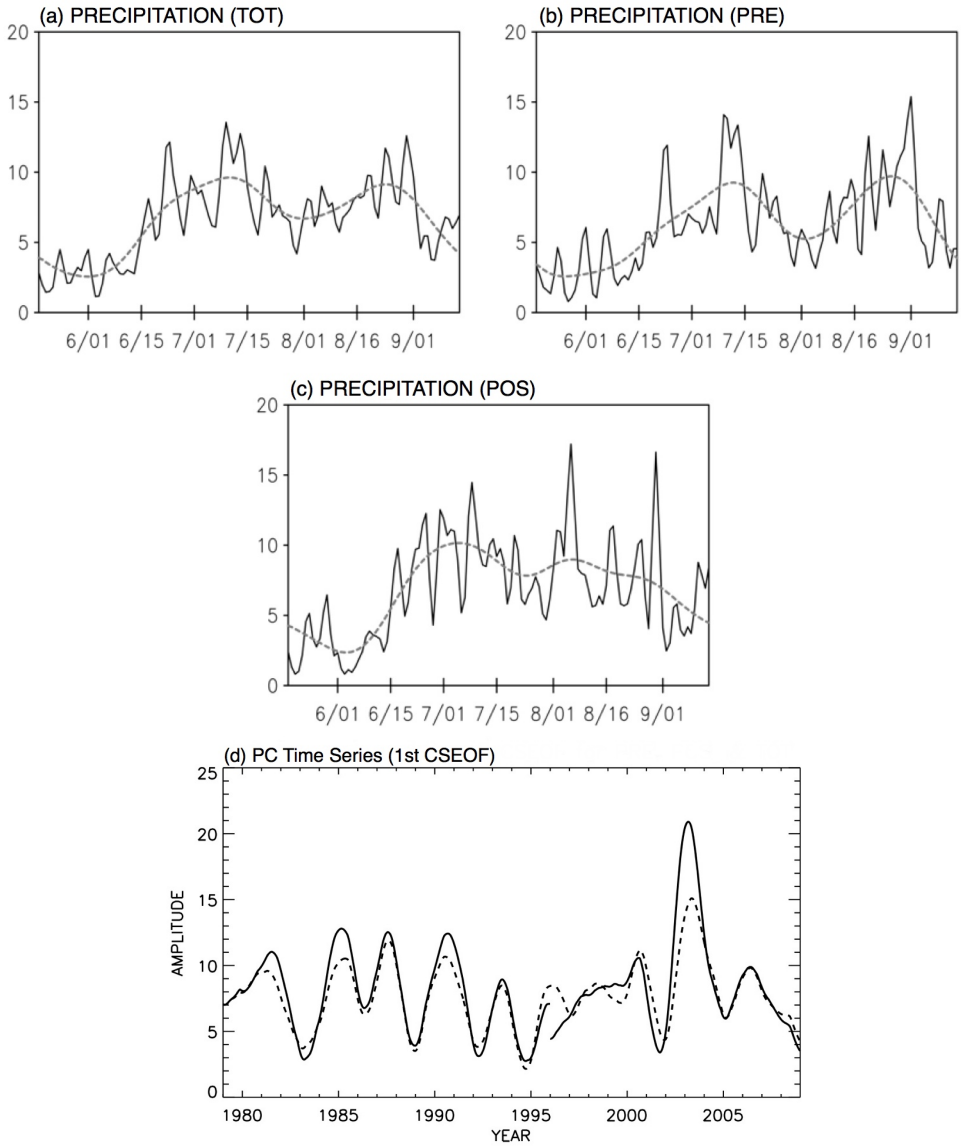

Figure 3.11. The first CSEOF of summertime precipitations at 61 KMA stations in Korea: precipitation in mm/day averaged over all 61 stations (solid) and the seasonal evolution (dotted) after removing high-frequency (<10 days) and sub-seasonal (10-30 days) components of variability; (a), (b), and (c) of panels represent in total (TOT), PRE, and POS years, respectively; (d) PC times series for TOT (dotted), PRE (solid), and POS (solid) years.

Three distinct physical mechanisms associated with the seasonal cycle of Korean summertime precipitation variability (Kim et al., 2010) were shown in chapter 3.1. The 10-30 day sub-seasonal component of variability was obtained via band-pass filtering (Newton, 1988) with periods of 10-30 days. Similarly, high-frequency components of variability with periods shorter than 10 days were derived via high-pass filtering with a cut-off period of 10 days. The seasonal component of variability on time scales greater than 30-days was obtained by removing the sub-seasonal and the high-frequency components of variability from the seasonal cycle. Recent changes in the physical mechanisms of the seasonal cycle of precipitation will be addressed in terms of the three components of variability. It should be noted that this study investigates the sub-seasonal and the high-frequency components of variability associated with the seasonal cycle.

The dotted curves in Fig. 3.11 represent the seasonal evolution of the seasonal cycle in summertime precipitations in Korea after removing the sub-seasonal and high-frequency components of variability with time scales shorter than 30 days (hereafter seasonal component). The three figures represent TOT (1979-2008), PRE (1979-1995), and POS (1996-2008) observational records, respectively. The seasonal component of summertime precipitation variability based on the entire record is characterized by two main peaks in the first half of July and in the second half of August separated by a period of weakened

precipitation; the seasonal evolution in Figure 3.11a clearly exhibits the bimodal structure (Qian et al., 2002; Chen et al., 2003; Lee et al., 2010; Ho and Kang, 1988). The first precipitation spell is called Changma in Korea, and is also called Baiu in Japan and Mei-Yu in China. The second spell of precipitation is called the second Changma or post-Changma in Korea (Lim et al., 2002). Climatologically, the primary rainy period in Korea commences in late June in association with the eastward movement of the Tibetan High and the westward movement of the North Pacific High toward East Asia forming a monsoon trough over the Korean peninsula (Kang et al., 1999). As the monsoon trough moves further north to the northeast of Asia, the period of weakened precipitation develops over the Korean peninsula in early August. In late August, when the monsoon trough retreats southward to the Korean peninsula, the second Changma starts.

While the seasonal component of summer precipitation in Korea, based on the PRE record, exhibits the typical bimodal characteristics of summer precipitation, the seasonal evolution based on the POS record is different from that based on the PRE record. A comparison between PRE (Figure 3.11b) and POS (Figure 3.11c) data shows that the first spell of precipitation, which typically lasts from July 1 through July 20, appeared earlier in recent records and has increased significantly. The magnitude of the station-averaged precipitation, on average, has increased from 163 mm to 213 mm during the 20-

day (July 1-20) period, which is a 30% increase. The second peak has broadened significantly without a well-developed period of decreased precipitation. The PC time series in Figure 3.11d give an impression that the year 2003 may have caused the difference between the PRE record and the POS record shown in Figures 3.11b and 3.11c. CSEOF analysis on the POS records without the year 2003 results in the seasonal component (figure not shown), which is very similar to Figure 3.13; this confirms that the substantial difference between the PRE and the POS records is not due to the year 2003. In fact, a super typhoon "Maemi" in 2003 caused heavy precipitation in Korea. The direct and indirect influences of typhoons were separated mainly as the second and third modes; the seasonal cycle was not seriously contaminated by the typhoons particularly in 2003. Also, in a climatological sense, atmosphere is conditionally unstable throughout summer, as seen in the vertical structure of equivalent potential temperature (figure 3.12). As shown in Figure 3.12, low-level equivalent potential temperature in POS years much stronger than that in PRE years. The vertical gradient of equivalent potential temperature from 1000 hPa to 600 hPa, which is the minimum equivalent potential temperature vertically, is much increased in POS years, too. The increase of vertical gradient of equivalent potential temperature is one of the most important causes in heavy precipitation in Korea.

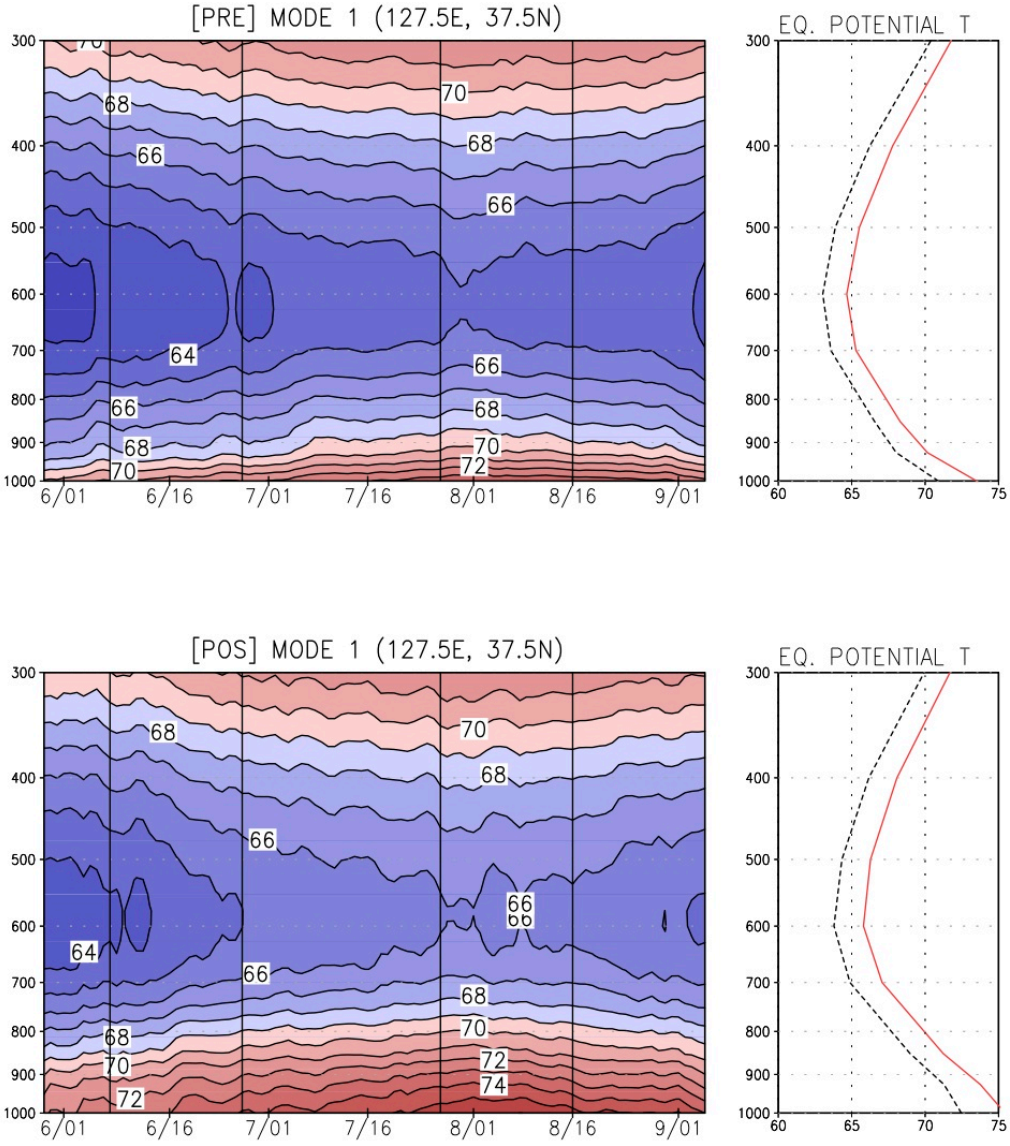

Figure 3.12. 300-100 hPa Vertical structures (Left two panels) of equivalent potential temperature evolution and the soundings (right two panels) in July 1 and August 1 in PRE years (upper panels) and in POS years (bottom panels). All values of equivalent potential temperature are indicated minus 273°

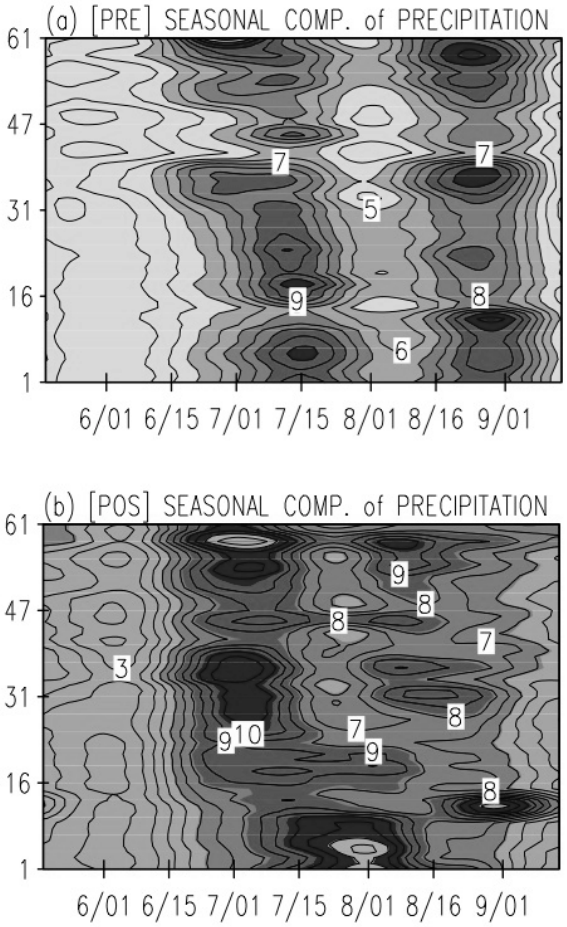

Figure 3.13. The seasonal component of summertime precipitation variability at each of the 61 KMA stations (y-axis) in South Korea for (a) PRE years and (b) POS years (contour intervals in unit, mm/day)

To investigate the spatial pattern of the decadal change, the seasonal components of summertime precipitation at 61 KMA stations in Korea (dotted lines in Figure 3.11) for PRE and POS years are shown in Figure 3.13. While the bimodal structure is clearly observed at most stations in PRE years (Figure 3.13a), it is not apparent at stations 1-25 in POS years (Figure 3.13b); these stations are located in the northern part of South Korea to the north of ~37°N and the western part to the north of ~36°N (see Figure 2.1). Excluding stations 11-14 with mountainous geographical characteristics, the seasonal components of precipitation in POS years (solid line) and in PRE years (dotted line) were compared between stations 1-25 and stations 26-61 in Figure 3.14. In the far-northern and the mid-western parts of South Korea, the seasonal component of summertime precipitation has only one peak in early August in POS years, while the bimodal structure is apparent in PRE years. By contrast, in the southern part of South Korea, the bimodal structures of precipitation are observed in both PRE and POS years, although the peaks appear earlier in POS years. Additionally, the first peak tends to be stronger in POS years.

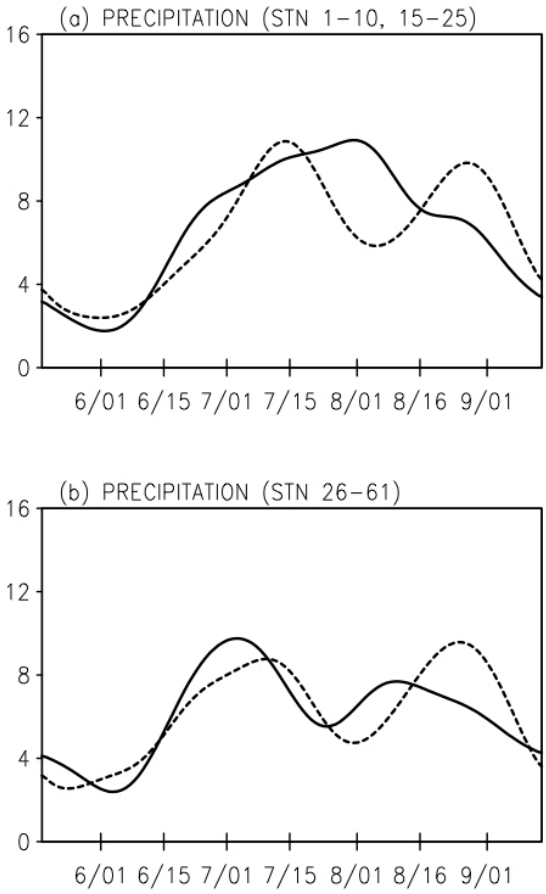

Figure 3.14. The seasonal component of summertime precipitations averaged over KMA stations 1-10 and 16-25, and stations 26-61 in Korea: averaged precipitation (dotted: PRE years; solid: POS years) in mm/day.

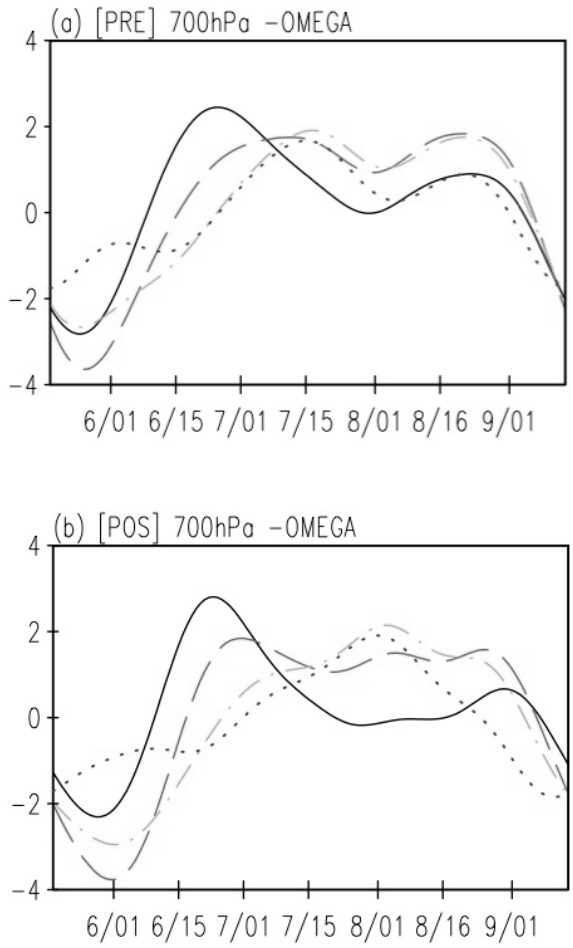

Figure 3.15. The seasonal component of the zonal-averaged (125°-130°E) evolution of the 700 hPa vertical velocity (interval: 1×10^{-2} Pa/sec) at 32.5°N (solid), 35°N (dashed), 37.5°N (dash-dotted), and 40°N (dotted).

Figure 3.15 shows the zonal-averaged (125°-130°E) evolution of the 700-hPa vertical velocities at four different latitudes (32.5°-40°N at 2.5° interval) in the seasonal component. The evolution of vertical velocity in the seasonal component depicts two peaks in PRE years, although the timings of the maxima differ with latitude; this evolution is associated with the migration of the monsoon precipitation band (Lim et al., 2002; Qian et al., 2002; Qian and Lee, 2000; Lau et al., 1988). However, the bimodal patterns are not clearly observed in the seasonal evolutions of the 700-hPa vertical velocities except at 32.5°N (solid line) in POS years. The maximum peak of the seasonal evolution of the 700-hPa vertical velocity appears in early August to the north of ~37°N in POS years.

3.2.3. Physical mechanism of the first spell of precipitation

To understand the detailed decadal change of the Korean summertime precipitation, physical patterns are shown for the first spell of precipitation (Figure 3.16), the period of decreased precipitation (Figure 3.17), and the second spell of precipitation (Figure 3.18), which represent the three important periods of summertime precipitation variability in Korea. Comparisons of the physical conditions associated with the seasonal component between the PRE and the POS records were done on specific calendar days so that difference in the days of comparison does not obscure true physical differences in the seasonal cycle;

insolation, a major driving force for the monsoon system, is virtually phase locked and the physical conditions in the ocean and the atmosphere vary with time.

Figure 3.16 (in PRE years) and Figure 3.17 (in POS years) shows the patterns of the physical conditions on July 1, which marks the peak stage of the first spell of precipitation in the seasonal component in POS years. In Figures 3.16a and Figure 3.17a, low-level moisture convergence/divergence around the Korean Peninsula in POS years is much stronger than in PRE years. The location of the moisture convergence band over the Korean Peninsula in POS years is shifted slightly northward relative to that in PRE years. This is consistent with the observation that the first peak of precipitation appears earlier and has increased in intensity in recent years. A stronger moisture convergence in POS years can be explained in terms of the change in the low-level circulation and the resulting moisture transport (Figures 3.16c and Figure 3.17c). A stronger pressure contrast between the Asian continent and the ocean induces stronger southwesterly anomalies along the eastern side of the Asian continent, which, in turn, increases moisture convergence over the East Asian countries; warm advection and moisture convergence over Korea by the southwesterly anomaly are regarded as the typical pattern of the East Asian summer monsoon front. The fact that the positive 850-hPa GPH anomaly to the

south of Korea is relatively closer to Korea in POS years explains the observation that the first Changma starts earlier in POS years.

Meanwhile, patterns of 500-hPa GPH and wind in PRE and POS years are similar to each other as shown in Figures 3.16b and Figure 3.17b. The meridional pressure gradient over the Korean peninsula, however, is stronger in PRE years; increased baroclinic instability associated with a stronger 500-hPa GPH gradient over Korea in PRE years leads to a stronger upward motion. Relatively strong upward motion over Korea is clearly observed at approximately 500 hPa in the meridional vertical section (Figures 3.16d and Figure 3.17b). Despite slightly decreased upper-level upward motion over Korea in POS years, relatively strong low-level convergence suggests increased precipitation in POS years.

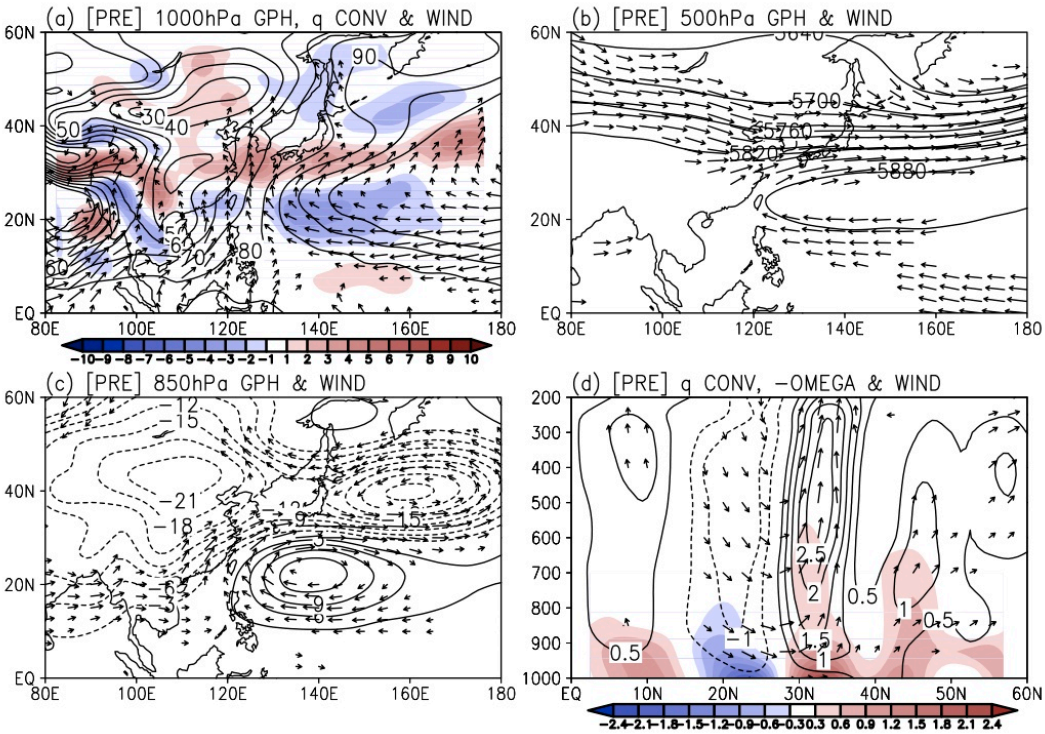

Figure 3.16. July 1 patterns of the seasonal evolution in PRE years in (a) 1000-850 hPa moisture convergence (shaded at 1×10^{-8} kg/kg/sec intervals) and 1000-hPa GPH (contoured at 10 gpm interval) and wind > 2 m/sec, (b) 500-hPa GPH (contoured at 60 gpm interval) and wind > 2 m/sec (vector), (c) 850-hPa GPH (contoured at 3 gpm) and wind anomalies > 1 m/sec (vector), and (d) vertical meridional section of moisture convergence (shaded at 1×10^{-8} kg/kg/sec intervals), vertical velocity anomalies (contoured at 1×10^{-2} Pa/sec) and wind anomalies > 1 m/sec along averaged 125°-130°E. The vertical component of wind has been amplified by a factor of 100.

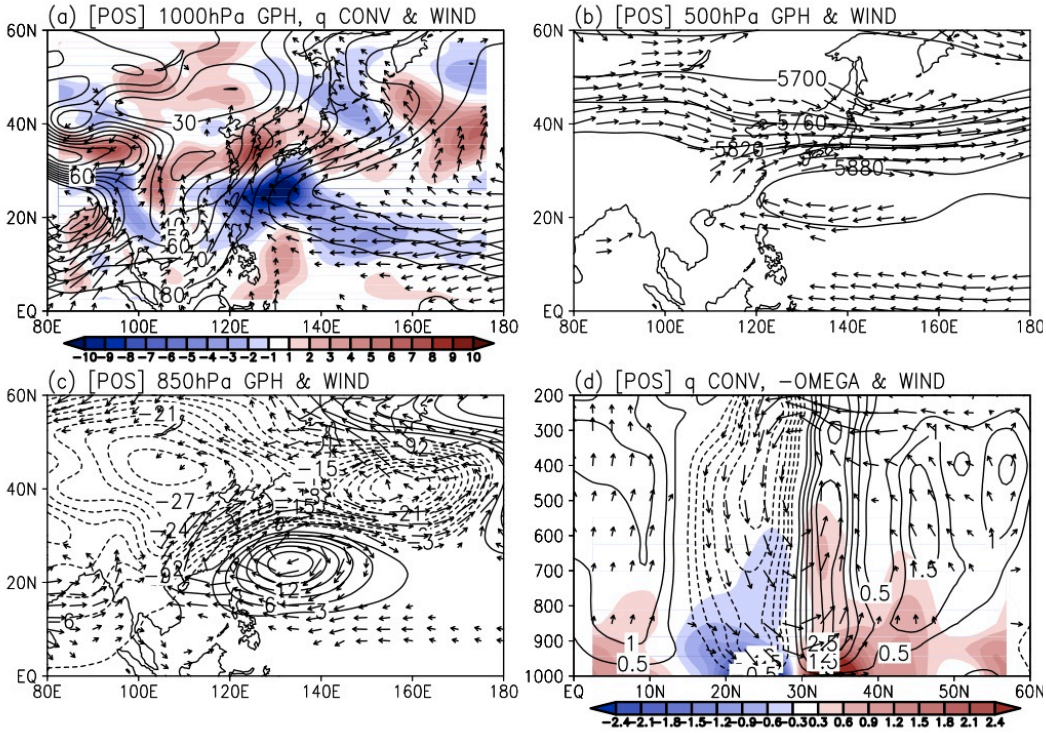

Figure 3.17. July 1 patterns of the seasonal evolution in POS years in (a) 1000-850 hPa moisture convergence (shaded at 1×10^{-8} kg/kg/sec intervals) and 1000-hPa GPH (contoured at 10 gpm interval) and wind > 2 m/sec, (b) 500-hPa GPH (contoured at 60 gpm interval) and wind > 2 m/sec (vector), (c) 850-hPa GPH (contoured at 3 gpm) and wind anomalies > 1 m/sec (vector), and (d) vertical meridional section of moisture convergence (shaded at 1×10^{-8} kg/kg/sec intervals), vertical velocity anomalies (contoured at 1×10^{-2} Pa/sec) and wind anomalies > 1 m/sec along averaged 125°-130°E. The vertical component of wind has been amplified by a factor of 100.

3.2.4. Physical mechanism of the decreased period of precipitation

A remarkable change in physical structures associated with the seasonal component of precipitation is also observed in early August. Figures 3.18 represents the August 1 physical condition during the period of decreased precipitation in PRE years, whereas Figures 3.19 describes the physical condition on the same day in POS years. The pressure gradient between the Asian continent and the surrounding oceans is no longer strong enough to support the southwesterly anomalies along the east coast of the Asian continent. Instead, low-level (925 hPa) easterly and southeasterly anomalies develop in conjunction with the positive GPH anomalies to the east of Korea and negative GPH anomalies to the south of Korea (Figures 3.18a and Figure 3.19a). In POS years, the positive GPH anomaly to the east of Korea was located closer to the Korean Peninsula; as a result, stronger southerly anomalies were induced toward the Korean peninsula than in PRE years. Increased warm advection and moisture advection toward Korea by the stronger low-level southerly anomaly (comparison between Figure 3.18a and Figure 3.19a) enhances convective instability of the atmosphere in POS years as a comparison between Figures 3.18d and Figure 3.19d shows.

Figures 3.18c and Figure 3.19c show a zonal band of 500-hPa positive vertical velocity anomalies at ~15°N, a band of negative vertical velocity

anomalies at ~25°N, and a band of positive vertical velocity anomalies at ~35°N; these are aligned in the meridional direction in the zonal band of 110°-130°E. It appears that an enhanced upward motion in the tropics (~10°-15°N) produced by strong convective instability induces upper-level divergence and low-level convergence. As a result, a downward motion is induced in the subtropics (~20°-25°N) with upper-level convergence and lower-level divergence. Nitta (1987), in his observational study, showed that an anticyclonic circulation associated with strong convective motions in low latitudes (~15°-20°N) of the western Pacific is highly correlated with a circulation of opposite sign to the north. Then, an upward motion is induced in the mid-latitudes (~30°-35°N). In this way, meridionally oscillating patterns of 500-hPa vertical velocities appear over the western North Pacific (Figure 3.18c and Figure 3.19c). Similarly, oscillating patterns of relative vorticity anomalies in the meridional direction are observed at 500 hPa (Figure 3.18b and Figure 3.19b). The centers of these oscillation patterns are located closer to the Asian continent in POS years than in PRE years (Figures 3.18b-c and Figures 3.19b-c). As a result, stronger negative relative vorticity and positive vertical velocity anomalies are observed over Korea in POS years than in PRE years (Figures 3.18b, 3.18d, Figures 3.19b, and 3.19d). In addition, Korea is located at the rear right of the entrance region of the upper-level jet (Figures 3.18b and 3.19b). Korea is closer to the entrance region of the jet in POS years, which suggests that upper-level divergence

becomes stronger in POS years (Bluestein, 1993; Keyser and Shapiro, 1986). The role of the secondary circulation around the upper level jet in regard to summertime heavy rainfall in Korea has been studied in many case studies (Lee et al., 2008; Lee et al., 1998). Thus, relatively active convective motions are observed over Korea in POS years due to stronger low-level south wind anomalies, more active convective motion in the tropics, and the enhanced secondary circulation near the entrance of the upper-level jet. For these reasons, a period of decreased precipitation is not clearly observed in POS years.

3.2.5. Physical mechanism of the second spell of precipitation

Figure 3.20 and Figure 3.21 show the physical patterns on August 26 in PRE years and in POS years; this figure represents the period of the second rainy spell caused by the reversal of the pressure gradient between the continent and the ocean (Lim et al., 2002). A positive 925-hPa GPH anomaly is observed over the Asian continent and a negative GPH anomaly is observed over the southwestern North Pacific (Figures 3.20a and 3.21a), resulting in a strong pressure gradient between the two. Despite a weaker pressure gradient at 925 hPa, the easterly anomaly over Korea is stronger in PRE years. The location of a negative GPH anomaly is partly responsible for stronger easterly anomaly in PRE years. Specifically, the center of positive vertical velocity in the tropics (~15°-20°N) is located at ~130°E in PRE years (Figure 3.20c) whereas it is

located at ~140°E in POS years (Figure 3.21c); as a result of this locational difference, stronger vertical velocity is induced over Korea in PRE years, as shown in the meridional vertical cross section (Figures 3.20d and 3.21d). In addition, the upper-level jet over Korea in PRE years is also stronger, inducing stronger upper-level divergence than in POS years. These physical conditions on August 26 explain the clear second spell of precipitation in PRE years, while the second spell of precipitation in recent years is broader and weaker, as a comparison between Figures 3.1b and 3.1c shows.

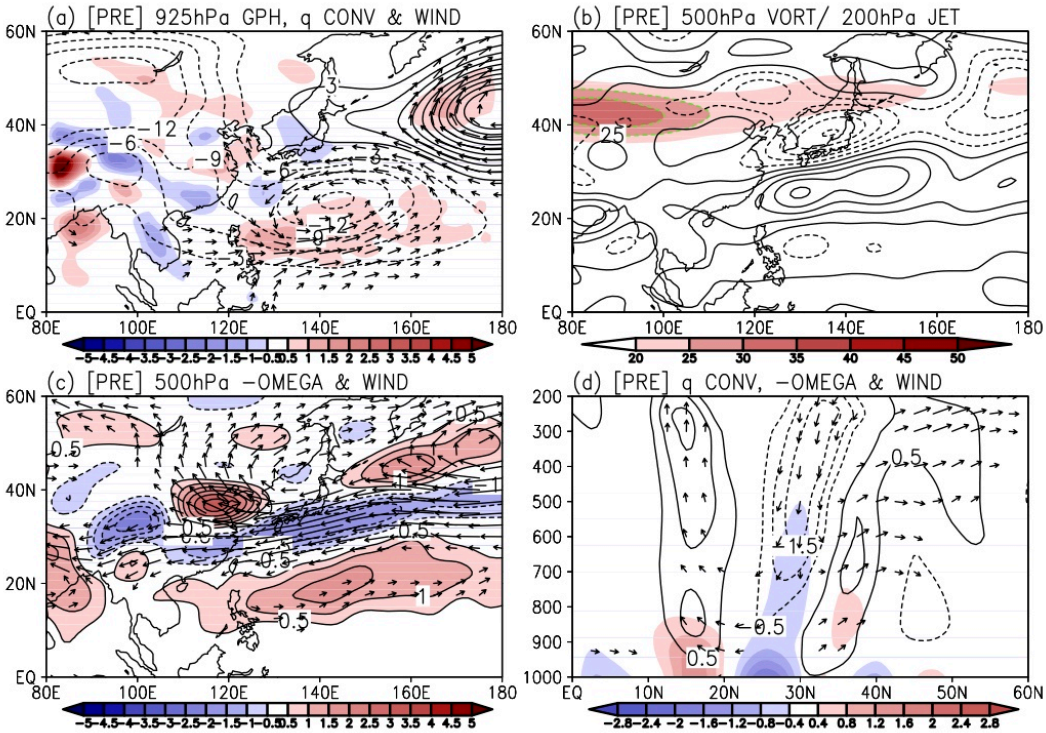

Figure 3.18. August 1 patterns of the seasonal evolution in PRE years of (a) 925-hPa moisture convergence (shaded at 1×10^{-8} kg/kg/sec intervals) and GPH anomalies (contoured at 3 gpm interval) and wind anomalies > 1 m/sec, (b) 500-hPa relative vorticity anomalies (contoured at 1×10^{-5} sec^{-1} interval) and 200-hPa zonal wind ≥ 25 m/sec (shaded at 5 m/sec intervals), (c) 500-hPa vertical velocity anomalies (contoured at 1×10^{-2} Pa/sec) and wind anomalies > 1 m/sec (vector), and (d) vertical meridional section of moisture convergence (shaded at 1×10^{-8} kg/kg/sec), vertical velocity anomalies (contoured at 1×10^{-2} Pa/sec) and wind anomalies > 1 m/sec along 125°-130°E. The vertical components of wind have been scaled up by a factor of 100.

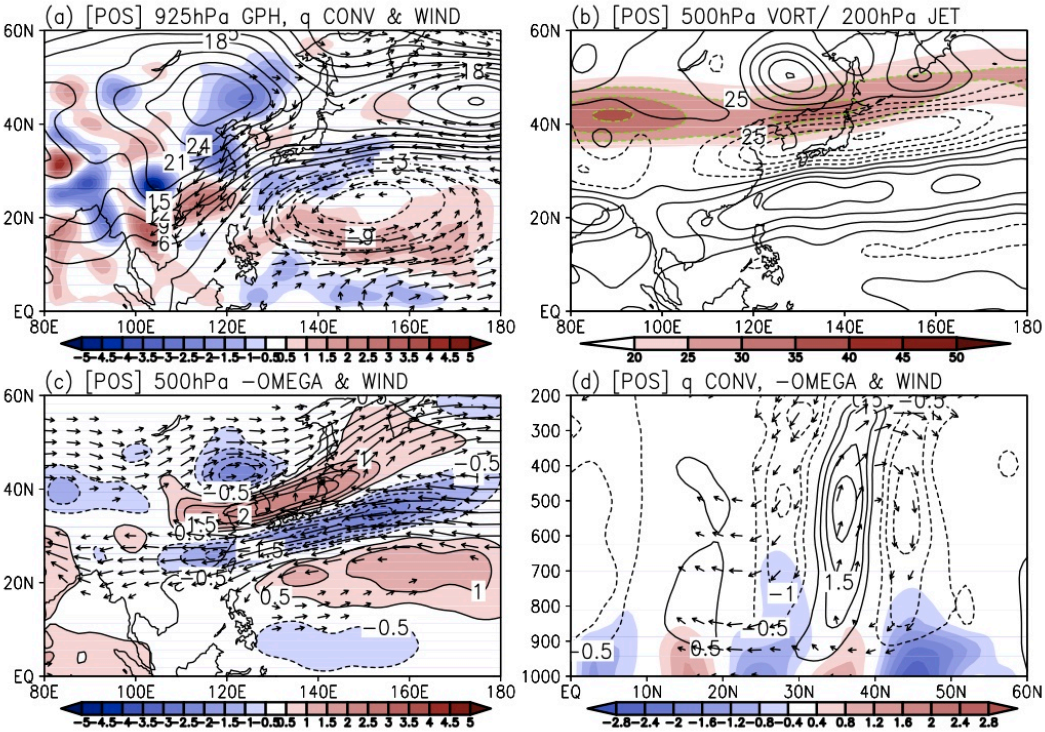

Figure 3.19. August 1 patterns of the seasonal evolution in POS years of (a) 925-hPa moisture convergence (shaded at 1×10^{-8} kg/kg/sec intervals) and GPH anomalies (contoured at 3 gpm interval) and wind anomalies > 1 m/sec, (b) 500-hPa relative vorticity anomalies (contoured at 1×10^{-5} sec^{-1} interval) and 200-hPa zonal wind ≥ 25 m/sec (shaded at 5 m/sec intervals), (c) 500-hPa vertical velocity anomalies (contoured at 1×10^{-2} Pa/sec) and wind anomalies > 1 m/sec (vector), and (d) vertical meridional section of moisture convergence (shaded at 1×10^{-8} kg/kg/sec), vertical velocity anomalies (contoured at 1×10^{-2} Pa/sec) and wind anomalies > 1 m/sec along 125°-130°E. The vertical components of wind have been scaled up by a factor of 100.

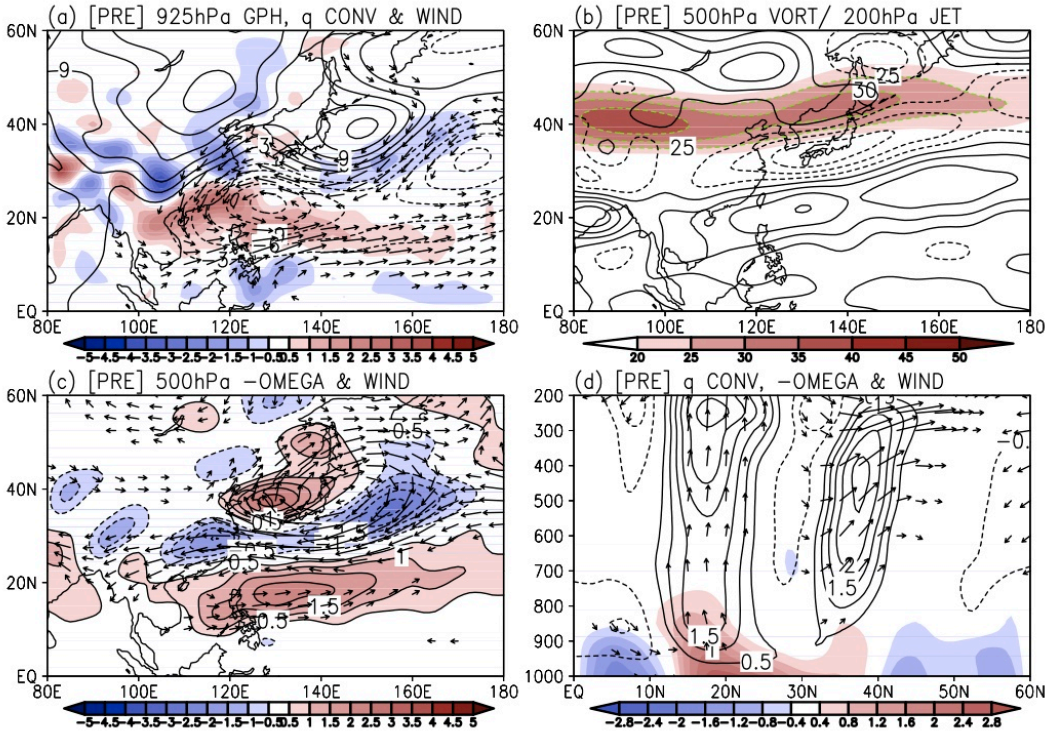

Figure 3.20. Same as Figure 3.18 except for August 26.

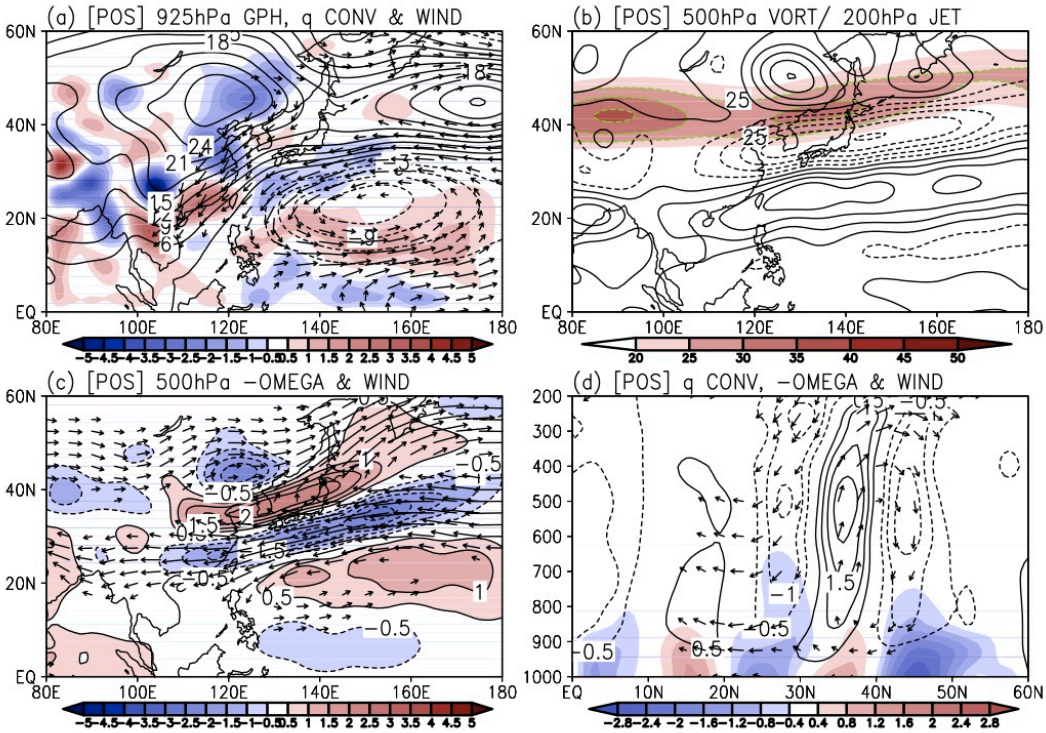

Figure 3.21. Same as Figure 3.19 except for August 26.

Figure 3.22 shows the zonal-averaged (125°-130°E) evolutions of the 500-hPa vertical velocity in the seasonal component. The positive 500-hPa vertical velocity anomaly in POS years migrates from ~27°N in early June to ~32°N in early July, which corresponds to the initiation of the first Changma in Korea. In POS years, the positive vertical velocity anomaly arrives in Korea earlier and the strength is greater than in PRE years. Compared with the PRE years, this frontal band has also broadened in August without a significant weakening, particularly in the northern part of Korea. As mentioned above, bands of vertical velocity anomalies with alternating signs are observed in the meridional direction. A north-south pair of positive vertical velocity anomalies separated by a negative velocity anomaly is clearly observed from early August to late August in PRE years and from mid-July to mid-August in POS years. In fact, the 500-hPa positive vertical velocity anomaly at (127.5°E, 35°N) is positively correlated at over 0.8 with a low-latitudinal counterpart at (125°E, 10-15°N) during the period of active convections (July 16 to August 15) in POS years. In PRE years, this correlation is over 0.9 during the period of August 1 to August 31. Thus, the climatological variation of the seasonal component of summertime precipitation variability in Korea appears to be correlated with the tropical variability of convection.

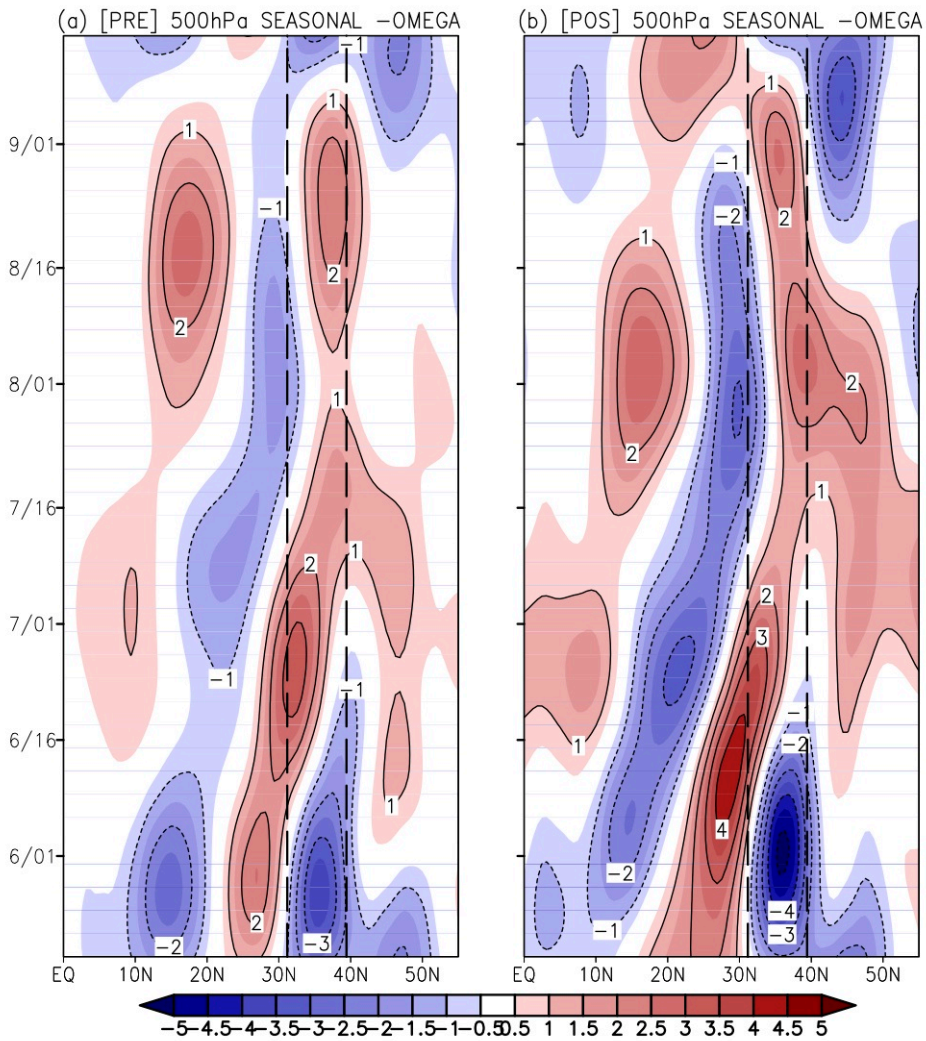

Figure 3.22. The seasonal component of the zonal-averaged (125°-130°E) evolution of the 500-hPa vertical velocity (interval: 1×10^{-2} Pa/sec). The two vertical dashed lines denote the meridional extent of the 61 KMA stations.

3.3. Decadal change of sub-seasonal component of the seasonal cycle

Figure 3.23 and Figure 3.24 represents the 10-30-day band-pass filtered and zonally averaged (127.5°-130°E) precipitation and low-level moisture convergence anomalies from the seasonal cycle in PRE years and in POS years. The sub-seasonal component of the seasonal cycle of Korean summertime precipitation variability based on the measurements at 61 KMA stations is reasonably similar to that derived from the NCEP/NCAR reanalysis data; the sub-seasonal component of the NCEP/NCAR precipitation averaged within the two vertical dotted lines (Figure 3.23a and Figure 3.24a) is correlated with coefficients of 0.61 and 0.81 with that of the KMA precipitation in PRE years and in POS years (Figure 3.23b and Figure 3.23b), respectively. Anomalies with alternating signs appear to propagate northward with an averaged period of ~15 days in PRE years and ~13 days in POS years (e.g., Wang et al., 2007). It should be noted, however, that the impact of these seemingly northward propagating oscillations is limited to the southern part of South Korea (Figure 3.23 and Figure 3.24). In the other hand, in the period of strong activity of sub-seasonal precipitation, northward propagation oscillation was seen in both figures 3.23 and 3.24.

Sub-seasonal oscillations of precipitation and moisture convergence are not conspicuous throughout the entire 120-day period. In PRE years, sub-seasonal oscillations between approximately 10°N and 30°N are not clearly observed, except for from late August through early September. Instead, seemingly southward propagation from ~40°N to ~30°N appears in mid-July, which is the period of relatively active sub-seasonal precipitation in Korea in PRE years. Sub-seasonal oscillations are active from mid-July to mid-August in POS years; the magnitudes of the precipitation and the low-level moisture convergence in the Asian domain are almost doubled in POS years compared with PRE years.

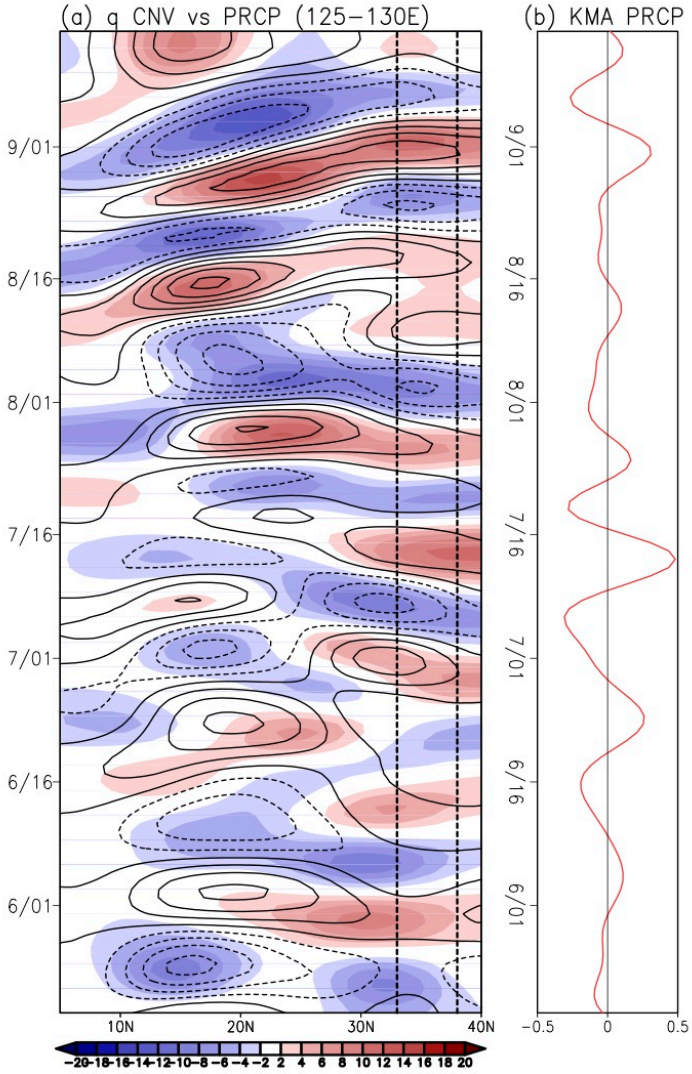

Figure 3.23. (a): Sub-seasonal (10-30 day) component of precipitation (contours: 0.3 mm/day) and low-level (1000-850 hPa) moisture convergence (shade: 1×10^{-9} kg/kg/sec) anomalies along 125°-130°E in the seasonal cycle, and (b): sub-seasonal component of precipitation (mm/day) in Korea averaged over the 61 KMA stations in PRE years. The two vertical dotted lines in (a) denote the meridional extent of the 61 KMA stations.

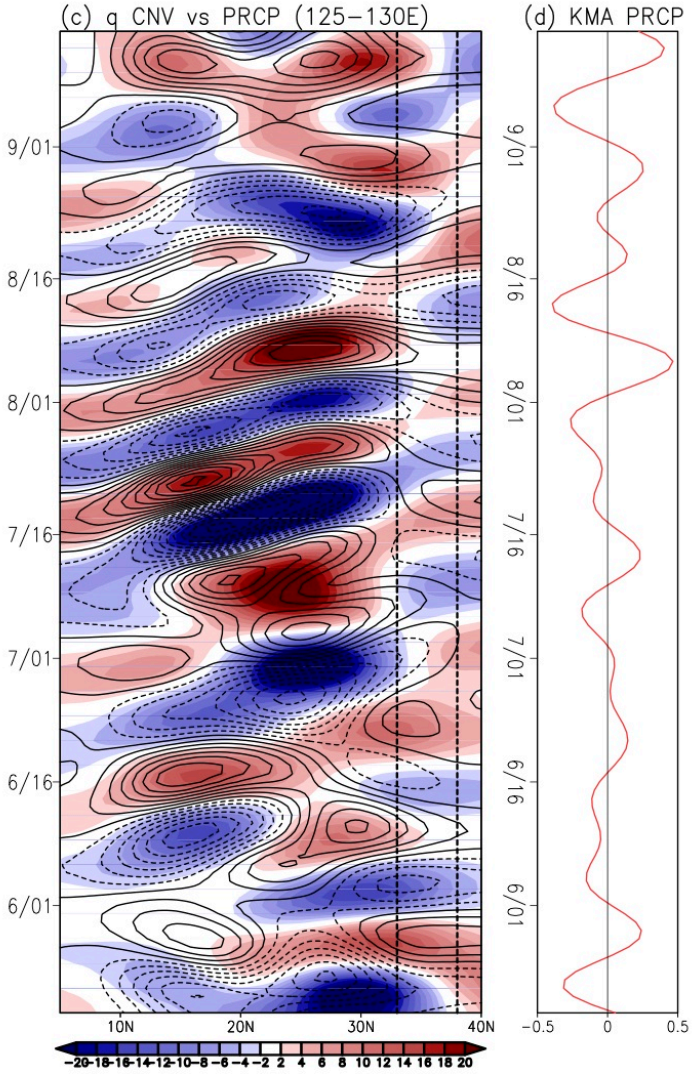

Figure 3.24. Same as Figure 3.23 except for POS years.

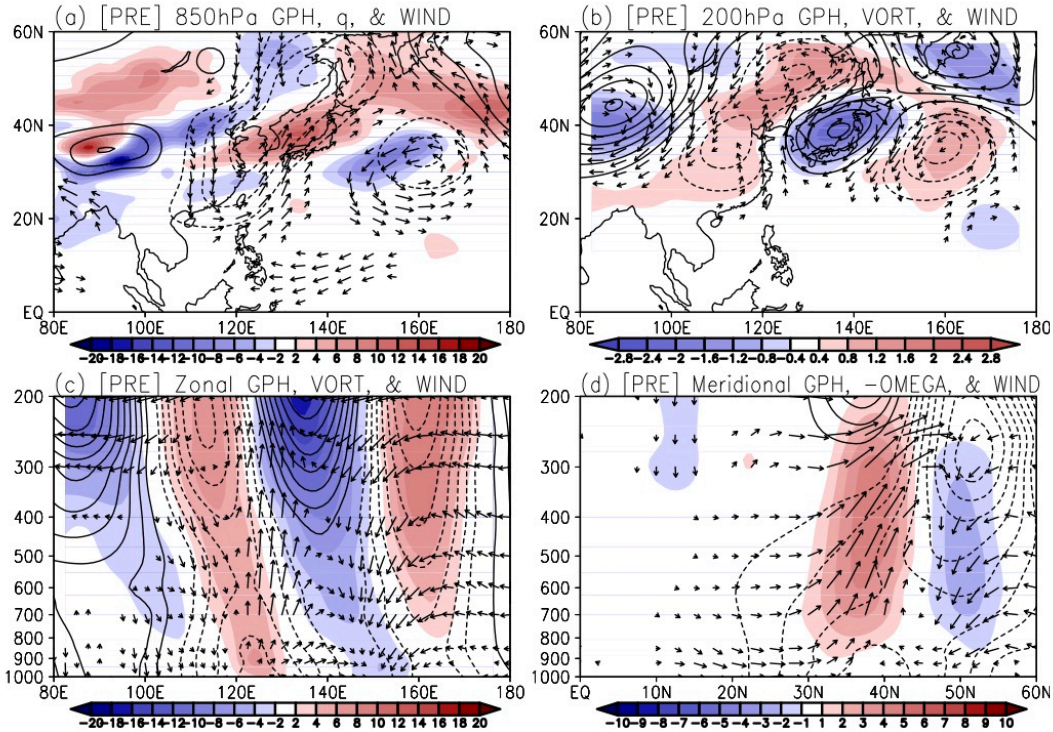

Figure 3.25. Positive composite of the sub-seasonal component of variability in PRE years: (a) 850-hPa GPH (contour: 5 gpm), specific humidity (shade: 1×10^{-4} kg/kg/sec), and wind > 0.5 m/sec; (b) 200-hPa GPH (contour: 10 gpm), relative vorticity (shade: 1×10^{-5} sec^{-1}), and wind > 2 m/sec; (c) zonal cross section of GPH (contour: 4 gpm), relative vorticity (shade: 1×10^{-6} sec^{-1}), and wind (u, $-\Omega$) > 0.5 m/s along the 32.5°-40°N band; (d) meridional cross section of GPH (contour: 4 gpm), vertical velocity anomalies (shade: 1×10^{-2} Pa/sec), and wind (v, $-\Omega$) > 0.5 m/s along the 122.5°-130°E band.

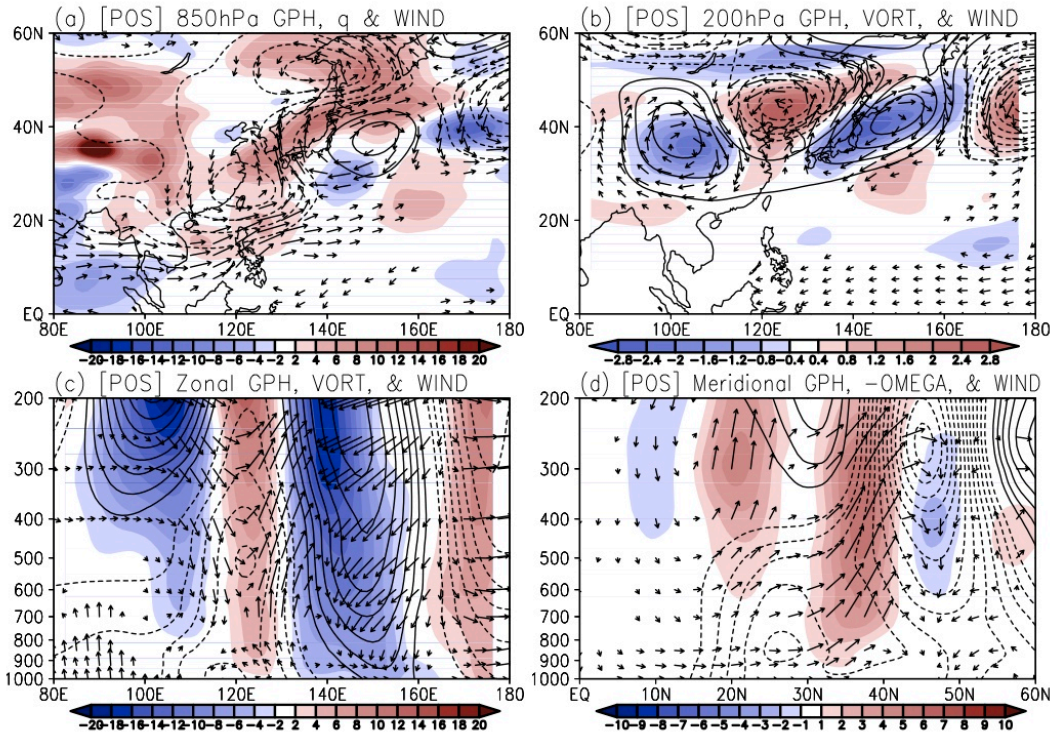

Figure 3.26. Same as Figure 3.26 except for POS years.

Figure 3.25 and Figure 3.26 represent the positive composite fields associated with the sub-seasonal component of the seasonal cycle. A positive composite pattern is defined by

$$C^{(+)}(r) = \sum_{P_f(t)>a} P_f(t) \cdot LVP_f(r,t) \Big/ \sqrt{\sum_{P_f(t)>a} P_f^2(t)}\,, \tag{3.2}$$

where $LVP_f(r,t)$ denotes the sub-seasonal evolution of a predictor variable and $P_f(t)$ is the sub-seasonal evolution of the summertime precipitation over Korea (Figures 3.23b and 3.24b). Equation (3.2) is essentially a weighted average of $LVP_f(r,t)$ with respect to the weight $P_f(t)$. Note in (3.2) that $LVP_f(r,t)$ is averaged only when $P_f(t) > a$ mm/day and the threshold value a is 0.122 and 0.131 mm/day for PRE years and POS years, respectively; these threshold values are taken to be a half of the respective standard deviations. Negative composite patterns can be obtained in a similar manner (not shown).

During the positive phase of the sub-seasonal precipitation anomalies, oscillating patterns of GPH anomalies are observed at 200-hPa along ~40°N and corresponding anomalies of the same sign are observed between ~110°E and 170°E at 850 hPa along ~40°N (Figures 3.25a, 3.25b, Figures 3.26a, and 3.27b). The seemingly northward propagations in Figure 3.23 and Figure 3.24 seem to represent oscillations of meridional circulation cells due to nearly standing oscillations of mid-latitude disturbances aloft (Figure 3.25b and Figure 3.26b), as

also addressed in Kim et al. (2010). The origin of the 200-hPa GPH anomalies at ~40°N is not clear but appears to be related to the typical mid-latitude baroclinic waves (Holton, 1992). A negative 850-hPa GPH anomaly is observed to extend from the northeast of Korea (~45°-50°N) to the southwest of Korea (~25°-30°N) in Figure 3.25a and Figure 3.26a. Such a structure is reminiscent of a typical synoptic-scale background related to summertime heavy rainfall events in Korea addressed in previous case studies (e.g., Lee et al., 2008; Kim and Lee, 2006; Hong, 2004; Ninomiya, 2001; Ninomiya, 2000; Lee et al., 1998; Ninomiya and Mizuno, 1987). Lee et al., (1998) noted in a study of 10 heavy rainfall cases over Korea that a favorable synoptic background for heavy rainfall consists of warm advection from the south and cold advection from northern China or Manchuria. As a result of this configuration, strong baroclinicity builds up over the Korean Peninsula and its vicinity. Warm advection to the east of Korea and cold advection to the west of Korea in conjunction with the negative GPH anomaly residing over Korea (Figure 3.25a and Figure 3.26a) produce a favorable synoptic background for heavy rainfall.

In PRE yeas, a positive 850-hPa specific humidity (SHUM) anomaly with a southwesterly wind anomaly covers Korea and Japan. A negative SHUM anomaly appears to the northwest of Korea with a northerly anomaly (Figure 3.25a). The zonal vertical section (32.5°-40°N) shows that strong baroclinicity builds up over Korea due to cold advection from the northeast and warm

advection from the southwest (Figures 3.25c and 3.25d). Cold advection from a shortwave trough to the north of Korea and warm advection from the south with the supply of warm moist air constitute an important mechanism of sub-seasonal variability from late June through mid-July. In POS years, warm advection is relatively strong because of the increased pressure gradient to the south of Korea (Figures 3.26c and 3.26d). Considering that the active period of the sub-seasonal fluctuation is later in POS years than in PRE years (see Figure 3.23 and Figure 3.24), positive GPH anomalies to the southeast of Korea are relatively strong and are shifted further northward in POS years; this results in stronger warm advection in POS years. On the other hand, cold advection is relatively weak. The zonal cross section (32.5°-40°N) clearly shows a barotropic structure in POS years (Figure 3.26c). Figure 3.25c and Figure 3.26c suggest that the atmosphere is more barotropic than baroclinic because of increased warm advection and decreased cold advection in recent years (Figure 3.25d and 3.26d). As a result, convective (barotropic) instability increases and is an important mechanism of the sub-seasonal variability in POS years.

3.4. Decadal change of high-frequency component of the seasonal cycle

To investigate any physical change in the high-frequency component of precipitation variability, high-pass filtering was conducted on the seasonal cycle using a 10-day cutoff period. Figure 3.27 and Figure 3.28 show the 10-day high-pass filtered precipitation in comparison with the high-pass filtered upper-level (200- to 600-hPa) GPH anomalies and low-level (850- to 1000-hPa) moisture convergence anomalies at (130°E, 37.5°N) over Korea in PRE years and in POS years. Relatively strong upper-level GPH anomalies appear in late May through early July in PRE years and in early July through mid-August in POS years. Low-level moisture convergence is relatively strong in early June and early September in PRE years. In POS years, on the other hand, low-level moisture convergence is relatively strong in late June and in August. There seems to be a reasonable level of physical consistency between the high-frequency component of precipitation variability, derived from both the gauge data and the upper-level GPH anomalies, and the low-level moisture convergence anomalies, derived from the NCEP/NCAR reanalysis data. The latter variables are both correlated with the precipitation anomalies with a coefficient of ~0.6. The magnitude of the high-frequency component of precipitation variability in Korea has increased by ~25% in POS years. Such an increase suggests that

dynamic and thermodynamic processes have been enhanced in POS years, particularly in early July through mid-August.

Figure 3.29 shows the positive composite maps of the high-frequency component of variability. Negative GPH anomalies over Korea and positive GPH anomalies to the east of Korea at the 850-hPa height (Figure 3.29a) are shifted eastward from the corresponding GPH anomalies at the 300-hPa level, forming westward tilt of GPH anomalies with elevation in PRE years (Figure 3.29b). Upper-level divergence over Korea is clearly observed in the vertical zonal section (Figure 3.29b). This structure indicates that baroclinic waves are a dominant ingredient for the high-frequency variability of precipitation with periods of approximately 6-8 days in Korea. In POS years, composite patterns are similar to those of PRE years. While a baroclinic structure is also observed in the vertical section (Figure 3.29d), 850-hPa negative GPH anomalies over Korea are much stronger in POS years. As a result, stronger south and southwest wind anomalies, which result from a shortwave trough over Korea and a ridge to the east of Korea, increase the transport of warm and moist air into Korea in POS years; this explains the strengthened upward motion in POS years at ~130°E (Figure 3.29d). In the meridional vertical cross section, upward motion is also observed to be stronger in POS years (figure not shown).

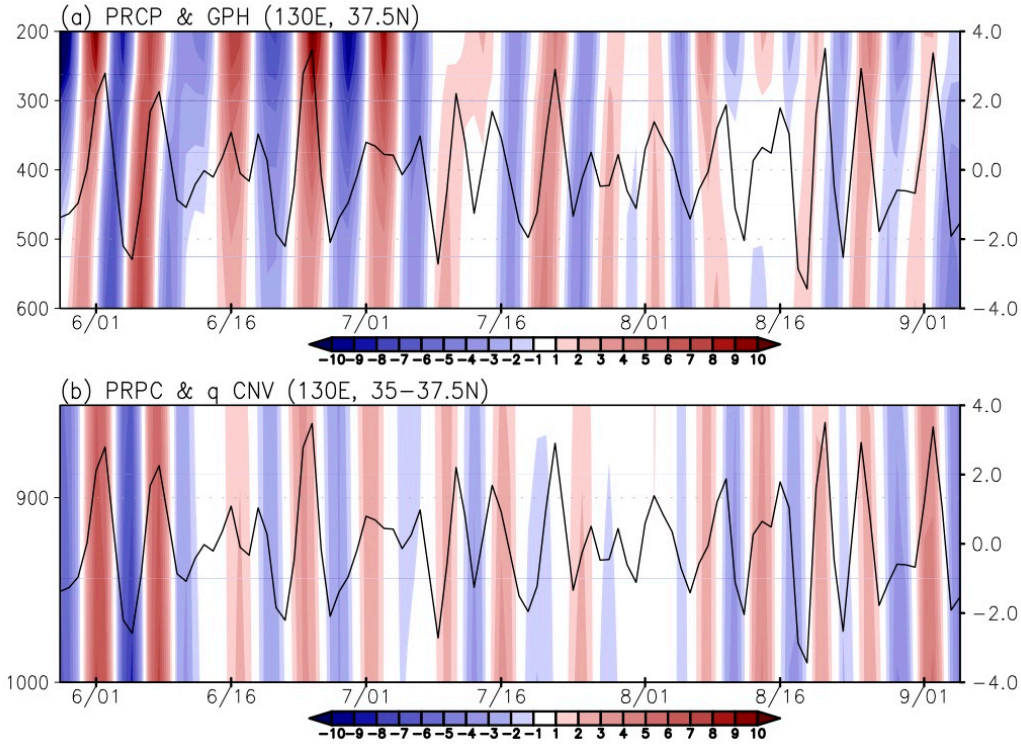

Figure 3.27. High-frequency component of precipitations (line), (a) GPH anomalies (red/blue shading: positive/negative) at 200-600 hPa, and (b) low-level (850-1000 hPa) moisture convergence anomalies (shading) in the high-frequency component in Korea (130°E, 37.5°N) in PRE years. The right axis denotes the precipitation scale (mm/day).

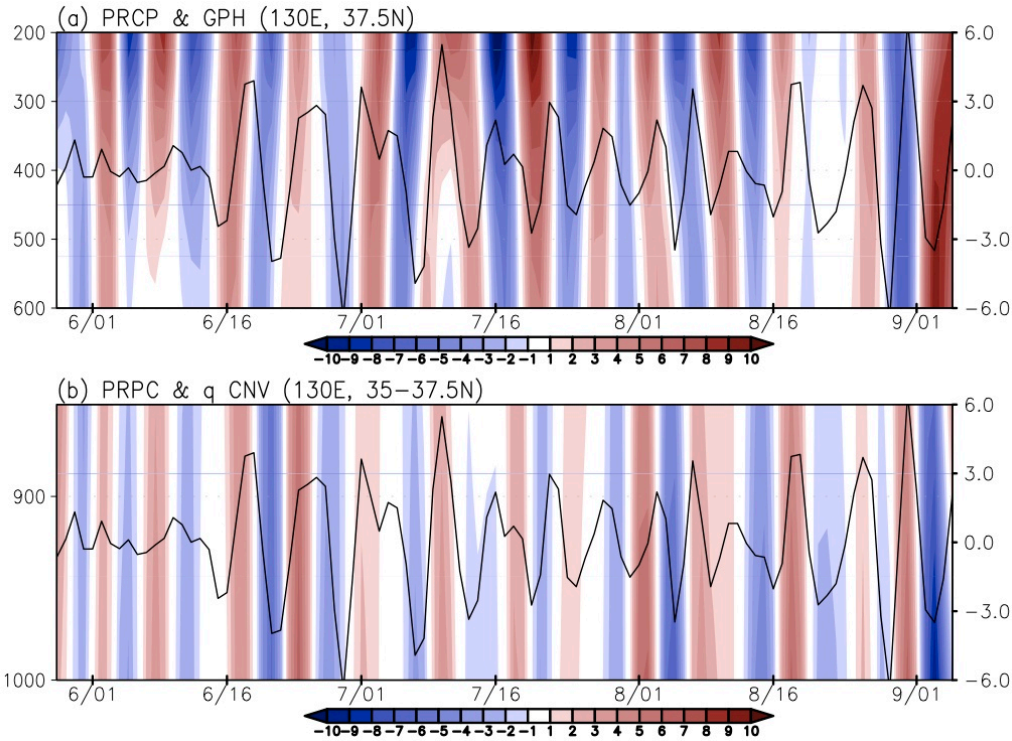

Figure 3.28. Same as Figure 3.27 except for POS years.

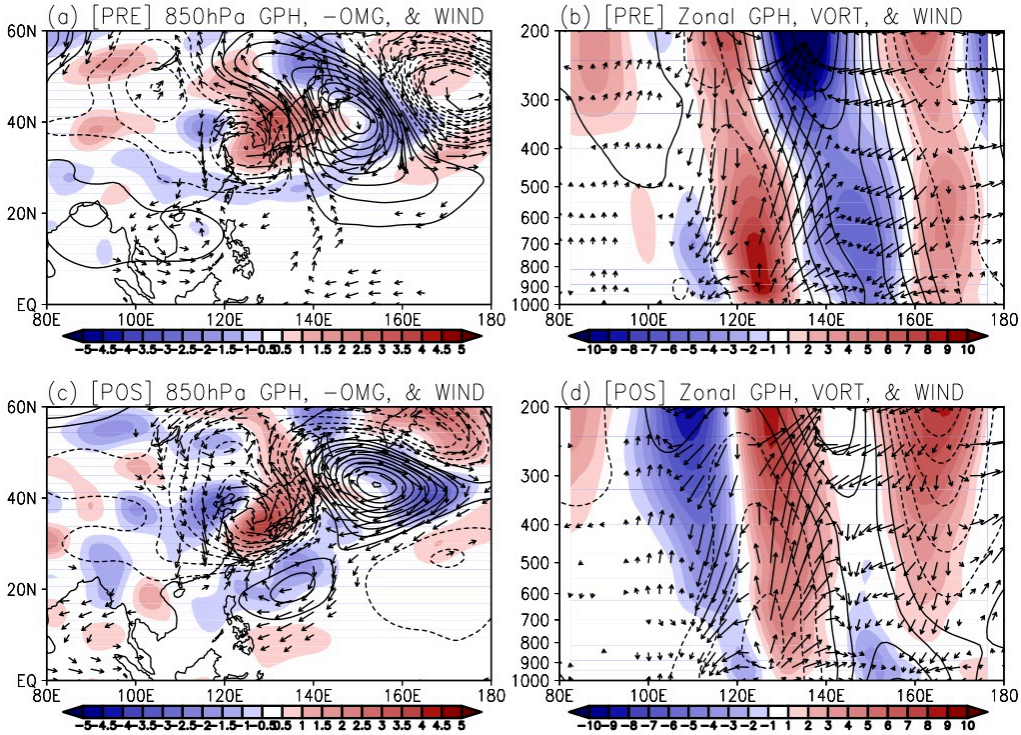

Figure 3.29. Positive composite of the high-frequency component of variability: (a and c) 850-hPa GPH (contour: 2 gpm), vertical velocity (shade: $1'10^{-2}$ Pa/sec), and wind > 0.5 m/sec; (b and d) zonal cross section of GPH (contour: 5 gpm), relative vorticity (shade: $1'10^{-6}$ sec^{-1}), and wind (u, -W) > 0.5 m/s along the 32.5°-37.5°N band. (a and b) are for PRE years and (c and d) are for POS years.

3.5. Decadal change of localized heavy rainfall

3.5.1. The second and the third cyclostationary empirical orthogonal function modes

Figure 3.30 shows the second and third CSEOFs of summertime precipitation variability in Korea averaged over all 61 stations. In TOT years, the second and third CSEOF modes explain 7.0% and 5.6% of the total variance, respectively. The evolution of precipitation associated with the second CSEOF loading vector (CSLV) averaged over 61 KMA stations in TOT years is well correlated with the second CSLV in POS years with the correlation coefficient of 0.96 (Figures 3.30a and 3.30c). The third CSLV in TOT years is well correlated with the second CSLV in PRE years with the correlation coefficient of 0.96 (Figures 3.30b and 3.30d). The second CSEOF modes in PRE years and in POS years explain 10.5% and 14% of the total variance, respectively. These relationships suggest that the nature of localized heavy rainfall events has changed significantly around 1996 (Kim and Suh, 2009). As shown in the second CSLV and the third CSLV, large fluctuations of precipitation on a short time scale are obvious in early August and in early September. Especially, the extreme localized heavy rainfall event, which is distributed out of the width of three standard deviations for 120 summer days, appears at September 3 (the 108th summer day) in the second CSEOF of PRE years (Figure 3.30d). In the

second CSEOF of POS years, however, the extreme heavy rainfall events are seen at August 7 (the 81th summer day) and August 31 (the 105th summer day) (Fig. 3.30c). The relatively stronger fluctuations of PC time series corresponding to the second CSEOF in TOT years are noticeably concentrated after mid-1990s. In contrast, those of PC time series of the third CSEOF are concentrated before mid-1990s. On considering the characteristics of heavy rainfall on a short time period and the occurrence of heavy rainfall at specified dates during August to early September, the CSEOF modes of precipitation variability could be due to the direct and indirect effects of tropical cyclone (Qian et al., 2002). The heavy rainfall occurring when the tropical cyclone penetrates into Korea is regarded as the direct effect of tropical cyclone. The indirect effect of tropical cyclone means that the increased moisture advection induces heavy rainfalls in Korea when the tropical cyclone or depression is mainly located around southern China and the south area of Korea. The typical physical structure of heavy rainfall related to the indirect effect of tropical cyclone in Korea was well studied by previous works (e.g., Lee et al., 2008; Kim and Lee, 2006; Lee and Lee, 2003).

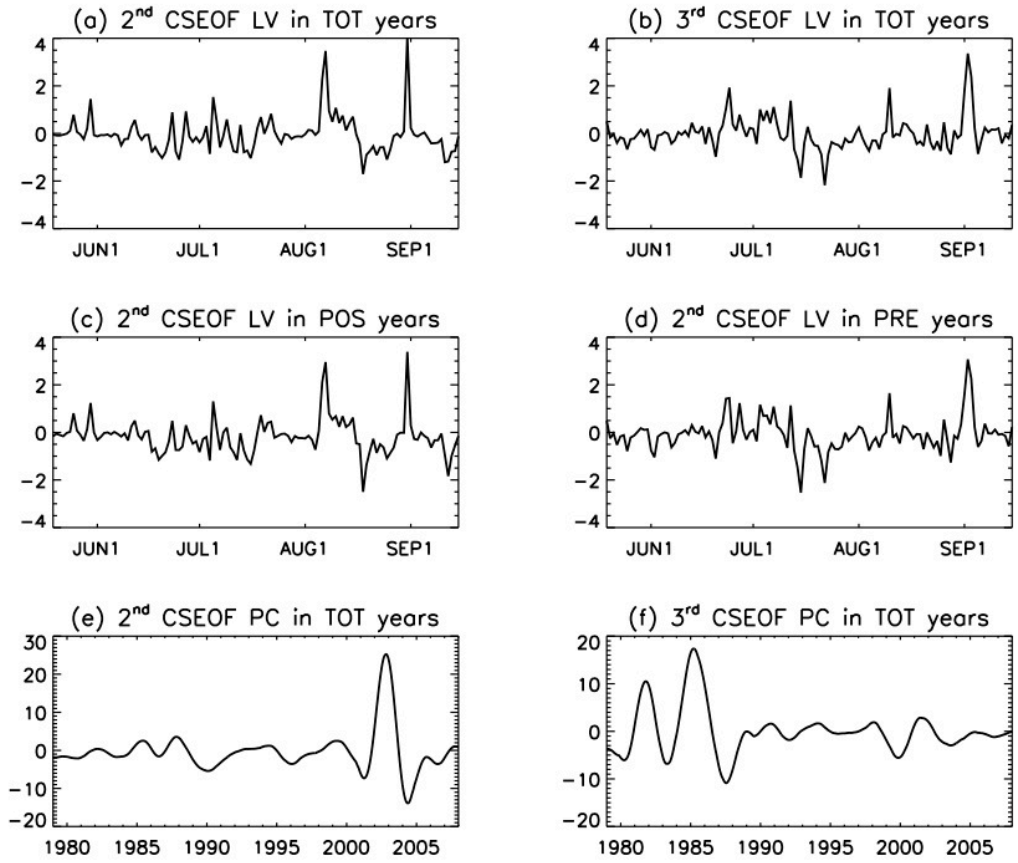

Figure 3.30. The second and third CSEOF modes of summertime precipitation [mm/day] averaged over 61 KMA stations in Korea; (a) and (b) of panels represent the second and third CSEOF loading vectors (CSLV) averaged 61 KMA stations during 120 summer days in TOT years, respectively; (c) and (d) of panels represent the second CSLVs in POS years and PRE years, respectively; (e) and (f) represent the second and third PC time series from 1979 to 2008 in TOT years.

In order to investigate in more detail second and third CSEOF modes of the summertime precipitation variability in Korea, precipitation data have been reconstructed using the CSLVs and the corresponding PC time series. Figure 3.31a and Figure 3.31b represent the reconstructed precipitation based on the second and the third modes of CSEOF in TOT years, respectively. In the second CSEOF of precipitation variability in TOT years (Figure 3.31a), the precipitation variability from 1996 to 2008 matches well with that in the second CSEOF in POS years (Figure 3.31c). Similarly, reconstructed precipitation records of the third CSEOF in TOT years (Figure 3.31b) are much similar to those of the second CSEOF in PRE years (Figure 3.31d). Therefore, it seems to be reasonable that the year 1996 is the optimal dividing point of the decadal change of precipitation, especially in terms of localized heavy rainfalls in the Korean Peninsula. In this study, the case of precipitation amount over 150 mm/day is defined as heavy rainfall events. Table 3.1 and Table 3.2 show heavy rainfall events over 150 mm/day averaged over 61 stations. The selected cases are mainly related to the direct/indirect effect of tropical cyclones. The name, location, and centered pressure of corresponding typhoon at 00 UTC for the selected cases in PRE years and in POS years are described in Table 3.1 and Table 3.2, respectively. The 13 cases appeared in POS years during 13 years in comparison to the 7 cases in PRE years during 17 years. The localized heavy rainfalls over 150 mm/day have remarkably increased in POS years.

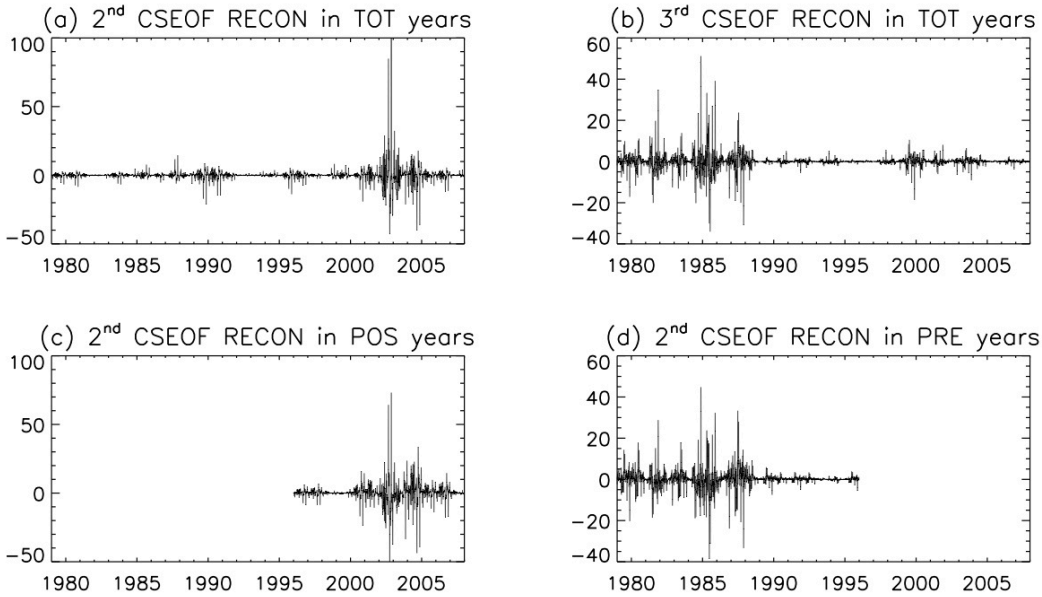

Figure 3.31. Reconstructions between CSLV and PC time series of the second and third modes of CSEOF in summertime precipitation averaged over 61 KMA stations in Korea; (a) and (b) represent the second and third mode in TOT years, respectively; (c) represents the second mode in POS years; (d) represents the second mode in PRE years.

Table 3.1. The cases over 150 mm/day based on the reconstruction of rainfall in PRE years. The information of corresponding typhoon is listed.

Date (yyyy.mm.dd)	TY Name	Latitude (°N)	Longitude (°N)	Pressure (hPa)
1981. 09. 02	Agnes	32.2	123.5	970
1984. 09. 02	June	30.0	119.0	1002
1984. 09. 03	June	34.0	127.0	1004
1985. 06. 24	Hal	22.1	115.1	975
1985. 09. 02	*NO TYPHOON*	•	•	•
1987. 07. 15	Thelma	29.9	125.5	950
1987. 07. 22	Vernon	30.8	123.4	1000

Table 3.2. Same as Table 3.1 except for POS years.

Date (yyyy.mm.dd)	TY Name	Latitude (°N)	Longitude (°N)	Pressure (hPa)
2002. 07. 05	Rammasoon	32.2	123.7	965
2002. 08. 06	Kammuri	27.0	115.2	996
2002. 08. 07	Kammuri	28.4	114.2	1000
2002. 08. 31	Rusa	32.6	127.1	960
2003. 09. 12	Maemi	30.5	126.5	930
2003. 09. 13	Maemi	39.1	131.8	975
2004. 06. 20	Dianmu	26.9	129.7	945
2004. 07. 04	Mindulle	33.1	124.5	984
2004. 07. 12	Compasu	20.0	133.5	1008
2004. 07. 14	Compasu	20.9	124.3	998
2004. 07. 17	*NO TYPHOON*	•	•	•
2004. 08. 18	Megi	28.4	125.3	970
2004. 08. 19	Megi	35.6	129.7	970

3.5.2. Decadal change of precipitation variability related to tropical cyclones

Figure 3.32 shows the patterns of 850-hPa NCEP reanalysis GPH and horizontal wind fields at 00 UTC in the heavy rainfall cases in Table 3.1. The tracks in Figures 3.32a, 3.32b, and 3.32d can be suggested by the direct effect of tropical cyclone on heavy rainfalls in which the cyclonic circulations are matched with typhoon tracks located over the Korean Peninsula. In Figure 3.32c and 3.32e, tropical cyclones are located in the lower Yangtze River and southern China with the cyclonic circulation. The strong south and southwest winds, which are strengthened by the cyclonic circulation to the southwest area of Korea and the anti-cyclonic circulation to the southeast area of Korea, were seen at the date of heavy rainfall case. It seems that tropical cyclones had an indirect effect on the heavy rainfall in Korea due to the warm and abundant moisture advections by the south and southwest wind. For such a reason, in POS years, the direct effect of tropical cyclones can be suggested on the heavy rainfall cases such as Figures 3.33a, 3.33c, 3.33d, 3.33f, and 3.33h. Figures 3.33b, 3.33e, and 3.33g represent the indirect effect of tropical cyclones on the heavy rainfall in Korea in POS years. Such as the difference of tracks of tropical cyclone in PRE years and in POS years can be suggested to regional changes in localized heavy rainfall distribution over Korea.

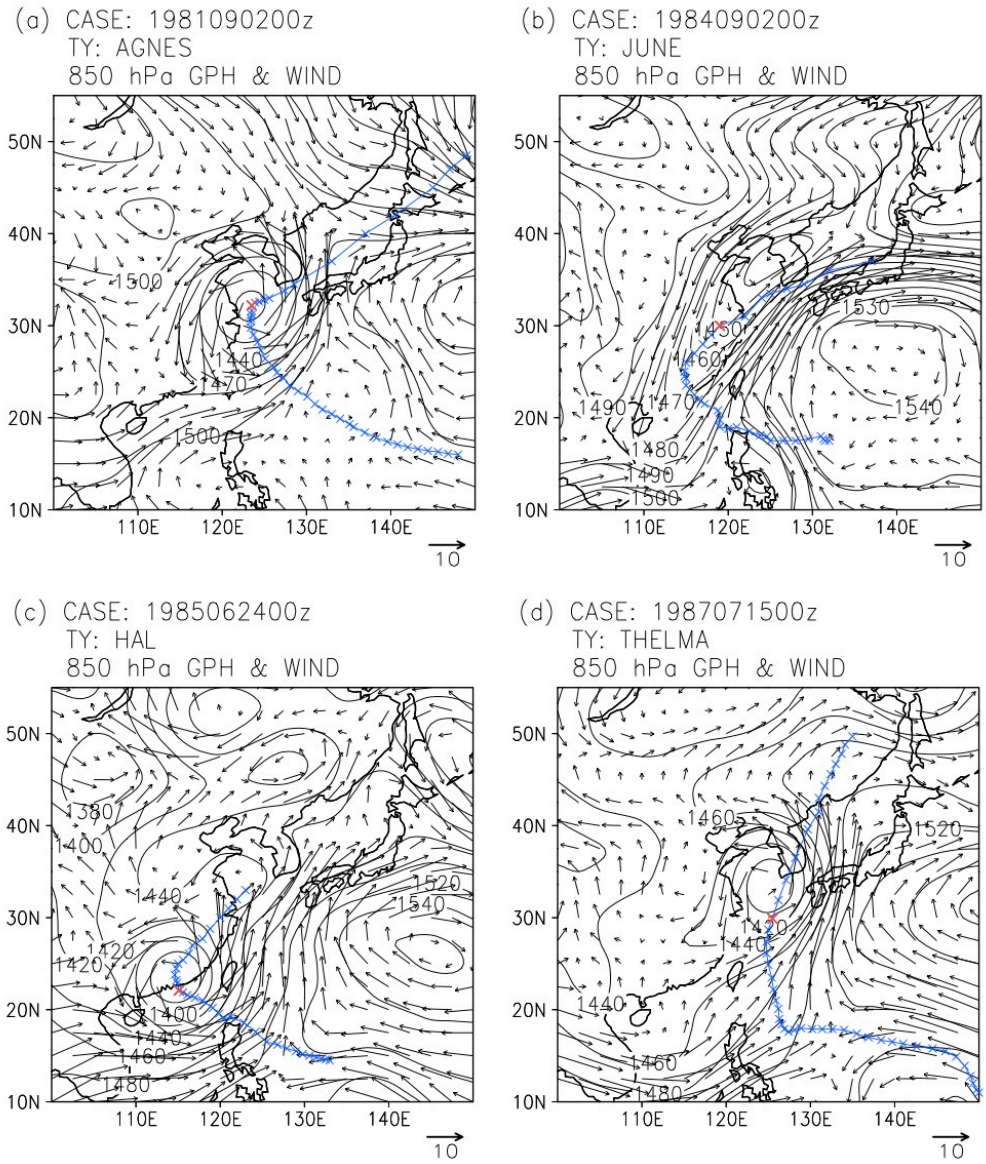

Figure 3.32. The 850-hPa geopotential height (gpm) and wind (m/s) in the cases over 150 mm/day in PRE years. Blue crosses and lines indicate JTWC best tracks of typhoon associated with heavy rainfall in Table 3.1. Each bold red cross is the location of tropical cyclone at the time of each case.

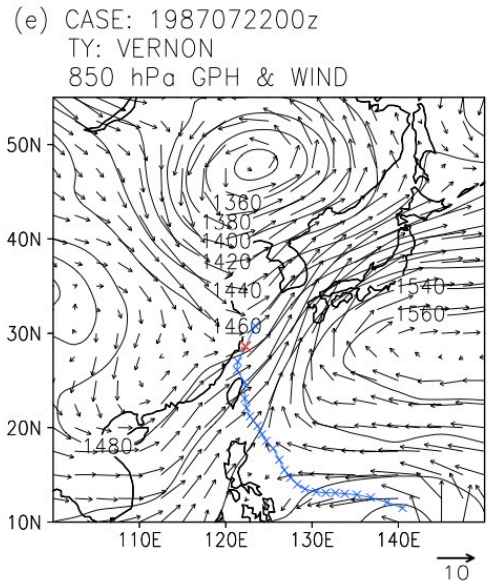

Figure 3.32. (Continued).

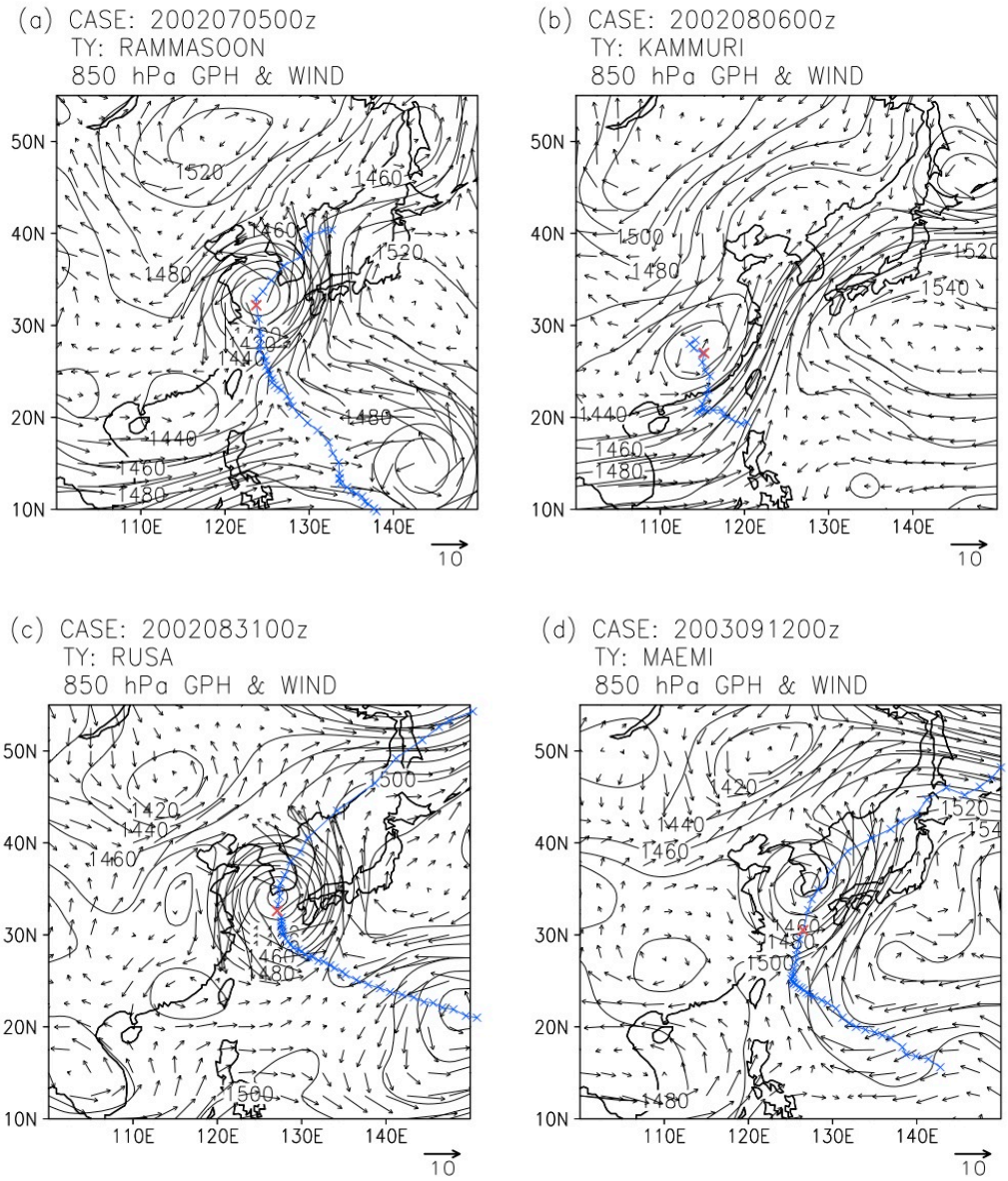

Figure 3.33. The 850-hPa geopotential height (gpm) and wind (m/s) in the cases over 150 mm/day in POS years. Blue crosses and lines indicate JTWC best tracks of typhoon associated with heavy rainfall in Table 3.2. Each bold red cross is the location of tropical cyclone at the time of each case.

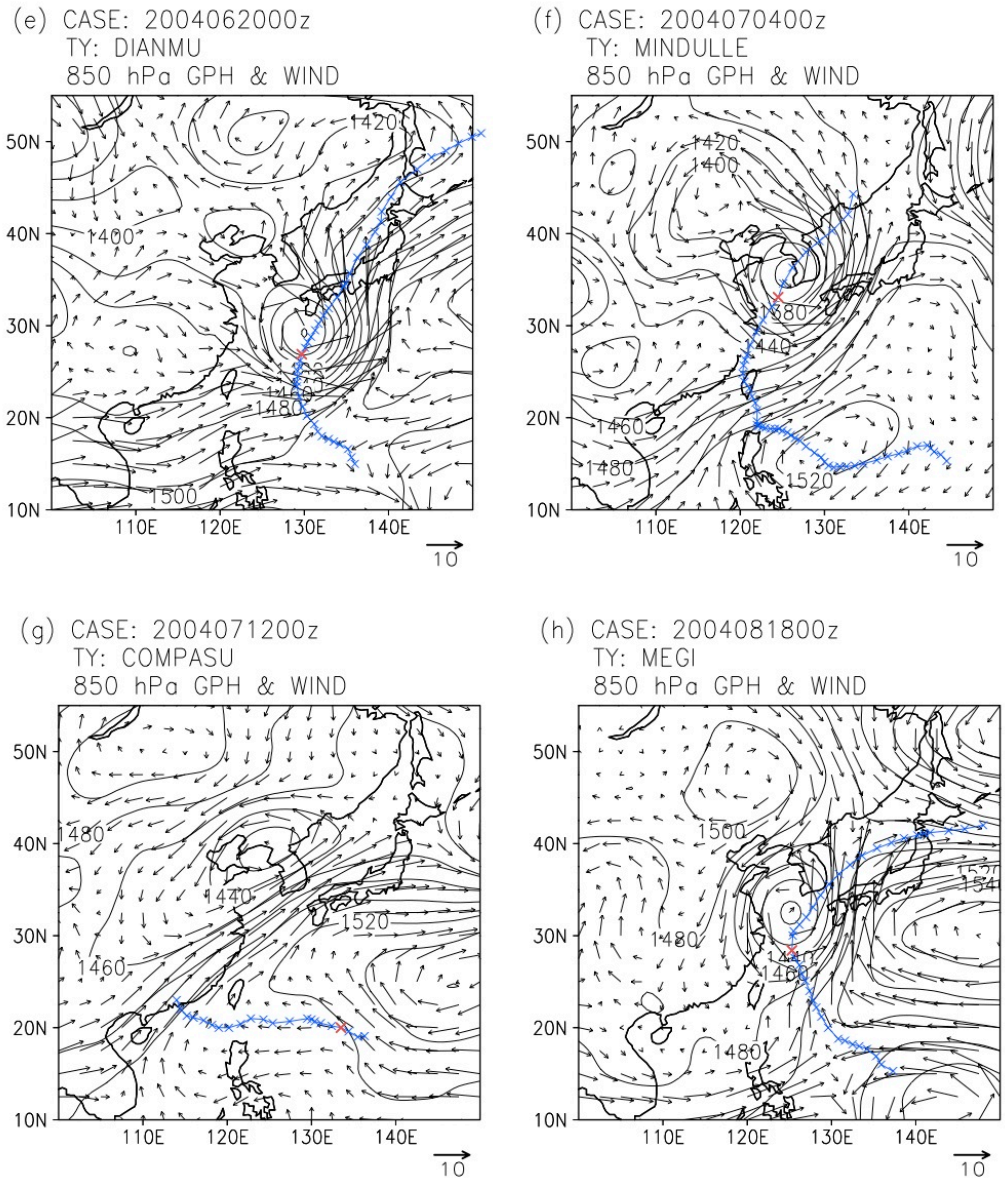

Figure 3.33. (Continued).

In order to investigate the regional changes in localized extreme heavy rainfall distribution, the local distributions of high-precipitation stations in PRE years and in POS years are represented in Figure 3.34. As mentioned above, the extreme heavy precipitation events, which are appeared at September 3 (the 108th summer day) in PRE years (Figure 3.34a), at August 7 (the 81th summer day), and at August 31 (the 105th summer day) in POS years (Figure 3.34b and Figure 3.34c), are selected to be out of the width of three standard deviations for 120 summer days in PRE years and in POS years. Thus, the high-precipitation stations of localized heavy rainfalls have been positioned in the western and central area of South Korea at August 7 and in the eastern area at August 31 after 1996, while the localized heavy precipitation had occurred in the southern area of South Korea at September 3 before 1996. Thus, the remarkable decadal change of summertime localized heavy precipitation in the Korean Peninsular is predominant.

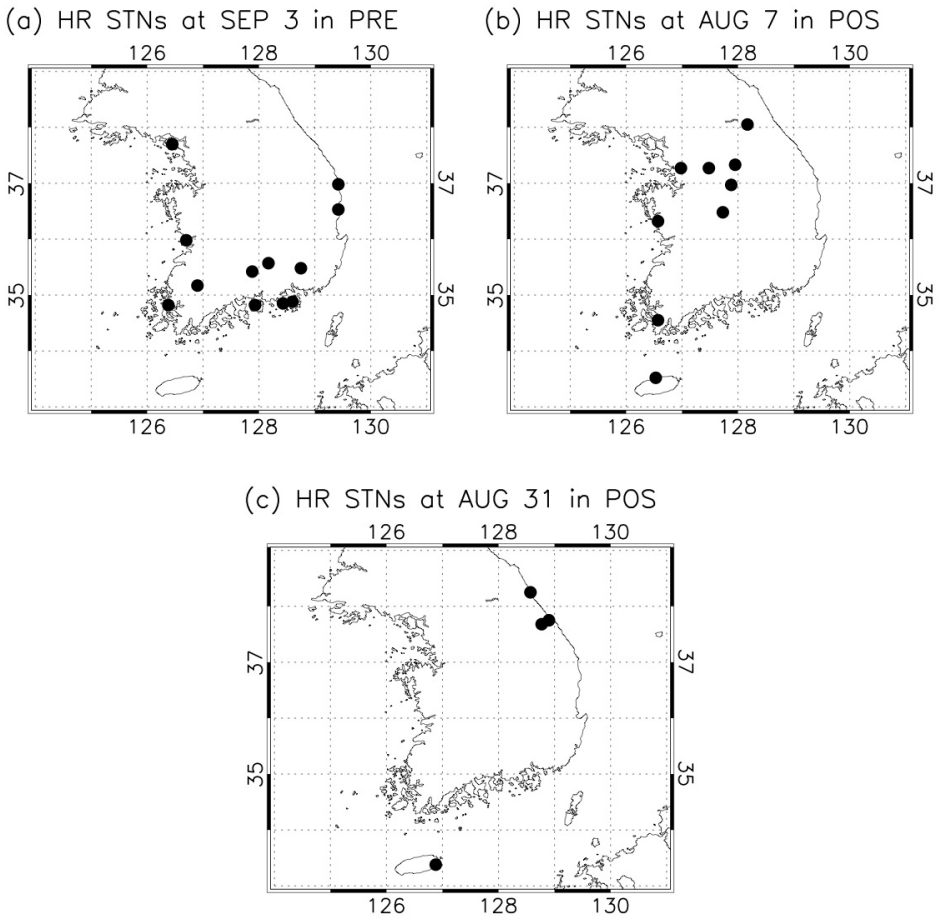

Figure 3.34. The local distributions of typical heavy rainfall stations (HR STN) (a) at September 3 in the second CSEOF in PRE years, (b) at August 7 in the second CSEOF in POS years, and (c) at August 31 in the second CSEOF in POS years.

The change of physical structures associated with the localized heavy precipitation has been investigated. The physical evolutions of 850-hPa spatial patterns of geopotential height anomalies, relative vorticity anomalies, and wind anomalies are shown in Figure 3.35. This figure represents the evolution of cyclonic circulations from September 1 to September 3, which is associated with the heavy rainfall case in the second CSEOF in PRE years. The negative GPH anomalies accompanying to positive relative vorticity anomalies located on the southeast coast of China at September 1 (Figure 3.35a) arrive to the Yellow Sea and the western area of the Korean Peninsular (see Figure 3.35b). As shown in Figure 3.35c, negative GPH anomalies accompanying the maximum positive relative vorticity anomalies, which is associated with a tropical cyclone, occupy the Korean Peninsula at September 3, which is corresponding to the extreme heavy precipitation day in PRE years. Although the physical evolution shown in Figure 3.35 is a representative pattern of a negative GPH anomaly, which is caused to localized heavy rainfall, the tracks of tropical cyclones, which put their turning point to the vicinity of the South China Sea, were seen to be well matched in the aspect that tropical cyclones moved from the vicinity of the South China Sea to the Korean Peninsula.

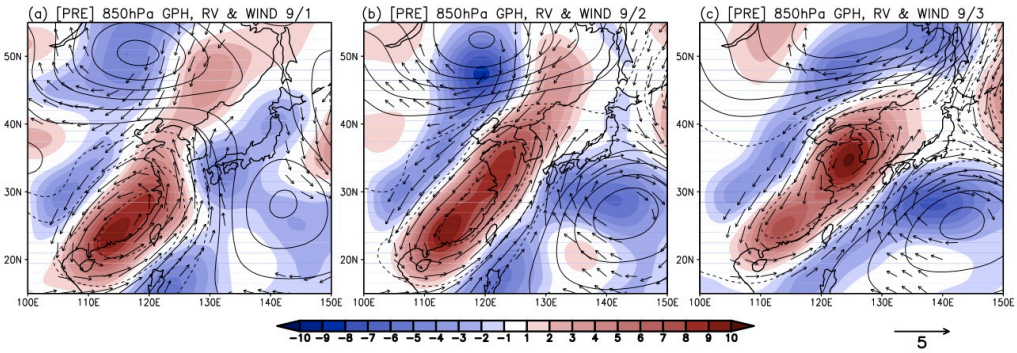

Figure 3.35. The 850-hPa geopotential height anomalies (solid/dashed lines are positive/negative geopotential height; contoured at 3 gpm interval), relative vorticity anomalies (red/blue shadings are positive/negative values; 10^{-6} sec^{-1}), and wind vector anomalies (> 1m sec^{-1}) in (a) September 1, (b) September 2, and (c) September 3 in the second CSEOF of PRE years.

Figure 3.35 represents the 850-hPa physical evolutions of two extreme heavy rainfall cases, which appeared at August 7 and August 31, over three times of standard deviations for 120 summer days in POS years. The negative GPH anomalies combined with positive relative vorticity anomalies on the southeast coast of China at August 5 (Figure 3.35a) reach to the Yellow Sea, and take up the Korean Peninsula at August 7 (Figure 3.35c). The evolution of negative GPH anomalies at August 7 in POS years is much similar to that at September 3 in PRE years. However, in early September, which is the period of the retreat of East Asian summer monsoon front, positive GPH anomalies on the continent are stronger than those in early August. Positive GPH anomalies, which is corresponding to the western North Pacific, to the southeastern are of Korea in early September are relatively shifted southward in comparison with those in early August (Kim et al., 2010; Lime et al., 2002). The negative GPH anomalies associated with tropical cyclone tracks in the case of August 7 in POS years can be shifted northward in comparison with those in the case of September 3 in PRE years since positive GPH anomalies on the northern area of Korea are relatively weaker and positive anomalies on the southwestern area of Korea are relatively stronger. The local distributions of high-precipitation stations at September 3 in PRE years (Figure 3.34a) and at August 7 in POS years (Figure 3.34b) can be roughly explained. In the 850-hPa spatial pattern of physical evolution from August 29 to August (Figures 3.36d to 3.36f) in POS

years, negative GPH anomalies, which are also going together anti-clockwise pattern of wind anomalies and positive relative vorticity anomalies, to the southeastern area of Korea at August 29 (Figure 3.36d) proceed slowly northward (Figure 3.36e). Then, negative GPH anomalies with the maximum positive relative vorticity anomalies occupy the Korean Peninsula at August 31 in POS years. In comparison to Fig. 18c, the local distribution of heavy rainfall stations at August 31 in POS years can be considered with the path of tropical cyclone. A negative GPH anomaly on the South China Sea in August 5 of POS years is the weaker than that in September 1 of PRE years on comparing the magnitude of relative vorticity anomaly corresponding to GPH anomaly. However, a negative GPH anomaly on the northeast area of Korea in August 5 of POS years accompanying to strong positive relative vorticity anomaly were seem to be gradually combined with a negative GPH on the South China Sea to August 6. In August 7 of POS years, a negative GPH anomaly on the Korean Peninsula accompanying to the strengthened positive relative vorticity anomaly was seen in Figure 3.36c. In contrast to, a negative GPH anomaly on the South China Sea in September 1 of PRE years moved northeastward by degree. Thus, the decadal change in tropical cyclone tracks seems to be associated with the physical pattern change, especially the subtropical high pattern change.

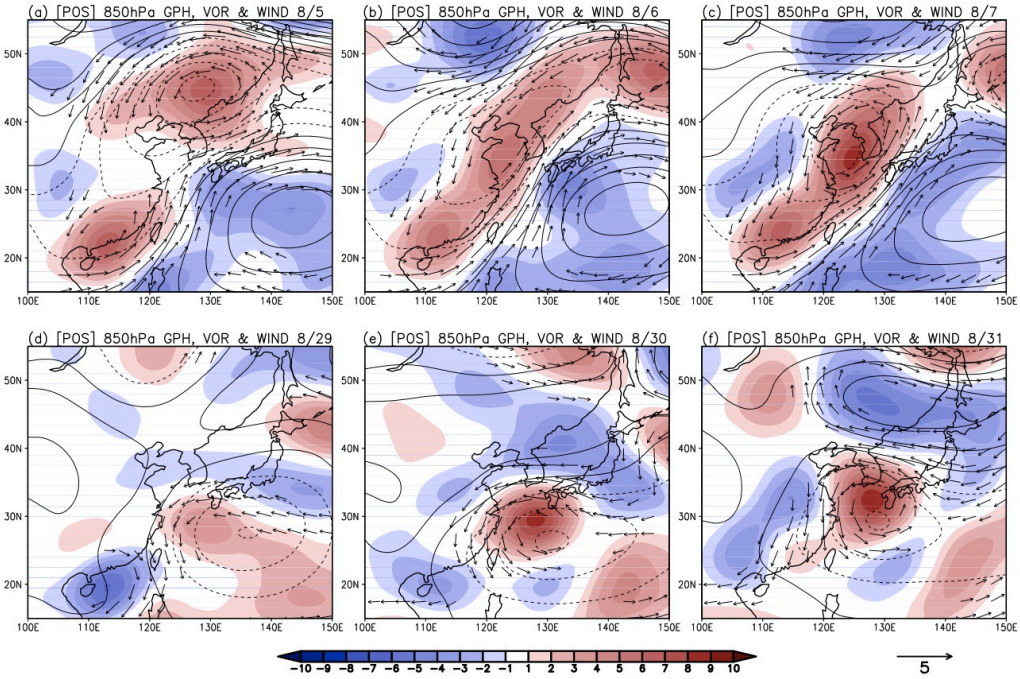

Figure 3.36. The same as Figure 3.35 except for (a) August 5, (b) August 6, (c) August 7, (d) August 29, (e) August 30, and (f) August 31 in the second CSEOF of POS years.

4. Summary and conclusion

The level of summertime precipitation in Korea has changed significantly in recent years, with frequent occurrences of very heavy rainfall. The total amount of precipitation seems to have increased by approximately 25% in the recent decade compared with the climatology preceding 2000. In this study, the recent decadal change in precipitation has been investigated in the context of the underlying physical mechanisms.

The seasonal cycle, the first CSEOF, of the summer precipitation in Korea consists primarily of three different physical mechanisms: the seasonal evolution, the sub-seasonal evolution, and the high-frequency evolution associated with Rossby waves. The seasonal evolution of the summer precipitation in Korea is strongly associated with the evolution of land/ocean contrasts in sea level pressure, as described in previous studies related to Changma front and East Asian summer monsoon. The pattern of sea level pressure and, consequently, of low-level circulation exhibits a complex evolution pattern caused by the huge difference in heat capacity between the Asian continent and the surrounding oceans. The first peak, called the Changma (first precipitation spell), is slightly stronger than the second peak, called the post-Changma; they are separated by a brief spell of weakened precipitation, resulting in a bimodal structure. During the first precipitation spell, excessive

moisture comes from the southwest, following a strong, steep sea level pressure gradient along the southeastern coast of the Asian continent. During the period of the weakened precipitation, the sea level pressure contrast between the Asian continent and the western Pacific is weak; as a result, moisture transport to Korea is reduced significantly. The second precipitation spell is associated with positive sea level pressure anomalies over the continent and negative anomalies over the western Pacific. As a result of this reversed sea level pressure contrast, excessive moisture is transported into Korea from the northwestern Pacific. The seasonal component, on average, explains 6.40 mm/day during the 120 summer days (standard deviation, 3.08 mm/day).

The sub-seasonal variability of precipitation in Korea is associated with the seemingly northward propagation of ~10–30 day oscillations of precipitation from lower latitudes with the mean period of ~15 days. The sub-seasonal component of variability in Korea is strongly associated with the upper-level wave-like disturbances propagating eastward. This upper-level disturbance at ~30°N–40°N alters the strength of the meridional circulations with decreased (increased) downward motion underneath and increased (decreased) upward motions to the north and to the south of the disturbance. The fluctuations of the upper-level disturbance therefore generate alternating signs of moisture and precipitation anomalies at low latitudes. As the upper-level disturbance moves eastward and is replaced by a disturbance of the opposite sign, the low-level

precipitation and moisture convergence anomalies appear to be drawn to the newly arrived upper-level divergence, giving it an appearance of northwestward migration from low latitudes. The standard deviation of the sub-seasonal component of precipitation in Korea is 1.13 mm/day.

Baroclinic instability is well developed when Rossby waves pass Korea with axes at ~40°N. As a result, high-frequency variability of precipitation is seen clearly throughout Korea. The standard deviation of the high-frequency component is 2.11 mm d^{-1}. The present study indicates that variability with periods of less than 10 days is stronger than the sub-seasonal component of variability.

Using the concept of three distinct physical mechanisms of summertime precipitation variability in Korea, decadal change is investigated in an effort to understand precipitation variability in Korea from a physical and dynamical point of view. Bridging local precipitation and regional physical processes is crucial not only in understanding local variability in the context of regional physical mechanisms, but also in understanding how the changing regional physical processes affect precipitation locally. While addressing precipitation changes in terms of intensity, amount, and timing is important, it will also be crucial to understand whether and how physical mechanisms of precipitation vary as a consequence of climate changes. Thus, this study offers

means of addressing local precipitation change in the context of bigger regional impacts of climate changes and physical mechanisms that affect local precipitation. In a sequel paper, we will address the effect of climate changes in the physical and dynamical characteristics of the summertime precipitation in Korea. We emphasize that the present approach to the physical decomposition of precipitation should apply equally well to local precipitation in many other midlatitude locations.

In seasonal component of seasonal cycle of summertime precipitation variability in Korea, the bimodal pattern of precipitation and the associated dynamic and thermodynamic patterns in the seasonal-scale variability are associated with the temporally varying pressure contrast between the Asian continent and the surrounding oceans. It appears that the first peak has increased by more than 25% and tends to appear earlier in recent years; this is due to the change in low-level circulation, which transports more moisture during the mature stage of the Asian summer monsoon. As a result, commencement of the East Asian monsoon front occurred earlier and the associated low-level moisture convergence strengthened in POS years.

The typical spell of decreased precipitation is not clear in POS years because of the strengthened convective activity over Korea. The increased convective activity is due to the strengthened low-level southerly anomalies. In

addition, both active convective motion in the subtropics and the increased divergence near the entrance of the upper-level jet seem to facilitate convective activity over Korea.

During the period of the post-Changma, convective activities over Korea have weakened in recent years. This is because the negative pressure anomaly over the northwestern Pacific has retreated further to the east; as a result, moisture convergence over Korea is much weaker. This retreat of the lower pressure center is also observed in the weakened convective activity in the subtropics along ~130°E. As a result, the second peak has broadened without a well-developed period of decreased precipitation in POS years.

The sub-seasonal variability with 10-30-day time scales describes alternating signs of precipitation seemingly propagating northward from ~20°N with an average period of ~15 days in PRE years and ~13 days in POS years. The sub-seasonal component of variability exhibits a substantial increase in strength in POS years. Relatively strong sub-seasonal activities occur in late June through mid-July in PRE years, in contrast to later activities in August through mid-September in POS years. This difference in timing suggests that cold advection is more important in PRE years than in POS years, whereas warm advection is more important in POS years than in PRE years.

Fluctuation of cold advection induced by the shortwaves to the northeast of Korea appears to modulate baroclinic instability over Korea. Fluctuation of warm advection by low-level southerly winds, on the other hand, seems to modulate convective instability over Korea. Convective instability, as indicated by the nearly barotropic structure of the atmosphere, is much stronger throughout the summer in recent years; as a result, the magnitude of sub-seasonal variability has significantly increased in POS years.

The high-frequency component of precipitation formed by the baroclinic waves and their (Kim et al., 2010) remains nearly the same in its physical structures between PRE years and POS years. The magnitude, however, has increased by approximately 25%; this implies that dynamic and thermodynamic processes leading to baroclinic instability have strengthened in POS years.

Due to a significant change in the heat distribution between the continent and the oceans, the seasonal cycle of the Asian summer monsoon has strengthened by approximately 25% in recent years. Due to the enhancement of the Asian summer monsoon, more moisture is transported to northeastern countries, including Korea, Japan, and eastern China. As a result, East Asian regional monsoons, on average, have become stronger in the last decade. According to the results of this study, changes in the summertime precipitation

pattern in Korea are not just a matter of local interest but may have a much broader impact.

The localized heavy rainfalls are explained in the second and third CSEOFs for the entire period. The PC time series of the second (third) CSEOF fluctuates relatively stronger after (before) mid-1990s than before (after) mid-1990s. The evolution of precipitation associated with the second CSEOF loading vector (CSLV) averaged 61 stations in the entire period is highly correlated with the second CSLV in recent years, 1996-2008. However, the third CSLV for the entire period is well correlated with the second CSLV in 1979-1995. At the point time of 1996, the decadal change of summertime precipitation is clearly prominent.

As the second and the third CSLVs over three times of standard deviations shows the characteristics of heavy rainfalls in a short time on period from August to early September, these modes of precipitation variability could be the products due to the effect of tropical cyclone (Qian et al., 2002). In the reconstruction between CSLV and corresponding PC time series, it is confirmed that heavy rainfall cases over 150 mm/day averaged over 61 stations are mainly accompanying tropical cyclones in the second and third CSEOFs. The 13 cases appeared in POS years, during 13 years, in comparison to the 7 cases in PRE

years, during 17 years. The localized heavy rainfalls over 150 mm/day have remarkably increased in POS years.

The extreme localized heavy rainfall event, which is distributed out of the width of three times of standard deviations for 120 summer days, appeared in the southern provinces of Korea at September 3 (the 108th summer day) in the second CSEOF of PRE years. In the second CSEOF of POS years, however, the extreme heavy rainfall events at August 7 (the 81st summer day) and August 31 (the 105th summer day) occur dominantly in the central-west region and in the eastern part of the Korean Peninsula, respectively. The decadal change in the localized heavy rainfalls could be due to the tropical cyclone or depression activities. The location changes of positive GPH anomalies to the north of Korea and to the southeast of Korea have an effect on the changes of trajectory of negative GPH anomalies corresponding to tropical cyclone.

References

Allen, M. R., and M. J. Ingram, 2002: Constraints on future changes in climate and the hydrologic cycle, *Nature*, **419**, 224-232.

Annamalai, H., and J. Slingo, 2001: Active/break cycles: Diagnosis of the intraseasonal variability of the Asian summer monsoon, *Clim. Dyn.*, **18**, 85-102, doi:10.1007/s003820100161.

Booij, M. J., 2002: Extreme daily precipitation in western Europe with climate change at appropriate spatial scales. *Int. J. Climatol.*, **22**, 69-85.

Bluestein, H. B., 1993: *Synoptic-Dynamic Meteorology in Midlatitudes*, Oxford Univ. Press, New York.

Chen, J., H. Uyeda, and D. –I. Lee, 2003: A method using radar reflectivity data for the objective classification of precipitation during the Baiu season, *J. Meteorol. Soc. Jpn*, **81**, 229-249.

Ding, Y. H., 2004: Seasonal march of the East Asian summer monsoon, in *The East Asian summer monsoon*. Vol. 2, edited by C.-P. Chang, pp. 3-53, World Sci., Publ., Monterey, Cal., 564 pp.

_____, and D. R. Sikka, 2006: Synoptic systems and weather, in *The Asian Monsoon*, edited by B. Wang, 131-201 pp., *Praxis. Springer Publisher*.

Easterling, D. R., G. A. Meehl, C. Parmesan, S.A., 2000: Climate extremes: Observations, modeling, and impacts. *Science*, **289**, 2068-2074, doi:10.1126/sciences.289.5487.2068.

Emori, S. and S. J. Brown, 2005: Dynamic and thermodynamic changes in mean and extreme precipitation under changed climate. *Geophys. Res. Lett.*, **32**, L17706, doi:10.1029/2005GL023272.

Frich, P., L. V. Alexander, P. Della-Marta, B. Gleason, M. Haylock, A. M. G. Klein Tank, and T. Peterson, 2002: Observed coherent changes in climatic extremes during the second half of the twentieth century. *Climate Res.*, **19**, 193-212.

Groisman, P. Ya., and Coauthors, 1999: Changes in the probability of heavy precipitation. Important indicators of climatic change. *Climate Change*, **42**, 243-283.

_____, R. W. Knight, D. R. Easterling, T. R. Karl, G. C. Hegerl, and V. N. Razuvaev, 2005: Trends in intense precipitation in the climate record. *J. Clim.*, **18**, 1326-1350.

Grotjahn, R., 1993: *Global Atmospheric Circulations: Observations and Theories*, Oxford Univ. Press, New York.

Haylock, M., and N. Nicholls, 2000: Trends in extreme rainfall indices for an updated high quality data set for Australia, 1910-1998. *Int. J. Climatol.*, **20**, 1533-1541.

Held, I. M., and B. J. Soden, 2006: Robust responses of the hydrological cycle to global warming, *J. Clim.*, **19**, 5686-5699.

Ho, C.-H., and I.-S. Kang (1988), The variability of precipitation in Korea, *J. Korean Meteor. Soc.*, **24**, 38-48.

Holton J. R., 1992: *An Introduction to Dynamic Meteorology*, 3rd ed., 511 pp., Academic Press.

Hong, S.-Y., 2004: Comparison of heavy rainfall mechanisms in Korea and the central US, *J. Meteorol. Soc. Jpn*., **82**, 1469-1479.

Houghton, J. T., Y. Ding, D. J. Griggs, M. Noguer, P. J. van der Linden, X. Dai, K. Maskell, and C. A. Johnson, Eds., 2001: *Climate Change 2001*: The Scientific Basis. Cambridge Univ. Press, 881 pp.

Iwashima, T., and R. Yamamoto, 1993: A statistical analysis of the extreme events: Long-term trend of heavy daily precipitation. *J. Meteor. Soc. Japan*, **71**, 637-640.

Kajikawa, Y., and T. Yasunari, 2005: Interannual variability of the 10-25- and 30-60-day variation over the South China Sea during boreal summer, *Geophys. Res. Lett*., **32**, L04710, doi:10.1029/2004GL021836.

Kalnay, E., and Coauthors, 1996: The NCEP/NCAR 40-year reanalysis project. *Bull. Amer. Meteorol. Soc*., **77**, 437-471.

Kang, I.-S., Y.-K. Lim, C.-H. Ho, K.-M. Lau (1999), Principal modes of climatological seasonal and intraseasonal variations of the Asian summer monsoon, *Mon. Wea. Rev*., **127**, 322-340.

Karl, T. R. and R. W. Knight, 1998: Secular trends of precipitation amount, frequency, and intensity in the United States, *Bull. Am. Meteorol. Soc.*, **79**, 231-241.

_____, _____, and N. Plummer, 1995: Trends in high-Frequency climate variability in the 20th-Century, *Nature*, **377**, 217-220.

Kemball-Cook, S., and B. Wang, 2001: Equatorial waves and air-sea interaction in the boreal summer intraseasonal oscillation, *J. Clim*., *14*, 2923-2942.

Keyser, D., and M. A. Shapiro, 1986: A review of the structure and dynamics of upper-level frontal zones, *Mon. Wea. Rev.*, **114**, 452-499.

Kim, C., M.-S. Suh, and K.-O. Hong, 2009: Bayesian change analysis of the annual maximum of daily and subdaily precipitation over South Korea. *J. Clim.*, **22**, 6741-6757.

_____, and _____, 2009: Change-point and change pattern of precipitation characteristics using Bayesian method over South Korea from 1954 to 2007, *Atmosphere*, **19**, 199-211.

Kim, H.-W., and D.-K. Lee, 2006: An observational study of mesoscale convective systems with heavy rainfall over the Korean Peninsula, *Wea. Forecasting*, **21**, 125-148.

Kim, J.-H., C.-H. Ho, M.-H. Lee, J.-H. Jeong, and D. Chen, 2006: Large increase in heavy rainfall associated with tropical cyclone landfalls in Korea after the late 1970s. *Geophys. Res. Lett.*, **33**, L18706, doi:10.1029/2006GL027430.

Kim, K.-Y., J.-W. Roh, D.-K. Lee, and J.-G. Jhun, 2010: Physical mechanisms of the seasonal, subseasonal, and high-frequency variability in the seasonal cycle of summer precipitation in Korea, *J. Geophys. Res.*, 155, D14110, doi:10.1029/2009JD013561.

_____, and Y. Y. Kim, 2002: Mechanism of Kelvin and Rossby waves during ENSO events. *Meteor. Atmos. Phys.*, *81*, 169-189.

_____, and G. R. North, 1997: EOFs of harmonizable cyclostationary processes. *J. Atmos. Sci.*, **54**, 2416-2427.

_____, G. R. North, and J. Huang, 1996: EOFs of one-dimensional cyclostationary time series: Computations, examples and stochastic modeling. *J. Atmos. Sci.*, **53**, 1007-1017.

_____, K. Kullgren, G.-H. Lim, K.-O. Boo, B.-M. Kim, 2006: Physical mechanisms of the Australian summer monsoon. Part II: Variability of strength, onset and termination times. *J. Geophys. Res.*, **111**, D20105, doi:10.1029/ 2005JD006808.

Kullgren, K., and K.-Y. Kim, 2006: Physical mechanisms of the Australian summer monsoon. Part I: The seasonal cycle. *J. Geophys. Res.*, **111**, D20104, doi:10.1029/2005JD006807.

Kwon, M., J.-G. Jhun, B. Wang, S.-I. Ahn, and J.-S. Kug, 2005: Decadal change in relationship between east Asian and WNP summer monsoons, *Geophys. Res., Lett.*, **32**, L16709, doi:10.1029/2005GL023026.

Lau, K. –M., G. J. Yang, and S. H. Shen, 1988: Seasonal and intraseasonal climatology of summer monsoon rainfall over East Asia. *Mon. Weather Rev.*, **116**, 18-37.

Lee, D.-K., J.-G. Park, and J.-W. Kim, 2008: Heavy rainfall events lasting 18 days from July 31 to August 17, 1998, over Korea. *J. Meteor. Soc. Japan*, **86**(2), 313-333.

_____, 2004: Summertime climatology, in *Korean Climatology.*, edited, by H.-S. Chung, Meteorological Research Institute, Korea Meteorological Administration, 92-99.

_____, H.-R. Kim, and S.-Y. Hong, 1998: Heavy rainfall over Korea during 1980-1990. *Korean J. of Atmos. Sci., 1*, 523-547.

_____, J.-G. Jhun, S.-Y. Hong, and H.-R. Kim, 1993: Numerical simulations of a heavy rainfall case occurred over central Korea during 10-12 September 1990. *J. of Korean Meteor, Soc.*, **29**(2), 147-169.

_____, D.-E. Chang, and T.-K. Wee, 1992: Typhoon approaching Korea, 1960-1989. Part I: Statistics and synoptic overview. *J. of Korean Meteor, Soc.*, **28**(2), 133-147.

_____, and S.-Y. Hong, 1989: Numerical experiments of the heavy rainfall event occurred over Korea during 1-3 September 1984. *J. of Korean Meteor, Soc.*, **25**(4), 233-260.

Lee, M.-S. and D.-K. Lee (2003), An application of a weakly constrained 4DVAR to satellite data assimilation and heavy rainfall simulation, *Mon. Wea. Rev.*, **131**, 2151-2176.

Lee, S.-S., P. N. Vinayashandran, K.-J. Ha, and J.-G. Jhun, 2010: Shift of peak in summer monsoon rainfall over Korea and its association with El Nino-Southern Oscillation, J. Geophys. Res., **155**, D02111, doi:10.1029/2009JD 011717.

Lim, Y.-K., and K.-Y. Kim, 2007: ENSO impact on the space-time evolution of the regional Asian summer monsoons. *J. Clim.*, *20*, 2397-2415.

_____, _____, and H. S. Lee, 2002: Temporal and spatial evolution of the Asian summer monsoon in the seasonal cycle of synoptic fields. *J. Clim.*, **15**, 3630-3644.

Meehl, G. A., F. Zwiers, J. Evans, T. Knutson, L. Mearns, and P. Whetton, 2000: Trends in extreme weather and climate events: Issues related to

modeling extremes in projections of future climate change. *Bull. Amer. Meteorol. Soc.*, **81**, 427-436.

Meehl, G. A., and J. M. Arblaster, 2001: The tropospheric biennial oscillation and Indian monsoon rainfall. *Geophy. Res. Lett.*, *28*, 1731-1743.

Mitas, C. M. and A. Clement, 2005: Has the Hadley cell been strengthening in recent decades?. *Geophys. Res. Lett.*, **32**, L03809, doi:10.1029/2004GL 021765.

Newton, H. J., 1988: *TIMESLAB: A Time Series Analysis Laboratory.* Wadsworth and Brooks/Cole, 623 pp.

Ninomiya, K., 2001: Large λ-shaped cloud zone formed around July 6, 1991 with pole-ward moisture transport from intense reinfall area in Meiyu-Baiu front. *J. Meteor. Soc. Japan*, **79**(3), 805-813.

_____, 2000: Large- and meso-α-scale characteristics of Meiyu/Baiu front associated with intense rainfalls in 1-10 July 1991. *J. Meteor. Soc. Japan*, **78**, 141-157.

_____, and H. Mizuno, 1987: Variations of Baiu precipitation over Japan in 1951-1980 and large-scale characteristics of wet and dry Baiu. *J. Meteor. Soc. Japan*, **65**, 115-127.

Nitta, T., 1987: Convective activities in the tropical western Pacific and their impact on the Northern-Hemisphere summer circulation, *J. Meteor. Soc. Japan*, **65**, 373-390.

Qian, W. H., and D.-K. Lee, 2000: Seasonal march of Asian summer monsoon. *Intl. J. Climatol.*, **20**, 1371-1378.

_____, H.-S. Kang, and D.-K. Lee, 2002: Distribution of seasonal rainfall in East Asian monsoon region. *Theor. Appl, Climatol.*, **73**, 151-168.

Roh, J.-W., K.-Y. Kim, and J.-G. Jhun, 2011: Decadal changes in the physical mechanisms of the seasonal cycle of summertime precipitation variability in Korea, *J. Geophys. Res.*, doi:10.1029/2011JD017268, *in press*.

Roy, S. S., and R. C. Balling Jr., 2004: Trends in extreme daily precipitation indices in India. *Int. J. Climatol.*, **24**, 457-466.

Seo, K.-H., and K.-Y. Kim, 2003: Propagation and initiation mechanisms of the Madden-Julian oscillation. *J. Geophys. Res.*, 108(D13), 4384, doi:10.1029/ 2002JD002876.

Solomon, S., D. Qin, M. Manning, M. Marquis, K. Averyt, M. M. B. Tignor, H. L. Miller Jr., and Z. Chen, Eds., 2007: *Climate Change 2007: The Physical Science Basis*. Cambridge Univ. Press, 996 pp.

Tao, S. Y. and L. X. Chen, 1987: A review of recent research on the East Asian monsoon in China. In: Monsoon Meteorology. Ed. By C.-P. Chang and T.N. Krishnamurti, Oxford University Press, London, 60-92.

Trenberth, K. E., 1999: Atmospheric moisture recycling: Role of advection and local evaporation. J. Clim., **12**, 1368-1381.

Wang, B., J.-G. Jhun, and B.-K. Moon, 2007:Variability and singularity of Seoul, South Korea, rainy season (1778-2004). *J. Clim.*, **20**, 2572-2580.

_____, and Lin Ho, 2002: Rainy season of the Asian-Pacific summer monsoon. *J. Clim.*, **15**, 386-398.

Weare, B. C., and J. N. Nasstrom, 1982: Examples of extended empirical orthogonal function analysis, *Mon. Wea. Rev.*, **110**, 481-485.

Webster P. J., V. O. Magana, T. N. Palmer, J. Shukla, R. A. Tomas, M. Yanai, and T. Yasunari, Monsoon, 1998: Processes, predictability, and the prospects for prediction, *J. Geophy. Res.*, **103**(C7), 14451-14510.

Zhai, P., X. Zhang, H. Wan, and X. Pan, 2005: Trends in total precipitation and frequency of daily precipitation extremes over China. *J. Climate*, **18**, 1096-1108.

국문 초록

한국 여름 강수 변동성 기작의 십년 규모 변화

노 준 우
지구환경과학부
서울대학교 대학원

최근 강수 강도, 빈도, 강수 기록 지역의 급변화와 같은, 강수 변화와 관련된 문제들은 기후변화에 따른 가장 중요한 변화 현상이다. 극심한 폭우가 기록되는 지역의 변화는 전 지구적인 문제라기 보다는 일부 지역에 특히 제한적으로 나타난다. 따라서 특정 지역에서 그 규모의 집중 호우를 설명할 수 있는 더 자세한 물리적 기작에 관한 연구가 요구된다. 한반도와 주변 동아시아 지역은 여름 강수 변화가 최근 크게 바뀐 지역임으로, 한반도의 여름 강수의 변동성과 그 변화를 연구하였다.

한반도의 여름강수는 아시아 및 동아시아 여름 몬순과 관련된 장마전선, 중위도 경압파, 상층 제트 및 하층 제트의 강도와 위치, 북태평양 고기압대와 오츠크해 기단 등의 영향, 티벳 고원의 영향으로 파생되는 다양한 현상들 등으로부터 기인하는 다양하고 복잡한 원인으로 발생한다. 이러한 한반도 여름 강수 변동성을 분석하기 위해, 1979-2008 년 기상청 61 개 관측소의 일 강수량의 여름 기간 (5 월 19 일 – 9 월 15 일) 자료를 CSEOF 분석기법을 이용하여, 연주기 변동성을 추출하였다. 강수 변동성의 원인을 설명하는 물리적 기작을 시-공간 구조로 더 자세하게 구현하기 위해 아시아 영역에서의 NCEP/NCAR 재분석 자료의 물리 변수를 강수 변동성과 동일한 시간에 대하여 CSEOF 분석을 실시하였다. 한반도 여름 강수의 연주기 변동성을 시간 규모에 따른 세가지 주요 요소인 seasonal 요소, sub-seasonal 요소, high-frequency 요소로 나누었다. Seasonal 요소는, 아시아 대륙과 그를 둘러싼 바다 사이에서 형성되는 계절적 기단차의 결과로 발생하는 아시아 여름 몬순, 특히 동아시아 여름 몬순과 관련된 변동성을 설명한다. 몬순 전선대의 도달과 지속 시기는 한반도 여름 강수의 seasonal 요소의 추이를 주도적으로 형성한다. 두개의 강수 최대치 유형은 이러한 기단의 성질

변화에 의한 하층 순환계 변화에 기인한다. Sub-seasonal 요소는 10-30 일 시간 규모의 성격을 가지며 ~40°N 부근의 동진하는 상층 요란과 관련성을 가진다. 상층 요란은 하층 수렴/발산에 따른 남북 방향 순환에 영향을 끼친다. 7 월 중순부터 8 월 중순까지 기간에는, 초여름과 늦여름에 비해 진동 주기가 더 짧아진다. 10 일 미만의 시간 규모를 가진 high-frequency 요소는 종관규모 중위도 로스비 경압파와 관련된다. 상층 지위고도와 하층 습윤이류는 한반도 high-frequency 변동성과 높은 상관도를 가진다. 이 요소에서, 한반도에 비가 있을때, ~40°N 를 축으로 로스비 경압파에 의한 상층 발산이 위치하며, 주요 물리 변수로 구현하면, 상층 발산과 하층 수렴의 전형적인 경압 불안정 연직구조를 보였다.

이러한 결과를 이용하여, 최근 기후변화에 따른 한반도 지역 여름 강수 변동성의 변화를 각 시간규모에 따른 세가지 요소별 물리적 기작 변화를 기반으로 조사하였다. 1979-1995 년 (PRE) 과 1996-2008 년 (POS) 시기에 대하여 각각 위의 분석 설계와 동일하게 CSEOF 분석을 실시하였다. 동아시아 여름 몬순과 관련된 변동성을 설명하는 Seasonal 요소에서는, 하층 순환 유형의 변화에 의해, 동아시아 몬순 전선대의 전진, 지속, 후퇴가 최근의 주요한 변화 요인으로 밝혀졌다. 특히 한반도 1 차 장마에 의한 강수의 첫번째 최대 시기가 더 빨리 시작되고 그 강도도 증가하였다. 여름강수의 휴지기는 최근에 전반적으로 약해졌는데, 특히 한반도 중북부에서는 휴지기 유형이 거의 사라졌다. 2 차 장마에 의한 강수 최대 시기는 최근 시간적으로 완만하게 분포한다.

평균 15 일 주기를 가진 Sub-seasonal 요소의 강도는 최근 아열대와 중위도 사이의 남북방향 순환이 강화되면서 증가하였다. 최근 한반도 남쪽에서부터 온난이류와 습윤이류이 강해지고 북쪽에서 기인하는 한랭이류가 약화되면서 경압형 연직 구조가 이 규모의 강수를 주도했던 과거와 달리, 순압형 연직 구조가 최근 주를 이뤘다. 상대적으로 강한 sub-seasonal 요소의 활동은 과거 6 월 말에서 7 월 중순에 있었으나, 최근 8 월 초에서 9 월 초 시기로 이동하였다.

경압 불안정 구조로 형성되는 high-frequency 요소의 강수는 역학적 열역학적 요인의 진행이 강해지면서 최근 약 25% 증가하였고, 특히 8 월 초에서 중순에 두드러졌다.

전체 30 년기간의 두번째 CSEOF 와 세번째 CSEOF 모드는 열대성 저기압의 직/간접적 영향에 의한 국지적 집중호우 사례들을 설명한다. PRE 기간의 두번째 모드 로딩벡터는 전체기간의 세번째 모드의 그것과, POS 기간의 두번째 모드의 로딩벡터는 전체기간의 두번째 모드의 그것과 0.96 이상의 상관관계를 가진다. 과거기간의 두번째 모드는 9 월 3 일, 남해안 지역에서 강수 최대치가 나타났고, 최근기간의 두번째 모드에서는 8 월 7 일과 8 월 31 의 강수 최대치가 중서부 지역과 동부 지역에 각각 나타났다. 이러한 열대성 저기압의 직/간적접 영향에 의한 국지적 집중호우 변화는 열대성 저기압의 진로와 관련된 한반도 주변의 물리 구조 변화에 의한 것으로 나타났다.

주요어: 물리적 기작, 싸이클로스테이셔너리 경험 직교 함수,한반도 여름 강수 변동성, 십년 규모 변화

학번: 2005-30139

감사의 글

길었던 한 시기가 지금 이 한권의 논문앞에서 일단락되려 합니다. 되돌아보니 많은 분들의 가르치심과 조언, 격려가 있었기에 지금 여기에 이른듯 합니다.

참 많은 것이 부족했던 제자를 위해, 그 바쁘신 일정속에서도 열정적으로 가르쳐주시고 연구자의 자세를 일깨워주신 김광열 교수님께 깊이 감사드립니다. 바쁘신 와중에도 논문 심사와 지도를 아낌없이 해주신 임규호 교수님, 이동규 교수님, 전종갑 교수님, 서경환 교수님께도 깊은 감사를 드립니다. 대기과학이란 학문을 다져주신 교수님들께 감사 드립니다. 오랜 시간 함께 했었던 수치예보실험실 선후배님들과 통계기후학실험실 후배님들, 이웃 실험실들의 선후배, 동료들에게도 감사와 응원의 말을 남깁니다. 기상연구소장님과 예보연구과 직원분들께도 감사 드립니다. 험난했던 저의 이 시기에 크나큰 힘이 되어준, 제 삶 곳곳의 친구들에게 특별히 깊은 고마움을 전합니다.

늘 저를 믿어주시고, 지원을 아끼지 않으셨던 내 사랑하는 가족, 고맙습니다. 아버지, 고맙습니다. 큰누나, 작은누나, 큰 자형, 작은 자형, 동생, 제수씨 그리고 내 조카들 모두 고맙습니다. 최종 몇일전 갑작스레 하늘로 가신, 지금 그곳에서 보고 계실 어머니, 고맙습니다. 어머니께 이 논문을 바칩니다.

이제 겸허한 마음 가짐으로 새로운 단락을 펼치려 합니다.

이 논문이 나오기 까지 힘이 되어주신 분들께 다시 한번 감사드립니다.